N75-30955

FINAL REPORT

RESEARCH STUDY ON STABILIZATION AND CONTROL

MODERN SAMPLED-DATA CONTROL THEORY

SYSTEMS RESEARCH LABORATORY

P.O. BOX 2277, STATION A
3206 VALLEY BROOK DRIVE
CHAMPAIGN, ILLINOIS 61820

PREPARED FOR GEORGE C. MARSHALL SPACE FLIGHT CENTER

HUNTSVILLE, ALABAMA

FINAL REPORT

RESEARCH STUDY ON STABILIZATION AND CONTROL

– MODERN SAMPLED-DATA CONTROL THEORY

SUBTITLE: STABILITY ANALYSIS OF THE LOW-COST LARGE SPACE TELESCOPE SYSTEM

June 30, 1975 NAS8-29853

BY B.C. KUO
G. SINGH

PREPARED FOR GEORGE C. MARSHALL SPACE FLIGHT CENTER
HUNTSVILLE, ALABAMA

CONTRACT NAS8-29853 DCN 1-2-40-23018

SYSTEMS RESEARCH LABORATORY
P.O. BOX 2277, STATION A
CHAMPAIGN, ILLINOIS 61820

TABLE OF CONTENTS

1. Pointing Accuracy of the Low-Cost Large Space Telescope Due to Noise and Quantization

1-1. Introduction

The objective of this study is to conduct an investigation on the pointing stability of the low-cost Large Space Telescope (LST) system. The low-cost LST is characterized by the use of reaction wheels for the generation of control torques. Because of the critical requirement on the pointing accuracy of the LST, the nonlinear frictional characteristics of the bearings of the reaction wheels cannot be neglected. It is well known that the nonlinear friction can cause limit cycles in a closed-loop system.

Another possible source of pointing error in the LST is due to the effect of quantization and sensor noise. Since the LST is a digital system, D-A and A-D converters, and sensors for positional and rate feedbacks are used. Sensor noise and amplitude quantization will also cause pointing error in the LST. In addition, quantization is a nonlinear phenomenon so that it may also cause self-sustained oscillations in the closed-loop system.

The dynamic modeling of the single-axis LST is described in this chapter. Several methods of evaluating the attitude error of the digital LST due to quantization and noise inputs are given.

1-2. Dynamic Models of the Low-Cost LST System

The dynamic model of the single-axis low-cost LST system with sampled data is shown in the block diagram of Fig. 1-1. The rigid body is represented by the double-integrator transfer function. The controller is formed by proportional, rate, and integral feedbacks of the vehicle attitude. The nonlinear element N in the reaction wheel dynamics represents the rolling friction, and its functional description is given by the well-known Dahl model.

The definitions of variables and the values of parameters and constants are tabulated in Table 1-1 [1].

Table 1-1.

ϕ_c	Reference input command	
ϕ_B	Body attitude of LST	
$\dot{\phi}_B$	Body rate of LST	
T_c	Torque command of reaction wheel	
T_{RW}	Torque output of reaction wheel	
$\dot{\Theta}_{RW}$	Angular velocity of reaction wheel	
Θ_{RW}	Angular displacement of reaction wheel	
T_F	Frictional torque of reaction wheel	
ϕ_e	Attitude error	
K_p	Proportional gain of controller	1.65×10^6 N-m/rad
K_R	Rate gain of controller	3.71×10^5 N-m/rad/sec
K_I	Integral gain of controller	7.33×10^5 N-m/rad/sec
R_F	Feedback resistance	0.484 ohms
K_A	Voltage amplifier gain	10000

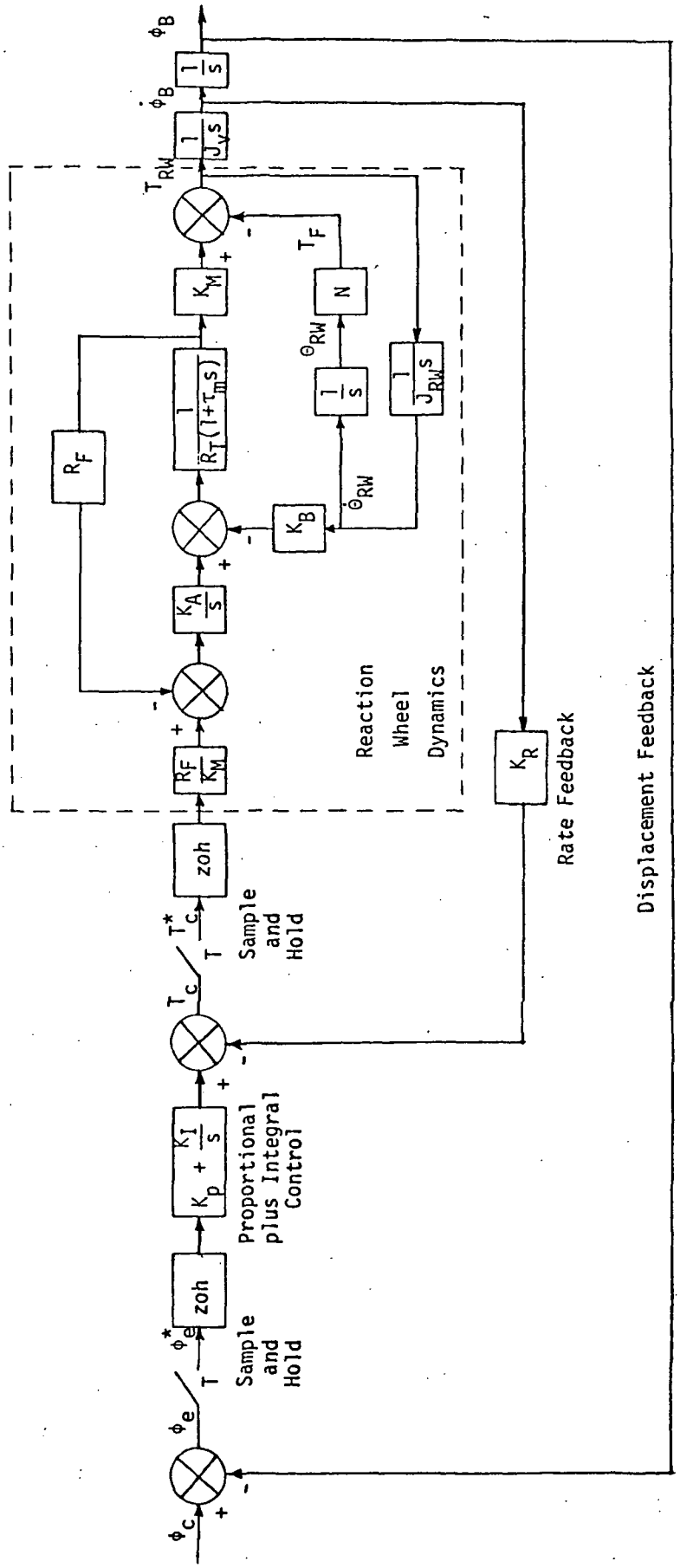

Figure 1-1. Digital low-cost LST system (single axis).

K_M	Motor torque constant	0.484 N-m/amp
K_B	Back emf constant	0.484 volt/rad/sec
J_{RW}	Moment of inertia of reaction wheel	0.2 Kg-m^2
J_v	Moment of inertia of vehicle about pitch axis	41822 Kg-m^2
τ_m	Motor time constant	0.002 sec
R_T	Motor resistance	10 ohms

Although the low-cost LST system has digital control, it is informative to analyze the system of Fig. 1-1 first without the sample-and-hold device. Figure 1-2 shows the signal flow graph of the continuous-data LST system. The characteristic equation of the system is determined from Fig. 1-2,

$$\Delta = 1 + R_F G_2 G_3 + K_B K_M G_3 G_6 + \frac{R_F K_M K_R}{K_M} G_2 G_3 G_4 + R_F G_1 G_2 G_3 G_4 G_5 + N(G_6 G_7 + R_F G_2 G_3 G_6 G_7) = 0 \tag{1-1}$$

where

$$G_1 = K_p + K_I/s$$

$$G_2 = K_A/s$$

$$G_3 = \frac{1}{R + (1 + \tau_m s)}$$

$$G_4 = \frac{1}{J_v s}$$

$$G_5 = \frac{1}{s}$$

$$G_6 = \frac{1}{J_{RW} s}$$

$$G_7 = \frac{1}{s}$$

and N denotes the analog describing function of the reaction wheel nonlinearity.

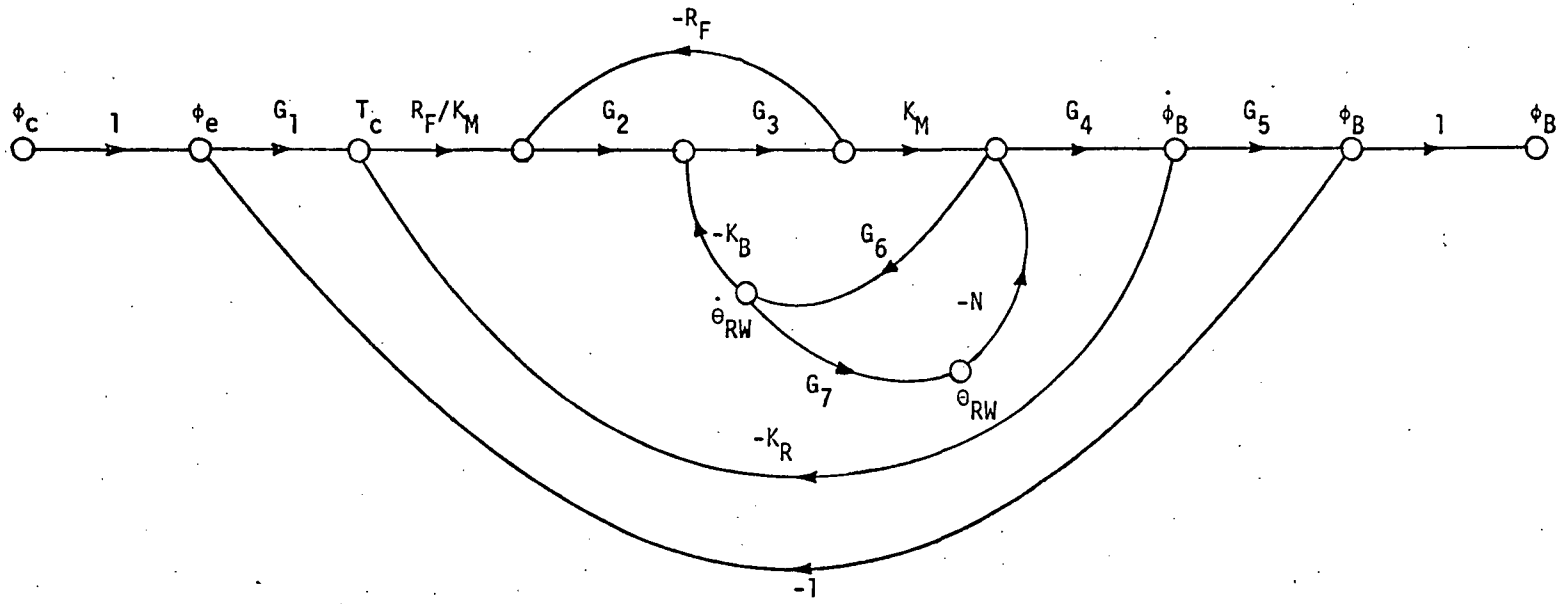

Figure 1-2. Signal flow graph of the continuous-data low-cost LST system.

For the linear model of the LST system, we set N = 0, and the characteristic equation becomes

$$\tau_m J_v R_T s^5 + J_v R_T s^4 + (J_v R_F K_A + \frac{K_B K_M J_v}{J_{RW}})s^3 + R_F K_R K_A s^2 + K_A R_F K_p s + K_A K_I R_F = 0 \quad (1\text{-}2)$$

It is of interest to investigate the dynamics of the reaction wheel and the vehicle. The open-loop transfer function between T_c and ϕ_B is

$$\frac{\phi_B}{T_c} = \frac{R_F K_A}{J_v s^2 (R_T \tau_m s^2 + R_T s + R_F K_A + \frac{K_M K_B}{J_{RW}})} \quad (1\text{-}3)$$

Substituting the system parameters into Eq. (1-3) gives

$$\frac{\phi_B}{T_c} = \frac{5.7865}{s^2(s^2 + 500s + 242058.5)} = \frac{5.7865}{s^2(s + 250 + j423.74)(s + 250 + j423.74)} \quad (1\text{-}4)$$

Thus, the reaction wheel is shown to have relatively fast dynamics.

Substitution of the values of the system parameters into Eq. (1-2), and simplifying, the characteristic equation of the linear LST system is written

$$s^5 + 500s^4 + 242058.5s^3 + 2.1468 \times 10^6 s^2 + 9.5476 \times 10^6 s + 4.24145 \times 10^6 = 0 \quad (1\text{-}5)$$

The roots of the characteristic equation are:

$s = -0.49659$

$s = -4.22743 + j4.25123$

$s = -4.22743 - j4.25123$

$s = -245.524 + j421.118$

$s = -245.524 - j421.118$

Note that the damping ratio of the dominant complex roots is 0.705, and the natural undamped frequency is 6 rad/sec or 0.954 Hz. These parameters are achieved by selecting the controller constants K_p, K_R and K_I at the indicated values. However, the poles of the reaction wheel dynamics at $s = -250 + j423.74$ and $s = -250 - j423.74$ are only slightly affected by the body controller and they account for the characteristic roots at $s = -245.524 + j421.118$ and $s = -245.524 - j421.118$ of the overall closed-loop system. Since these fast roots are very far away from the dominant ones, this means that for all practical purposes the dynamics of the reaction wheel can be neglected as far as the linear system is concerned. Figure 1-3 shows the block diagram of the simplified continuous-data low-cost LST system, and the digital system is shown in Fig. 1-4.

The closed-loop transfer function of the continuous-data system of Fig. 1-3 is

$$\frac{\Phi_B(s)}{\Phi_c(s)} = \frac{K_p s + K_I}{J_v s^3 + K_R s^2 + K_p s + K_I} \tag{1-6}$$

For the digital system of Fig. 1-4, the closed-loop transfer function is written

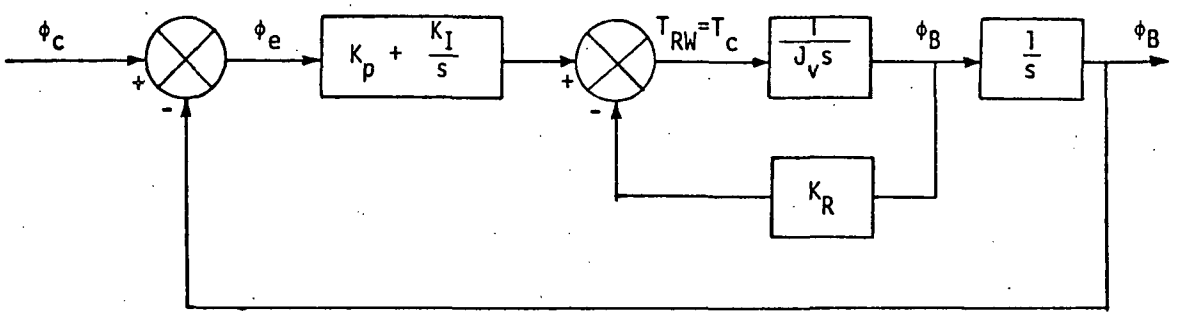

Figure 1-3. Simplified continuous-data low-cost LST system.

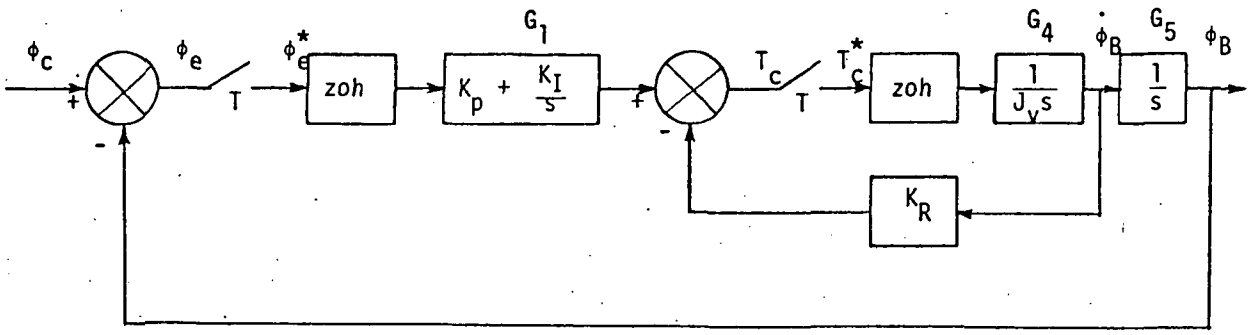

Figure 1-4. Simplified digital low-cost LST system.

$$\frac{\Phi_B(z)}{\Phi_c(z)} = \frac{G_A(z)G_B(z)}{1 + G_c(z) + G_A(z)G_B(z)} \tag{1-7}$$

where

$$G_{ho}(s) = \frac{1 - e^{-Ts}}{s}$$

$$G_A(z) = \mathcal{Z}(G_{ho}G_1) = (1 - z^{-1})\mathcal{Z}\left(\frac{K_I s + K_I}{s^2}\right) = \frac{K_p z + K_I T - K_p}{z - 1} \tag{1-8}$$

$$G_B(z) = \mathcal{Z}(G_{ho}G_4G_5) = (1 - z^{-1})\mathcal{Z}\left(\frac{1}{J_v s^3}\right) = \frac{T^2(z + 1)}{2J_v(z - 1)^2} \tag{1-9}$$

$$G_c(z) = \mathcal{Z}(G_{ho}G_4K_R) = K_R(1 - z^{-1})\mathcal{Z}\left(\frac{1}{J_v s^2}\right) = \frac{K_R}{J_v}\frac{T}{z - 1} \tag{1-10}$$

Equation (1-7) is simplified to

$$\frac{\Phi_B(z)}{\Phi_c(z)} = \frac{T^2(K_p z^2 + K_I T z + K_I T - K_p)}{2J_v z^3 + (T^2K_p + 2K_R T - 6J_v)z^2 + (6J_v - 4K_R T + T^2 K_I T)z + (2K_R T + K_I T^3 - 2J_v - K_p T^2)} \tag{1-11}$$

The characteristic equation of the system is

$$2J_v z^3 + (T^2K_p + 2K_R T - 6J_v)z^2 + (6J_v - 4K_R T + T^3 K_I)z + 2K_R T + K_I T^3 - 2J_v - K_p T^2 = 0 \tag{1-12}$$

Or,

$$83644z^3 + (1.65 \times 10^6 T^2 + 7.42 \times 10^5 T - 2.50932 \times 10^5)z^2$$
$$+ (2.50932 \times 10^5 - 14.84 \times 10^5 T + 7.33 \times 10^5 T^3)z$$
$$+ (-8.3644 \times 10^4 + 7.42 \times 10^5 T + 7.33 \times 10^5 T^3 - 1.65 \times 10^6 T^2) = 0 \quad (1\text{-}13)$$

The characteristic equation roots are tabulated below as functions of the sampling period T:

T (msec)	Roots
0.1	1, 0.998 ± j0.0025
0.5	1, 0.998 ± j0.0022
1	1, 0.996 ± j0.0043
5	0.998, 0.979 ± j0.0208
10	0.995, 0.957 ± j0.0411
25	0.987, 0.889 ± j0.0988
50	0.975, 0.766 ± j0.1825
100	0.950, 0.483 ± j0.2901
120	0.940, 0.356 ± j0.300
150	0.925, 0.150 ± j0.260
170	0.915, 0.0034 ± j0.144
180	0.910, 0.049, -0.195
200	0.900, 0.107, -0.571
220	0.890, 0.1116, -0.9078
230	0.885, 0.1085, -1.077 (unstable)

The root loci of Eq. (1-13) are sketched in Fig. 1-5 as a function of T. For small sampling periods, the characteristic roots are all located near

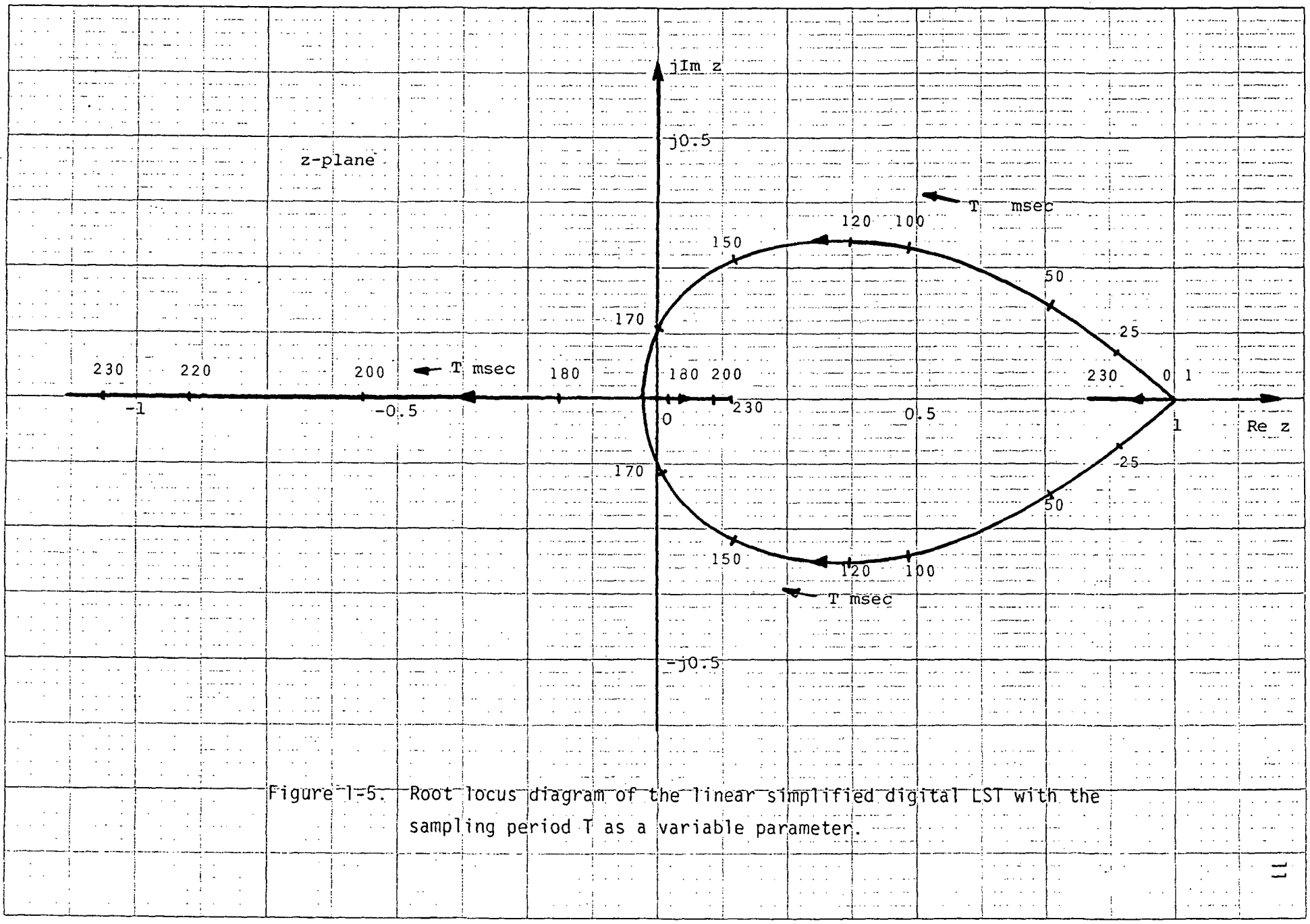

Figure 1-5. Root locus diagram of the linear simplified digital LST with the sampling period T as a variable parameter.

the $z = 1$ point. The linear digital LST system becomes unstable when T exceeds approximately 225 msec.

1-3. Effects of Quantization on Pointing Stability of the Low-Cost LST - Limit Cycle Conditions

Quantization occurs at at least three places in the LST system. Two are at the displacement sensor and the rate sensor where A-to-D converters are used. A quantizer is also needed at the control torque input to the reaction wheel since D-to-A conversion is effected there. In addition, if the integral control K_I/s is implemented digitally, quantization should be considered in the digital controller as well. Figure 1-6 shows the digital LST system with quantizers. The z-transfer functions are defined in Eqs. (1-8), (1-9), and (1-10). The quantizers at the displacement sensor, the rate sensor, and the reaction wheel control torque are denoted by Q_p, Q_R, and Q_T, respectively. The input-output relation of a quantizer is shown in Fig. 1-7. The quantization level is represented by h.

We shall analyze the effects of quantization on pointing stability or accuracy of the LST by means of three different methods. The first method utilizes the deterministic approach and establishes a least upper bound on the pointing error due to quantization. The second method relies on treating the quantizer as a noise source, and statistical analysis is applied. The third method is also a statistical approach which represents the quantizer by a linearized gain $K_{eq}(z)$.

It should be pointed out that a system with quantization is a nonlinear system and its behavior cannot be predicted by linear theory. One of the well-known phenomena of a nonlinear system is that sustained oscillations may occur. When a digital system has several quantizers, it is extremely difficult to predict the condition of self-sustained oscillations.

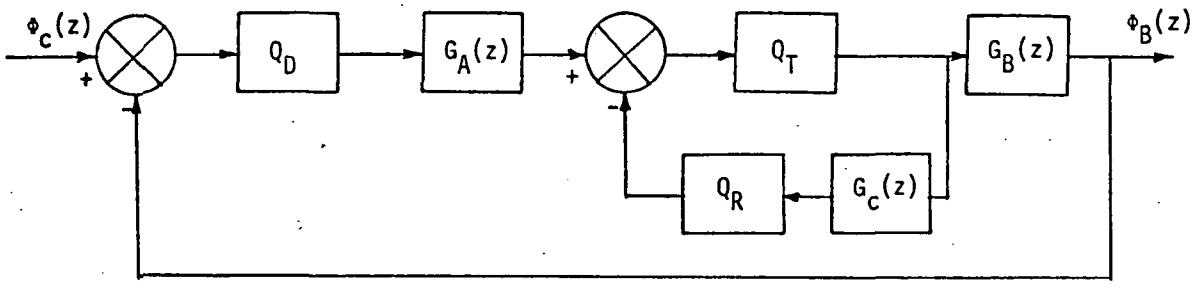

Figure 1-6. Simplified digital LST system with quantizers.

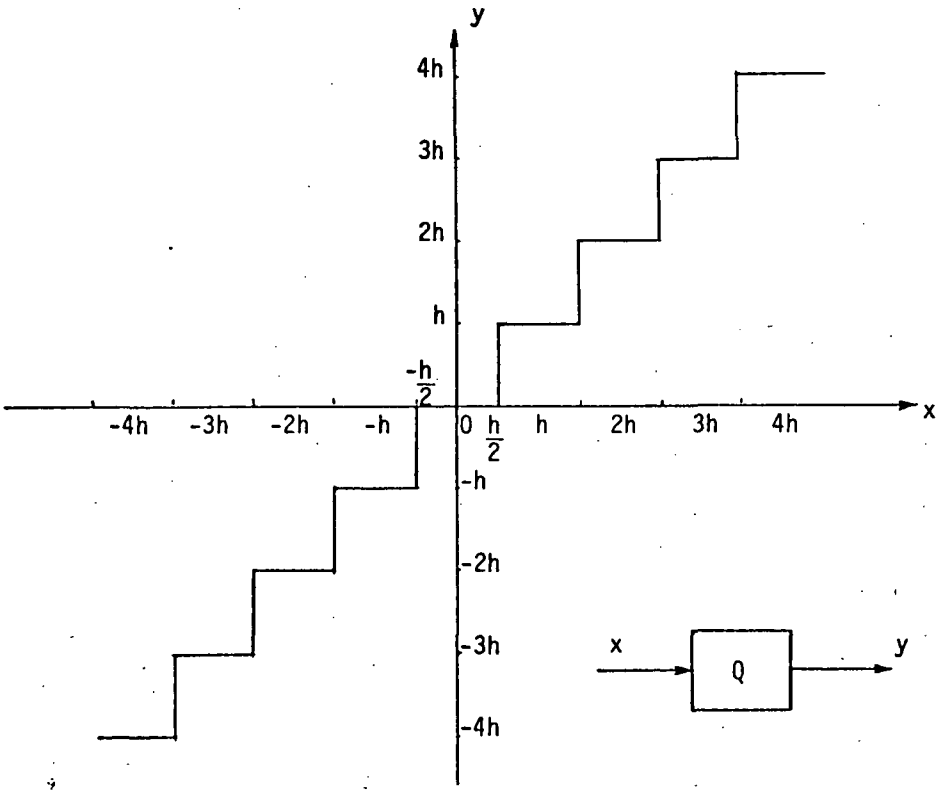

Figure 1-7. Input-output characteristics of a quantizer.

To illustrate the effects of quantization, and how quantization can cause sustained oscillations in an otherwise stable linear system, let us refer to the digital systems shown in Figs. 1-8 and 1-9. The difference between the two systems in Figs. 1-8a and 1-9a is that the former has negative feedback and the latter has positive feedback; but both systems are stable.

For $r(k) = 0$, both linear systems have zero steady-state values for $c(k)$; that is, $c(k) = 0$ for $k \to \infty$, for arbitrary initial state $c(0)$. We shall show that when quantization is considered, the system in Fig. 1-9b has a steady-state error, whereas the system in Fig. 1-8b exhibits a sustained oscillation.

Let the quantization level h be 2 in Fig. 1-7, and when the input is an integer, the output is the same integer. The state equation of the system in Fig. 1-9b is

$$c(k+1) = Q[0.9c(k)] \tag{1-14}$$

For $c(0) = 10$, it can be easily shown that $c(k) = 4$ for $k \geq 2$.

The state equation of the system in Fig. 1-8b is

$$c(k+1) = Q[-0.9c(k)] \tag{1-15}$$

For $c(0) = 10$, $c(k) = 8$ for $k \geq 2$ even, and $c(k) = -8$ for $k > 2$ odd. Thus, the state of the system oscillates between -8 and +8.

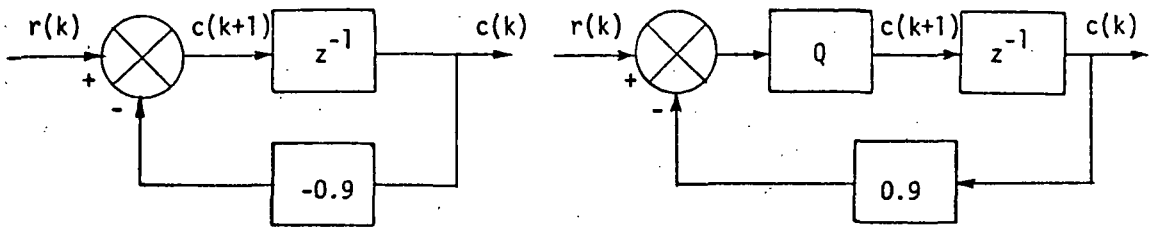

(a) Linear system (b) System with quantizer

Figure 1-8. Systems with quantizers.

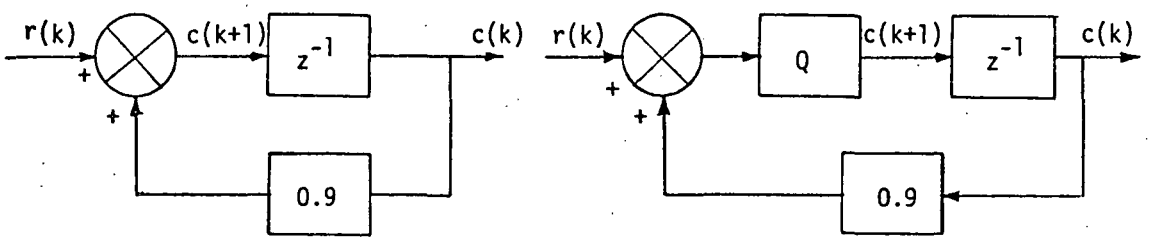

(a) Linear system (b) System with quantizer

Figure 1-9. Systems with quantizers.

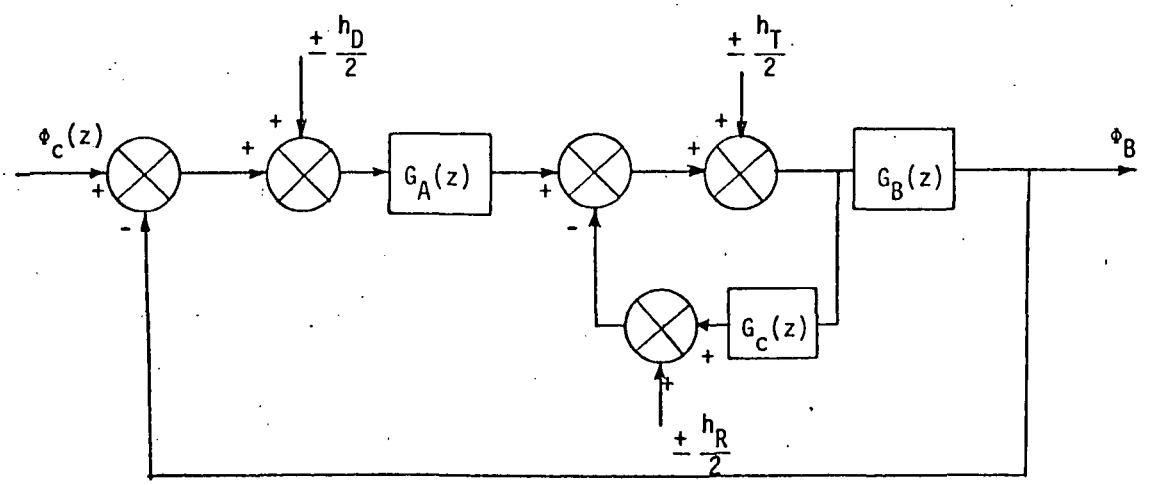

Figure 1-10. Digital LST system with quantizers replaced by deterministic noise sources.

1-4. Effects of Quantization on Pointing Stability of the Digital Low-Cost LST - Least Upper Bound Quantization Error

In this section the effects of quantization on the low-cost LST system are investigated using a deterministic approach. The method of analysis is based on the "worst" error condition due to quantization. In general, the analysis gives a conservative estimation of the quantization error.

Since the quantization error has a maximum bound of $\pm h/2$, the "worst" error due to quantization in a digital system can be studied by replacing the quantizer in the state diagram by a branch with unity gain and an external noise source with a signal magnitude of $\pm h/2$. The block diagram of the digital LST system with quantizers shown in Fig. 1-6 is redrawn in Fig. 1-10 with the noise sources. The transfer functions $G_A(z)$, $G_B(z)$, and $G_c(z)$ are defined in Eqs. (1-8), (1-9), and (1-10), respectively.

The z-transform of the body attitude of the LST due to the three quantizers when $\phi_c = 0$ is

$$\Phi_B(z) = \frac{z}{z-1} \frac{\pm \frac{h_D}{2} G_A(z) \pm \frac{h_T}{2} \pm \frac{h_R}{2}}{1 + G_A(z)G_B(z) + G_c(z)} G_B(z) \tag{1-16}$$

Substitution of Eqs. (1-8) through (1-10) into Eq. (1-16), and simplifying, we have

$$\Phi_B(z) = \frac{z}{z-1} \frac{[\pm \frac{h_D}{2}(K_p z + K_I T - K_p) \pm (\frac{h_T}{2} + \frac{h_R}{2})(z-1)]T^2(z+1)}{2J_v(z-1)^3 + T^2(z+1)(K_p z + K_I T - K_p) + 2TK_R(z-1)^2} \tag{1-17}$$

The steady-state error of the body attitude due to the quantization effects is obtained by applying the final-value theorem to Eq. (1-17), (if the system is stable).

Thus,

$$\lim_{k\to\infty} \Phi_B(kT) = \lim_{z\to 1} (1 - z^{-1})\Phi_B(z) = \pm\frac{h_D}{2} \tag{1-18}$$

It is interesting to explore the significance of this result on the error due to quantization. Firstly, the quantization error at the displacement sensor is propagated through the system without change in amplitude. Secondly, the errors due to the torque and rate sensor quantizers are completely eliminated at the output position. This is attributed to the integral control K_I/s in the forward path.

Digital Implementation of Forward Controller

If the proportional-plus-integral controller is implemented digitally, the transfer function $G_A(z)$ becomes

$$G_A(z) = K_p + \frac{TK_I(z + 1)}{2(z - 1)} \tag{1-19}$$

Substituting $G_A(z)$ from Eq. (1-19) into Eq. (1-16), we can again show that the steady-state error in $\Phi_B(kT)$ due to the three quantizers is $\pm h_D/2$, and the errors due to Q_R and Q_T are completely eliminated.

In reality, the digital implementation of the controller should also include quantization in the digital process. Figure 1-11 shows the block diagram of the LST system with quantizations also considered in the digital controller. The z-transform of the body attitude of the

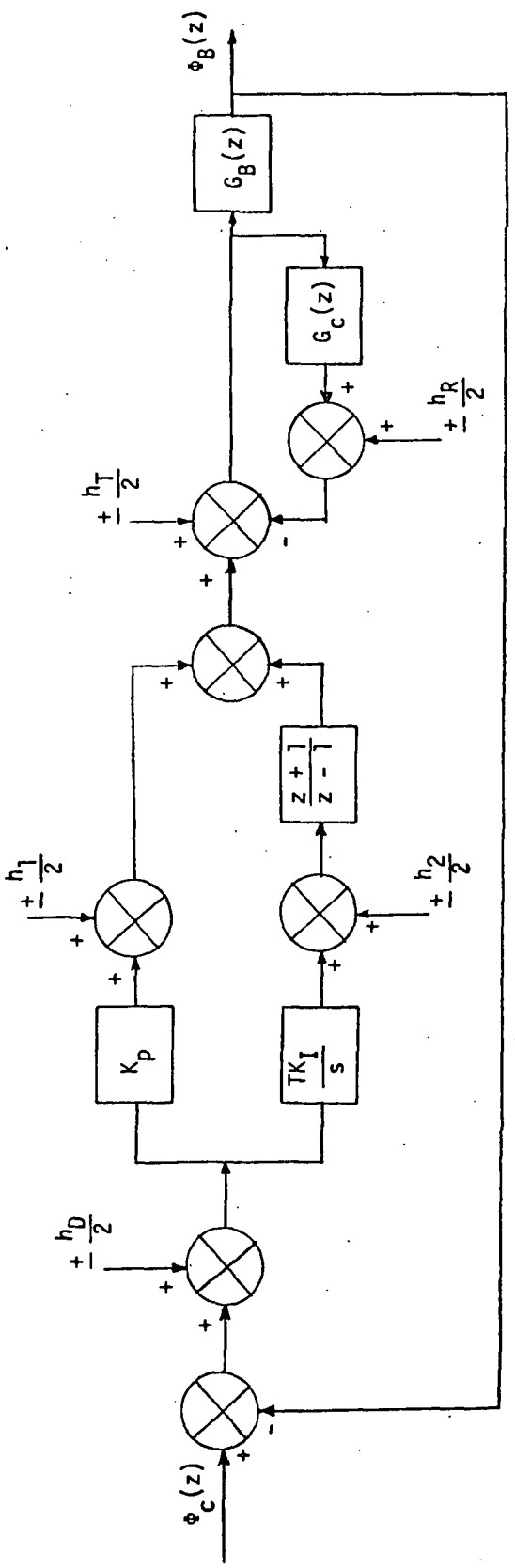

Figure 1-11. Digital LST system with quantizers in the digital controller.

LST due to the five quantizers when $\Phi_c = 0$ is

$$\Phi_B(z) = \frac{z}{z-1} \frac{\pm\frac{h_D}{2} G_A(z) \pm \frac{h_1}{2} \pm \frac{h_2}{2}\left(\frac{z+1}{z-1}\right) \pm \frac{h_R}{2} \pm \frac{h_T}{2}}{1 + G_A(z)G_B(z) + G_c(z)} G_B(z) \tag{1-20}$$

where $G_A(z)$ is given by Eq. (1-19) and $G_B(z)$ and $G_c(z)$ are given in Eqs. (1-9) and (1-10), respectively.

Applying the final-value theorem to Eq. (1-20), we have

$$\lim_{k\to\infty} \Phi_B(kT) = \frac{\pm h_2 \pm h_D K_I T}{2K_I T} = \pm\frac{h_D}{2} \pm \frac{h_2}{2K_I T} \tag{1-21}$$

It is interesting to note that the introduction of the integral control eliminates the noise signals that enter at all points after the integral control in the control loop; however, the digital implementation of this control in turn produces a quantization error which is bounded by $\pm h_2/2K_I T$, where h_2 is the quantization level.

1-5. Effects of Quantization on Pointing Stability of the Digital Low-Cost LST - Equivalent Noise Source, Statistical Analysis

In this section the pointing errors of the digital LST system due to quantizations in the displacement, rate, and torque channels are investigated by statistical means. The rms (root-mean-square) error in ϕ_B due to quantizations that are represented by equivalent Gaussian noise sources with zero mean, or white noise sources, is determined by setting $\phi_c = 0$. The results are then compared with those of the continuous-data LST obtained in reference [1].

The block diagram model of the continuous-data LST with the quantizers replaced by equivalent noise sources is shown in Fig. 1-12. The equivalent digital system is shown in Fig. 1-13. It is assumed that the equivalent noise sources that represent the quantization operations are white, so that their power spectral density functions in both the s and the z domains are constants. Therefore,

$\Phi_D(s)$, $\Phi_D(z) = \Phi_D$ = power spectral density of displacement quantizer

$\Phi_R(s)$, $\Phi_R(z) = \Phi_R$ = power spectral density of rate quantizer

$\Phi_T(s)$, $\Phi_T(z) = \Phi_T$ = power spectral density of rate quantizer

Let the rms attitude error of the continuous-data LST due to Φ_D be represented by σ_{BD}. The rms errors are given by the following relations:

Displacement:

$$\sigma_{BD} = \left[\frac{1}{2\pi j}\int_{-j\infty}^{j\infty} M_D(s)M_D(-s)ds \cdot \Phi_D\right]^{1/2} \tag{1-22}$$

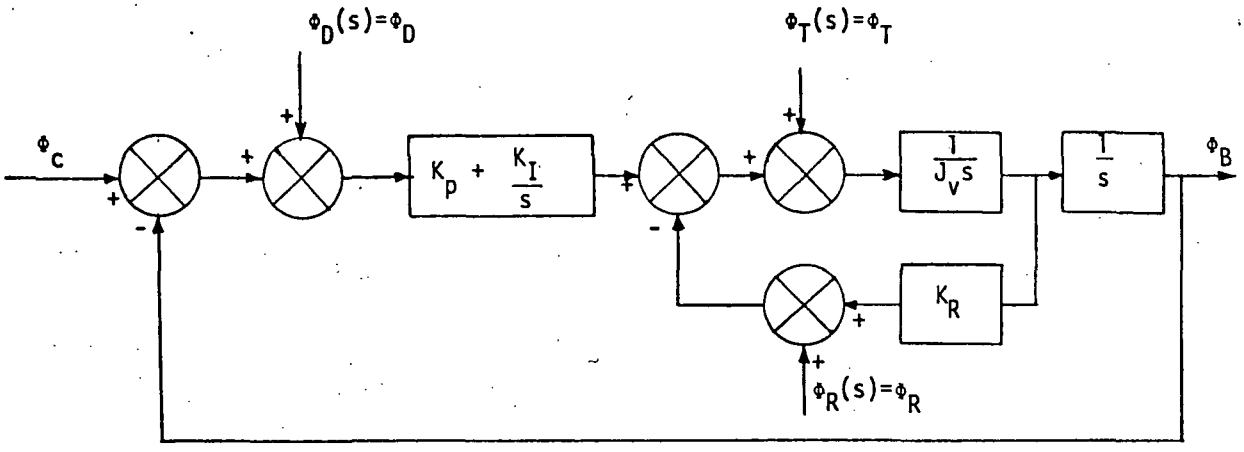

Figure 1-12. Continuous-data LST with quantizers represented by equivalent white noise sources.

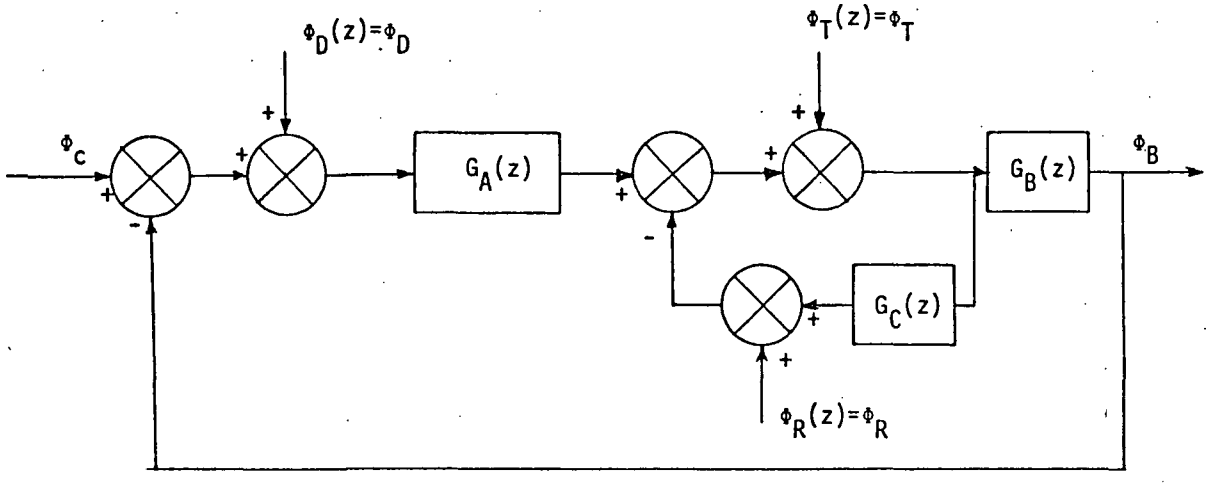

Figure 1-13. Digital LST with quantizers represented by equivalent white noise sources.

where $M_D(s)$ denotes the transfer function between $\Phi_D(s)$ and $\Phi_B(s)$,

$$M_D(s) = \frac{\Phi_B(s)}{\Phi_c(s)} = \frac{K_p s + K_I}{J_v s^3 + K_R s^2 + K_p s + K_I} \tag{1-23}$$

Similarly,

Rate:

$$\sigma_{BR} = \left(\frac{1}{2\pi j} \int_{-j\infty}^{j\infty} M_R(s) M_R(-s) ds \cdot \Phi_R \right)^{1/2} \tag{1-24}$$

Torque:

$$\sigma_{BT} = \left(\frac{1}{2\pi j} \int_{-j\infty}^{j\infty} M_T(s) M_T(-s) ds \cdot \Phi_T \right)^{1/2} \tag{1-25}$$

where

$$-M_R(s) = M_T(s) = \frac{\Phi_B(s)}{\Phi_T(s)} = \frac{s}{J_v s^3 + K_R s^2 + K_p s + K_I} \tag{1-26}$$

This result is obtained with the assumption that the quantizer noise is not multiplied by the sensor gain K_R, as in reference [1]; otherwise, the right-hand side of Eq. (1-26) should be multiplied by K_R.

The total rms attitude error due to all three quantizers is simply the sum of the errors due to each noise source acting alone; that is,

$$\sigma_B = \sigma_{BD} + \sigma_{BR} + \sigma_{BT} \tag{1-27}$$

From Eq. (1-26) it is easy to see that σ_{BR} and σ_{BT} have the same magnitude.

The line integral of the form of Eq. (1-22) can be evaluated by

contour integration, and then the residue theorem. An integral table is also available for the evaluation of the contour integral. Using Eqs. (1-23) and (1-26), the rms attitude errors of the continuous-data system are obtained as

$$\sigma_{BD} = \left[\frac{K_p^2 + K_I K_R}{2(K_R K_p - K_I J_v)}\,\Phi_D\right]^{1/2} = (2.5748\Phi_D)^{1/2} = 1.605\sqrt{\Phi_D} \tag{1-28}$$

$$\sigma_{BT} = \left[\frac{1}{2(K_R K_p - K_I J_v)}\,\Phi_T\right]^{1/2} = (0.8598 \times 10^{-12}\Phi_T)^{1/2}$$

$$= 0.927 \times 10^{-6}\sqrt{\Phi_T} \tag{1-29}$$

$$\sigma_{BR} = 0.927 \times 10^{-6}\sqrt{\Phi_R} \tag{1-30}$$

For the digital LST, the rms attitude errors are:

Displacement:

$$\sigma^*_{BD} = \left[\frac{1}{2\pi j}\oint M_D(z)M_D(z^{-1})z^{-1}dz \cdot \Phi_D\right]^{1/2} \tag{1-31}$$

Rate:

$$\sigma^*_{BR} = \left[\frac{1}{2\pi j}\oint M_R(z)M_R(z^{-1})z^{-1}dz \cdot \Phi_R\right]^{1/2} \tag{1-32}$$

Torque:

$$\sigma^*_{BT} = \left[\frac{1}{2\pi j}\oint M_T(z)M_T(z^{-1})z^{-1}dz \cdot \Phi_T\right]^{1/2} \tag{1-33}$$

The transfer functions, $M_D(z)$, $M_R(z)$, and $M_T(z)$ are determined from

Fig. 1-13.

$$M_D(z) = \frac{G_A(z)G_B(z)}{1 + G_A(z)G_B(z) + G_c(z)} \tag{1-34}$$

$$-M_R(z) = M_T(z) = \frac{G_B(z)}{1 + G_A(z)G_B(z) + G_c(z)} \tag{1-35}$$

where

$$G_B(z) = \frac{T^2(z + 1)}{2J_v(z - 1)^2} \tag{1-36}$$

$$G_c(z) = \frac{K_R T}{J_v(z - 1)} \tag{1-37}$$

and

$$G_A(z) = \frac{K_p z + K_I T - K_p}{z - 1} \qquad \text{(sample-and-hold and analog controller)} \tag{1-38}$$

$$G_A(z) = \frac{(2K_p + TK_I)z + TK_I - 2K_p}{2(z - 1)} \qquad \text{(digital implementation of controller)} \tag{1-39}$$

Substituting Eqs. (1-36) through (1-39) into Eqs. (1-34) and (1-35), we get the following transfer functions which are used for the computation of the rms attitute errors in Eqs. (1-31) through (1-33).

With zero-order hold and analog controller,

$$M_D(z) = \frac{T^2[K_p z^2 + K_I z + (K_I T - K_p)]}{\Delta_1} \tag{1-40}$$

$$-M_R(z) = M_T(z) = \frac{T^2(z^2 - 1)}{\Delta_1} \tag{1-41}$$

where

$$\Delta_1 = 2J_v z^3 + (-6J_v + 2K_R T + T^2 K_p)z^2 + (6J_v - 4K_R T + K_I T^3)z + (-2J_v + 2K_R T + K_I T^3 - K_p T^2) \tag{1-42}$$

With digitally implemented controller,

$$M_D(z) = \frac{T^2[(2K_p + TK_I)z^2 + 2TK_I z + TK_I - 2K_p}{\Delta_2} \tag{1-43}$$

$$-M_R(z) = M_T(z) = \frac{2T^2(z^2 - 1)}{\Delta_2} \tag{1-44}$$

where

$$\Delta_2 = 4J_v z^3 + (-12J_v + 2T^2 K_p + T^3 K_I + 4K_R T)z^2 + (12J_v + 2T^3 K_I - 8K_R T)z + (4K_R T + T^3 K_I - 2T^2 K_p - 4J_v) \tag{1-45}$$

A tabulation method or a numerical method [3] can be used to evaluate the contour integrals of Eqs. (1-31), (1-32), and (1-33), once the values of the parameters of the transfer functions are known. Table 1-2 gives the values of $(\phi_{B\,rms})^*_D$, $(\phi_{B\,rms})^*_T$ and $(\phi_{B\,rms})^*_R$ for various values of the sampling period T.

Table 1-2.

T (msec)	Sample-and-Hold with Analog Controller		Digitally Implemented Controller	
	$\frac{\sigma^*_{BD}}{\sqrt{\Phi_D}}$	$\frac{\sigma^*_{BT}}{\sqrt{\Phi_T}}$	$\frac{\sigma^*_{BD}}{\sqrt{\Phi_D}}$	$\frac{\sigma^*_{BT}}{\sqrt{\Phi_T}}$
0.01	0.0052	2.932×10^{-9}	0.0052	2.932×10^{-9}
0.1	0.0161	9.274×10^{-9}	0.0161	9.274×10^{-9}
1.0	0.0508	2.936×10^{-8}	0.0508	2.936×10^{-8}
5.0	0.1140	6.599×10^{-8}	0.1141	6.595×10^{-8}
10	0.1621	9.394×10^{-8}	0.1622	9.383×10^{-8}
25	0.2602	1.515×10^{-7}	0.2607	1.511×10^{-7}
50	0.3777	2.216×10^{-7}	0.3796	2.205×10^{-7}
100	0.5652	3.368×10^{-7}	0.5720	3.339×10^{-7}

The results tabulated in Table 1-2 show that the rms errors of the LST with sample-and-hold and the analog controller are very close to those of the LST with the controller implemented digitally.

It is interesting to show that the rms attitude errors of the digital LST due to quantization are related to those of the continuous-data system in Fig. 1-12.

Applying the limit as T approaches zero to Eq. (1-31), we get

$$\lim_{T\to 0} \sigma^*_{BD} = \lim_{T\to 0} \left\{ \frac{1}{2\pi j} \oint M_D(z) M_D(z^{-1}) z^{-1} dz \Phi_D \right\}^{1/2} \tag{1-46}$$

Since

$$\lim_{T\to 0} M_D(z) = M_D(s) \tag{1-47}$$

where $M_D(s)$ is given in Eq. (1-23), and $M_D(z)$ is given by either Eq. (1-40) or (1-43), depending on the way the controller is implemented, and

$$z^{-1}dz = T\,ds \tag{1-48}$$

Eq. (1-46) is written

$$\lim_{T\to 0} \sigma^*_{BD} = \left\{\frac{T}{2\pi j}\int_{-j\infty}^{j\infty} M_D(s)M_D(-s)ds\Phi_D\right\}^{1/2} = \sqrt{T}\,\sigma_{BD} \tag{1-49}$$

or

$$\sigma_{BD} = \frac{1}{\sqrt{T}} \lim_{T\to 0} \sigma^*_{BD} \tag{1-50}$$

The meaning of this relation is that the mean-square value of the attitude error of the continuous-data system is equal to 1/T times the attitude error of the digital system as T approaches zero. Table 1-3 gives the values of $\sigma^*_{BD}/\sqrt{T\Phi_D}$ and $\sigma^*_{BT}/\sqrt{T\Phi_T}$ for various values of T. These values are very close to the values of $\sigma_{BD} = 1.605$ and $\sigma_{BT} = 0.926 \times 10^{-6}$, respectively, especially at very small sampling periods.

These relations show that, in general, for small sampling periods, the attitude error due to a white noise input in a digital system will be less than that of the same system without sampling. For example, for T = 25 msec, the rms attitude error σ^*_{BD} is $0.2602\sqrt{\Phi_D}$, whereas σ_{BD} is $1.605\sqrt{\Phi_D}$. Therefore, the use of the continuous-data LST model of Fig. 1-12, as in [1], for the error analysis of the digital LST results in conservative results.

Table 1-3.

T (msec)	$\frac{\sigma^*_{BD}}{\sqrt{T\Phi_D}}$	$\frac{\sigma^*_{BT}}{\sqrt{T\Phi_T}}$
0.01	1.644	0.927×10^{-6}
0.1	1.610	0.927×10^{-6}
1.0	1.606	0.928×10^{-6}
5.0	1.612	0.933×10^{-6}
10	1.621	0.939×10^{-6}
25	1.645	0.958×10^{-6}
50	1.689	0.991×10^{-6}
100	1.787	1.065×10^{-6}

The results in Tables 1-2 and 1-3 again show that for the same quantization levels, the quantizer in the displacement channel produces far greater attitude errors than those due to the quantizers in the rate and torque channels.

1-6. Effects of Quantization on Pointing Stability of the Digital Low-Cost LST - Quasilinear Analysis, Statistical

In this section the effects of quantization on the low-cost LST are studied by means of a quasilinearized equivalent-gain approach [4], [5]. Although the analysis is conducted in the statistical sense, there is a basic difference between the present analysis and the one conducted in Section 1-5. In the previous section, the rms attitude error of the LST is evaluated by treating the quantizers as noise sources that are stationary Gaussian processes with zero means. In this section, the quantizer will be treated as a nonlinear element whose input is a random stochastic process. An equivalent gain, $K_{eq}(z)$, is derived for the quantizer. The attitude of the LST is then determined with the quantizer replaced by $K_{eq}(z)$, and when the system is subject to a stochastic input. The only restriction with this method is that only one quantizer can be considered at a time. Since it has been established that the attitude of the LST is more sensitive to the quantizer Q_D, we shall consider only the system model shown in Fig. 1-14.

The quantizer Q_D is isolated as shown by the block diagram in Fig. 1-15a; the input is x(t) and the output is y(t). Figure 1-15b shows the equivalent gain representation of Q_D. The equivalent gain of Q_D is defined as

$$K_{eq}(z) = \frac{\Phi_{xy}(z)}{\Phi_{xx}(z)} \tag{1-51}$$

where $\Phi_{xx}(z)$ denotes the z-transform of the autocorrelation function of x(t), and $\Phi_{xy}(z)$ is the z-transform of the crosscorrelation function of

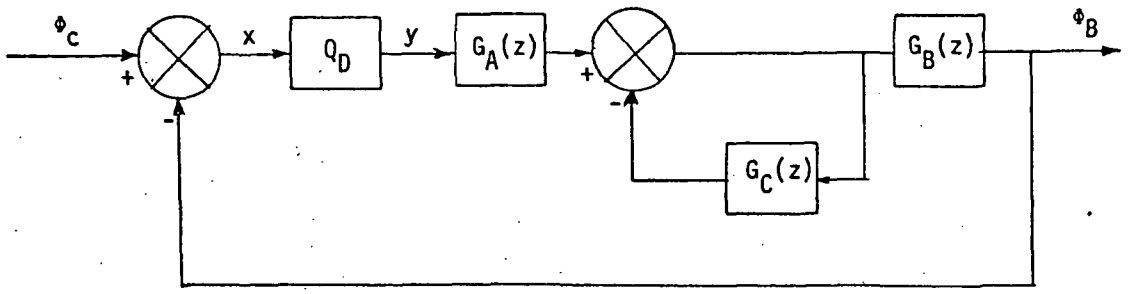

Figure 1-14. Digital LST with quantizer in the displacement channel.

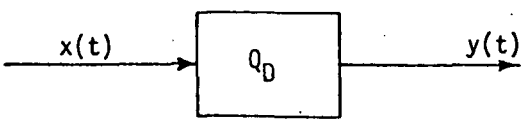

(a)

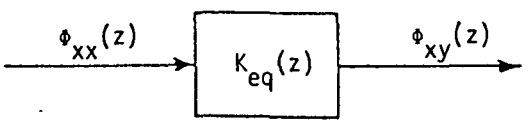

(b)

Figure 1-15. The representation of the quantizer with statistical input and output as an equivalent gain.

$x(t)$ and $y(t)$. In order to derive $K_{eq}(z)$, we consider that the input to Q_D is a stationary Gaussian process with zero mean so that the probability function is

$$p(x) = \frac{\exp(-x^2/2\sigma_x^2)}{\sqrt{2\pi}\,\sigma_x} \tag{1-52}$$

where σ_x is the standard deviation of $x(t)$.

The crosscorrelation function of $x(t)$ and $y(t)$ is given by

$$\Phi_{xy}(\tau) = \int_{-\infty}^{\infty} Q_D(\lambda)p(\lambda)\rho\lambda d\lambda \tag{1-53}$$

where

$$Q_D[x(t)] = y(t) \tag{1-54}$$

is the mathematical description of the quantizer, and

$$\rho = \frac{\Phi_{xx}(\tau)}{\sigma_x^2} \tag{1-55}$$

Thus,

$$\Phi_{xy}(\tau) = \frac{1}{\sigma_x^2}\,\Phi_{xx}(\tau) \int_{-\infty}^{\infty} Q_D(\lambda)p(\lambda)\lambda d\lambda \tag{1-56}$$

Taking the z-transform on both sides of Eq. (1-56) and rearranging, we have

$$K_{eq}(z) = \frac{\Phi_{xy}(z)}{\Phi_{xx}(z)} = \frac{1}{\sigma_x^2} \int_{-\infty}^{\infty} Q_D(\lambda)p(\lambda)\lambda d\lambda \tag{1-57}$$

Although the equivalent gain $K_{eq}(z)$ is indicated as a function of z, the nature of the right-hand side of Eq. (1-57) implies that it is always a constant. It is apparent that although our interest is centered on the quantizer nonlinearity, in general, the definition of $K_{eq}(z)$ can be applied to any comman nonlinearities found in control systems.

With reference to the quantizer characteristics of Fig. 1-7,

$$y(t) = 0 \qquad -h/2 < x < h/2$$

$$y(t) = -h \qquad -3h/2 < x \leq -h/2$$

$$y(t) = h \qquad h/2 \leq x < 3h/2$$

$$\vdots$$

$$y(t) = -(N-1)h \qquad -\frac{2(N-1)h}{2} < x \leq -\frac{(2N-3)h}{2}$$

$$y(t) = (N-1)h \qquad \frac{2(N-3)h}{2} \leq x < \frac{(2N-1)h}{2}$$

$$y(t) = -Nh \qquad -\infty < x \leq -\frac{(2N-1)h}{2}$$

$$y(t) = Nh \qquad \frac{2(N-1)h}{2} \leq x < \infty$$

where N is a positive integer.

Equation (1-57) gives

$$\begin{aligned} K_{eq}(z) = \frac{1}{\sigma_x^2}\Bigg[& \int_{-\infty}^{-(2N-1)h/2} (-Nh)p(\lambda)\lambda d\lambda \\ & + \int_{-(2N-1)h/2}^{-(2N-3)h/2} -(N-1)hp(\lambda)\lambda d\lambda + \cdots + \int_{-3h/2}^{-h/2} -hp(\lambda)\lambda d\lambda \\ & + \int_{h/2}^{3h/2} hp(\lambda)\lambda d\lambda + \cdots + \int_{(2N-3)h/2}^{(2N-1)h/2} (N-1)hp(\lambda)\lambda d\lambda \\ & + \int_{(2N-1)h/2}^{\infty} Nhp(\lambda)\lambda d\lambda \Bigg] \end{aligned} \tag{1-58}$$

Or,

$$K_{eq}(z) = \frac{1}{\sigma_x^2}\left[2h\int_{h/2}^{3h/2} p(\lambda)\lambda d\lambda + \cdots + 2(N-1)h\int_{(2N-3)h/2}^{(2N-1)h/2} p(\lambda)\lambda d\lambda + 2Nh\int_{(2N-1)h/2}^{\infty} p(\lambda)\lambda d\lambda\right] \tag{1-59}$$

Since all the integrals in the last equation have the same integrand, we evaluate one of the integrals as follows:

$$\int_{h/2}^{3h/2} p(\lambda)\lambda d\lambda = \int_{h/2}^{3h/2} \frac{\exp(-\lambda^2/2\sigma_x^2)}{\sqrt{2\pi}\,\sigma_x}\lambda d\lambda \tag{1-60}$$

Let

$$u = \lambda^2/2\sigma_x^2$$

Then

$$du = \frac{\lambda d\lambda}{\sigma_x^2} \qquad \text{or} \qquad \lambda d\lambda = \sigma_x^2 du$$

and

$$\int_{h/2}^{3h/2} p(\lambda)\lambda d\lambda = \frac{1}{\sqrt{2\pi}}\int_{h^2/8\sigma_x^2}^{9h^2/8\sigma_x^2} \exp(-u)\sigma_x du$$

$$= \frac{1}{\sqrt{2\pi}}\sigma_x\left[\exp\left(-\frac{9h^2}{8\sigma_x^2}\right) + \exp\left(-\frac{h^2}{8\sigma_x^2}\right)\right] \tag{1-61}$$

Thus, the equivalent gain for the quantizer with 2N levels of quantization is

$$K_{eq}(z) = \sqrt{\frac{2}{\pi}}\frac{h}{\sigma_x}\left[\exp\left(-\frac{h^2}{8\sigma_x^2}\right) + \exp\left(-\frac{9h^2}{8\sigma_x^2}\right) + \exp\left(-\frac{25h^2}{8\sigma_x^2}\right) + \cdots + \exp\left(-\frac{(2N-1)^2h^2}{8\sigma_x^2}\right)\right] \tag{1-62}$$

Although the equivalent gain has been derived from Q_D, the response of the closed-loop system of Fig. 1-14 cannot be determined by using $K_{eq}(z)$ directly, since σ_x, the standard deviation, of x(t) is not known. The analysis procedure is outlined as follows:

For a given σ_c, which is the rms value of the input,

(1) The equivalent gain $K_{eq}(z)$ is computed using Eq. (1-62) for various values of σ_x.

(2) The values of σ_x that correspond to the various values of $K_{eq}(z)$ obtained in step (1) are calculated from

$$\sigma_x = \left[\frac{1}{2\pi j}\oint M_x(z)M_x(z^{-1})\Phi_{cc}(z)z^{-1}dz\right]^{1/2} \tag{1-63}$$

where

$$M_x(z) = \frac{1}{1 + K_{eq}(z)G_A(z)G_B(z) + G_c(z)} \tag{1-64}$$

and

$$\Phi_{cc}(z) = \sigma_c^2$$

It is assumed that the input of the system is a white noise. The solution of σ_x for the given σ_c is determined when there is a match between σ_x from Eq. (1-63) and that used in step (1).

(3) The rms attitude response of the system is determined from

$$\sigma_B = \left\{\frac{1}{2\pi j}\oint M(z)M(z^{-1})\Phi_{cc}(z)z^{-1}dz\right\}^{1/2} \tag{1-65}$$

using the $K_{eq}(z)$ which corresponds to the σ_x obtained in step (2).

For the LST system, a quantization level of h = 0.003 is selected for Q_D. The quantizer is assumed to saturate after 5000 increments; that is, N = 5000 in Eq. (1-62). A digital computer program is prepared which automatically cuts off the series of Eq. (1-62) when an additional term is contributing less than 10^{-6} to the entire result. The sampling period T is chosen to be 25 msec, and the system transfer functions $G_A(z)$, $G_B(z)$, and $G_c(z)$ are given by Eqs. (1-38), (1-36), and (1-37), respectively. Following the procedure outlined above, the results of the analysis with several values of σ_c are tabulated in Table 1-4.

The results in Table 1-4 show that for a given set of quantization and saturation levels, both small and large input signals cause the quantizer to act as an attenuator. The true characteristics of the system as a function of the input σ_c are displayed by normalizing σ_B. The last column in Table 1-4 represents the normalized output σ_{BN}, which is defined as

$$\sigma_{BN} = \frac{\sigma_B}{\sigma_{B1}\sigma_c} \tag{1-66}$$

where

$$\sigma_{B1} = \sigma_B \quad \text{at} \quad \sigma_c = 1 \quad . \tag{1-67}$$

Table 1-4.

Input σ_c	σ_x	K_{eq}	No. of terms used in $K_{eq}(z)$	Output σ_B	Normalized output σ_{BN}
5×10^{-4}	5.318×10^{-4}	0.075	2	5.20×10^{-5}	0.4
10^{-3}	1.086×10^{-3}	0.797	3	2.40×10^{-4}	0.92
10^{-2}	1.093×10^{-2}	1.0	19	2.68×10^{-3}	1.0
10^{-1}	1.093×10^{-1}	1.0	176	2.60×10^{-2}	1.0
1	1.093	1.0	1753	2.60×10^{-1}	1.0
10	10.87	0.836	5000	2.383	0.916
50	53.37	0.22	5000	6.88	0.529

Figure 1-16 shows the plot of $K_{eq}(z)$ versus σ_x. The plot has the significance of a "statistical describing function" of the quantizer. This plot shows that for small inputs, when the input magnitude is comparable to the quantization level, h, the gain drops below unity, and the quantizer is attenuating the signal. For larger inputs the quantizer appears as a unity-gain element in a statistical sense, and for very large inputs, where the input magnitude is comparable to maximum output (N levels of h), the quantizer gain again reduces, and the input is attenuated.

Figure 1-17 gives a plot of σ_x versus σ_c which represents the solution of Eq. (1-63) and step (1) for the range of σ_c considered.

Figure 1-18 shows a plot of σ_{BN} versus σ_c. It is seen that the normalized output reduces from unity in the ranges of σ_c when $K_{eq}(z)$ is less than 1.

As an interesting comparison, the statistical method of Section 1-5 assumes $K_{eq}(z) = 1$ for all values of σ_c and, consequently, it always yields

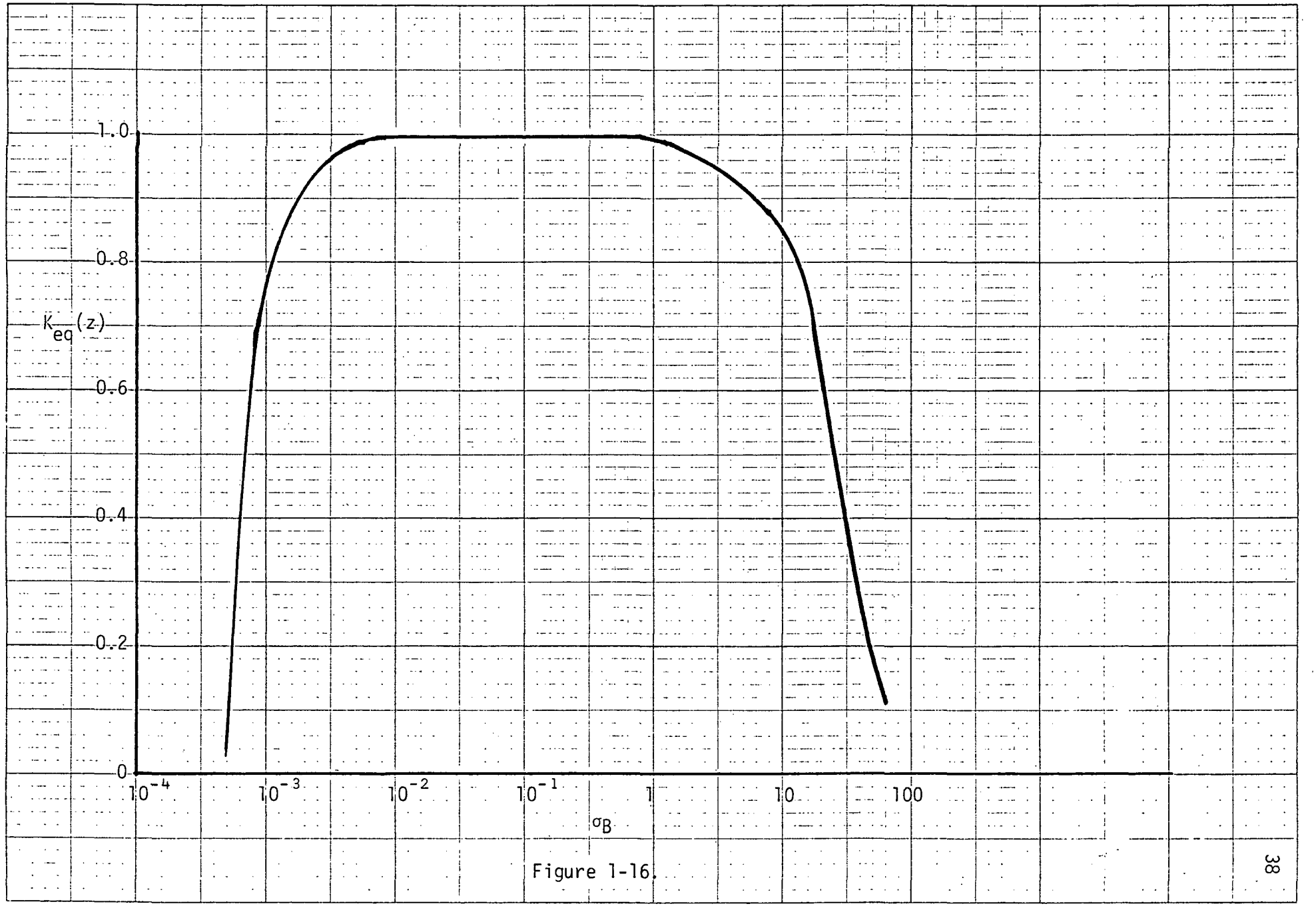

Figure 1-16

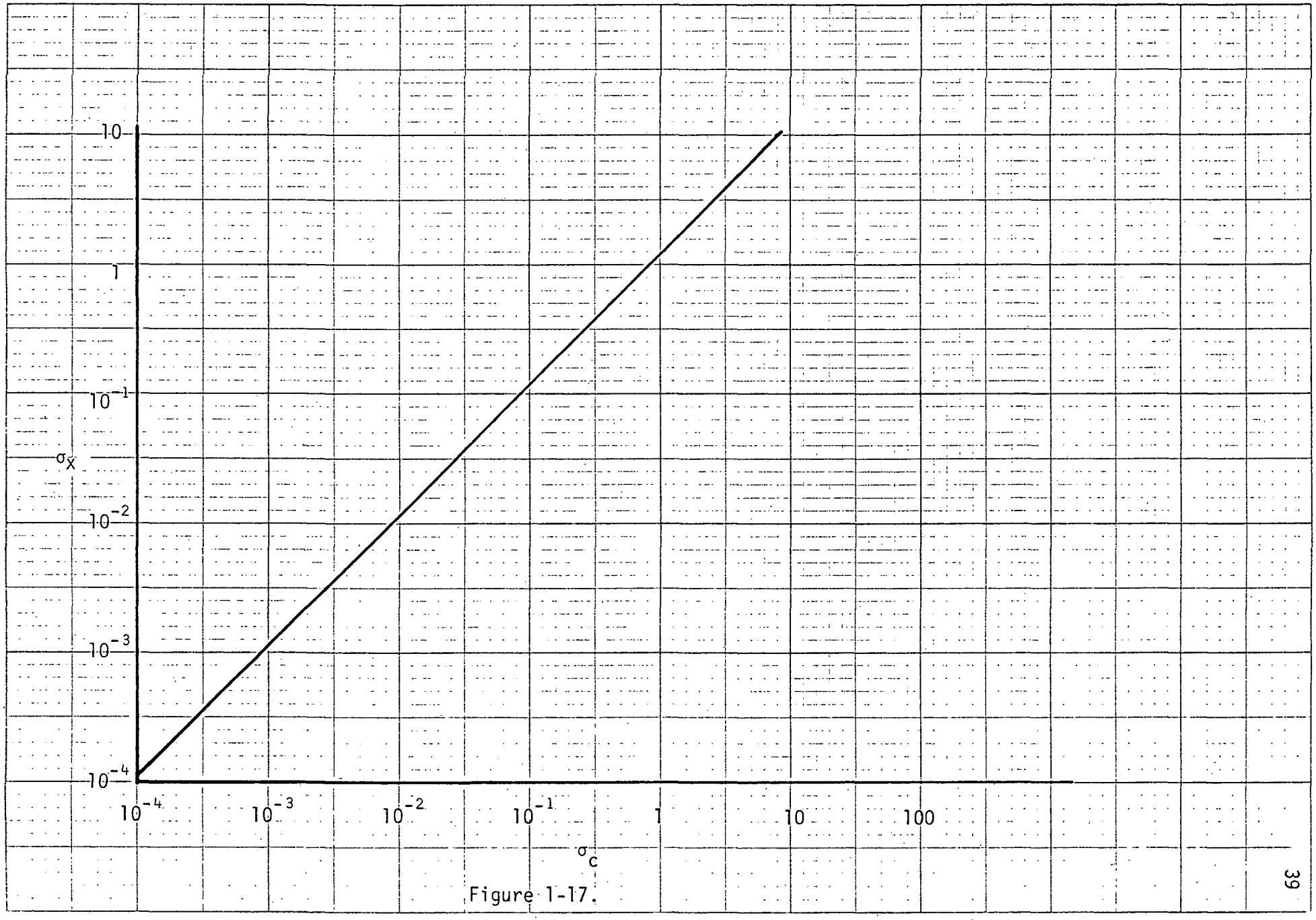

Figure 1-17.


1.0
0.8
σ_{BN}
0.6
0.4
0.2
0
10^{-4}
10^{-3}
10^{-2}
10^{-1}
1
10
100
0.033h
0.33h
3.33h
33.3h
333h
3333h
33333h
σ_c

Figure 1-18.

a result of $\sigma_{BN} = 1$. In this sense that method is more conservative and does not recognize the severity of the nonlinearity due to the quantizer at very small and very large input magnitudes.

2. Stability of the Analog Low-Cost Large Space Telescope Due to Quantization

2-1. Introduction

The objective of this chapter is to conduct an investigation on the pointing stability of the low-cost Large Space Telescope (LST) System under the influence of quantization at various locations of the system. Only the analog model of the LST system is considered in this chapter. The stability of the digital LST system with quantization is considered in Chapters 5 and 6.

The block diagram of the simplified analog LST system with quantizers is shown in Fig. 2-1.

The describing function method is used to determine the condition of self-sustained oscillation in the LST system due to the effect of each of the three quantizers acting alone. The present analysis considers only one quantizer at a time.

Let the analog describing functions of the quantizers Q_D, Q_T, and Q_R be represented by N_D, N_T, and N_R, respectively. In general, the describing function of a quantizer nonlinearity is a function of the input amplitude, E; quantization level, h; and the number of quantization levels, n, which depends on E.

For the LST system shown in Fig. 2-1, the "characteristic equations" of the system when each one of the quantizers is acting, are given as follows:

Displacement Quantizer Q_D:

$$J_v s^3 + N_D(K_p s + K_I) + K_R s^2 = 0 \tag{2-1}$$

Torque Quantizer Q_T:

$$J_v s^3 + N_T(K_R s^2 + K_p s + K_I) = 0 \tag{2-2}$$

Rate Quantizer Q_R:

$$J_v s^3 + K_p s + K_I + N_R K_R s^2 = 0 \tag{2-3}$$

These equations can be conditioned by dividing both sides of the equations by the terms that do not contain the describing function, so that the stability equation is expressed in the form of

$$1 + NG(s) = 0 \tag{2-4}$$

where N is the describing function, and G(s) is a linear transfer function. The condition of self-sustained oscillations is found by investigating the possible intersections between the trajectories of -1/N and G(s) in the complex plane.

For the equations given in Eqs. (2-1), (2-2) and (2-3), the equivalent transfer functions are

$$G_D(s) = \frac{K_p s + K_I}{s^2(J_v s + K_R)} \tag{2-5}$$

$$G_T(s) = \frac{K_R s^2 + K_p s + K_I}{J_v s^3} \tag{2-6}$$

$$G_R(s) = \frac{K_R s^2}{J_v s^3 + K_p s + K_I} \tag{2-7}$$

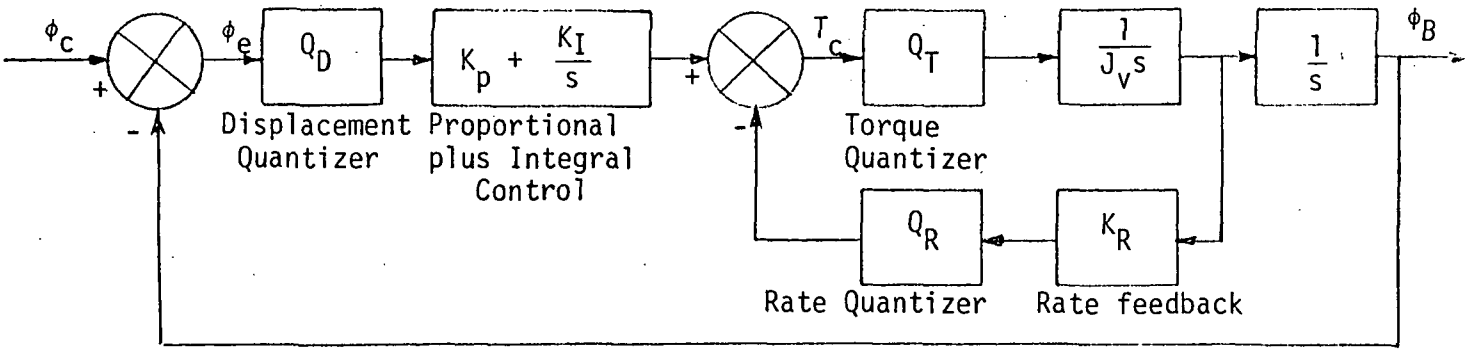

Figure 2-1. Simplified analog LST system with quantization.

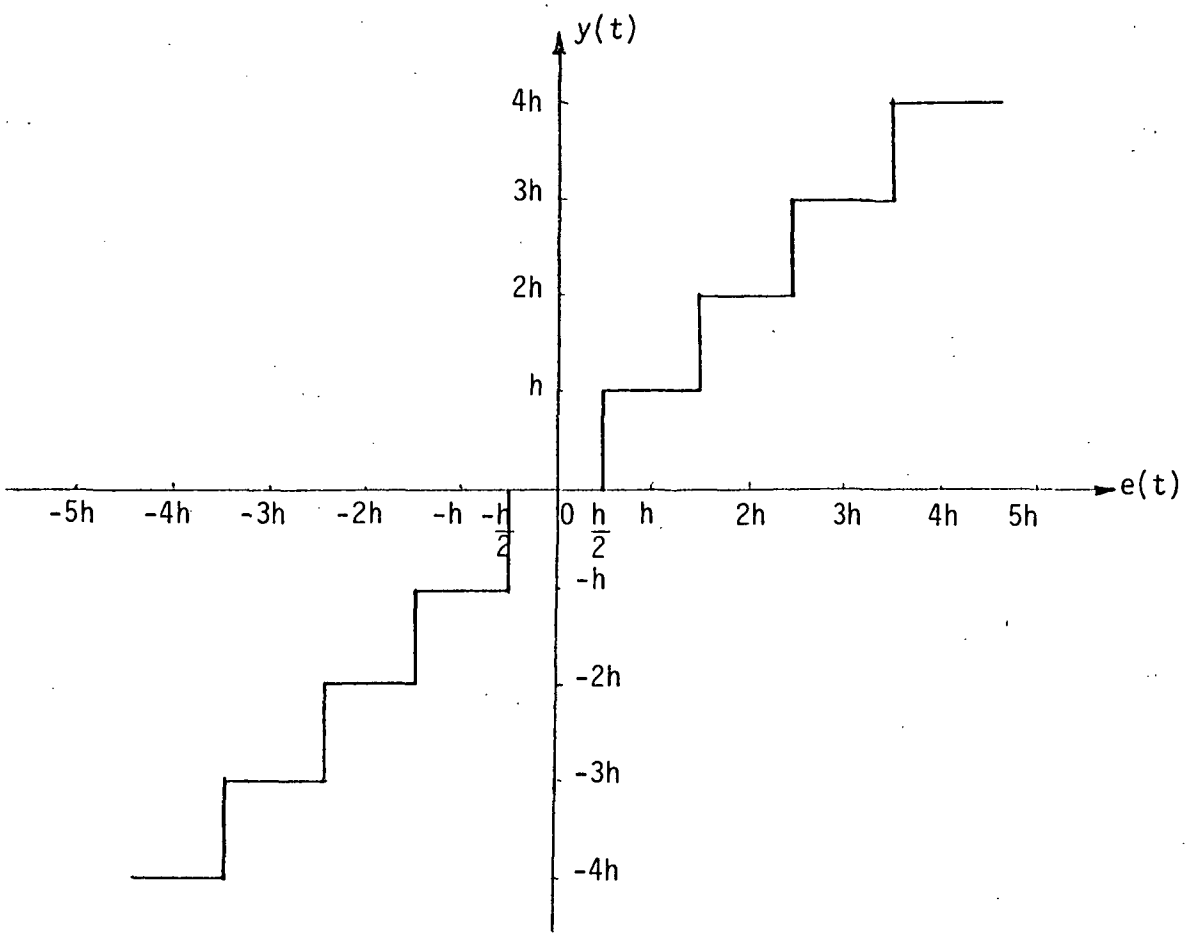

Figure 2-2. Input-output relation of a quantizer.

2-2. Analog Describing Function of the Quantizer Nonlinearity

Consider that a quantizer has the input-output relation as shown in Fig. 2-2. Let the input to the quantizer be a sine wave,

$$e(t) = E \sin \omega t \tag{2-8}$$

The quantization level is h, and let the magnitude of E be such that

$$\frac{(2n - 1)h}{2} \leq E < \frac{(2n + 1)h}{2} \tag{2-9}$$

where n is a positive integer. A typical output of the quantizer is shown in Fig. 2-3.

The fundamental component of the Fourier series expansion of y(t) is

$$y_1(t) = Y_1 \sin \omega t \tag{2-10}$$

where

$$Y_1 = \frac{4}{\pi} \int_{\alpha_1}^{\pi/2} y(t) \sin \omega t \, d\omega t \tag{2-11}$$

Evaluating the last integral, we have

$$\begin{aligned} Y_1 &= \frac{4}{\pi} \int_{\alpha_1}^{\alpha_n} y(t) \sin \omega t \, d\omega t + \frac{4}{\pi} \int_{\alpha_n}^{\pi/2} nh \sin \omega t \, d\omega t \\ &= \frac{4}{\pi} \sum_{i=1}^{n-1} \int_{\alpha_i}^{\alpha_{i+1}} ih \sin \omega t \, d\omega t + \frac{4}{\pi} \int_{\alpha_n}^{\pi/2} nh \sin \omega t \, d\omega t \end{aligned} \tag{2-12}$$

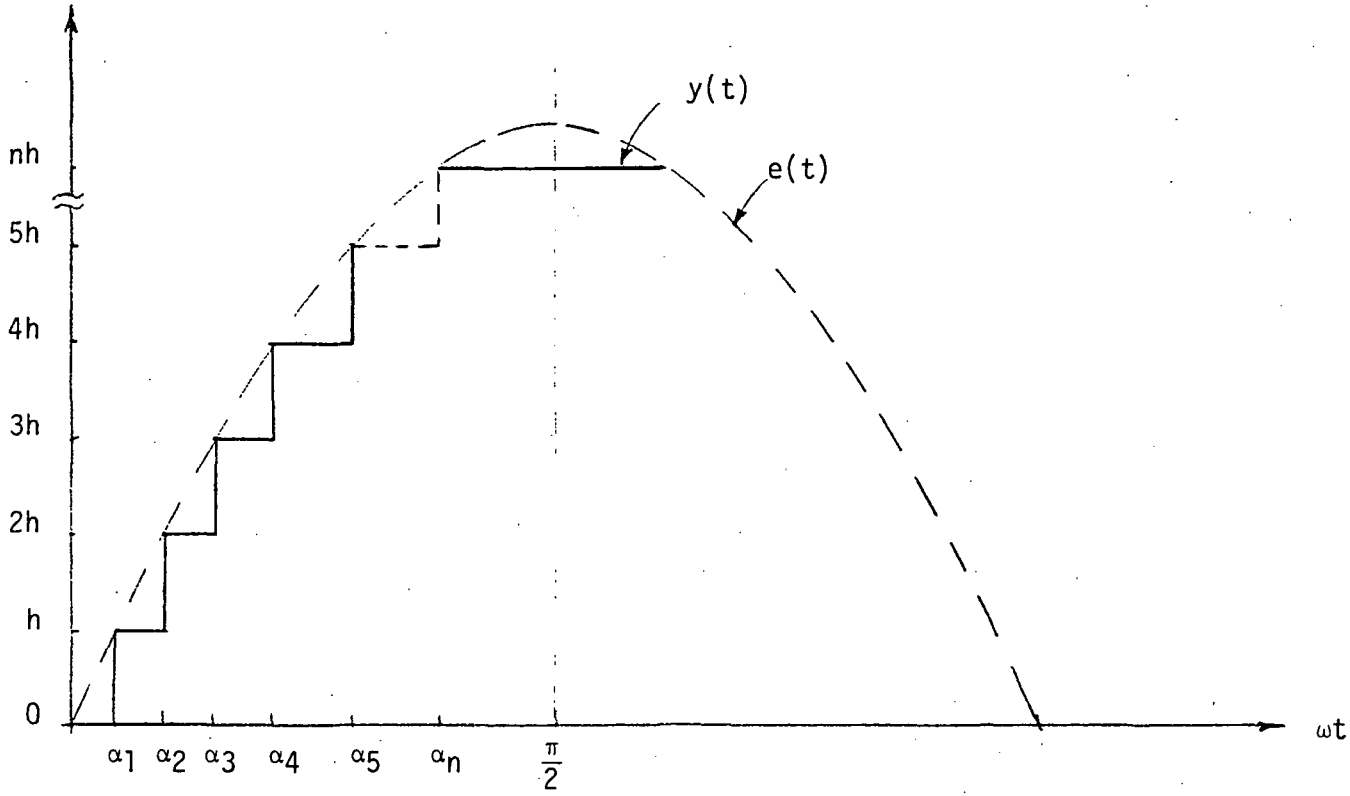

Figure 2-3. Output of a quantizer corresponding to a sinusoidal input.

Then,

$$Y_1 = -\frac{4h}{\pi}\sum_{i=1}^{n-1} i[\cos\alpha_{i+1} - \cos\alpha_i] + \frac{4nh}{\pi}\cos\alpha_n \tag{2-13}$$

Since

$$\sin\alpha_1 = \frac{h}{2E} \tag{2-14}$$

$$\sin\alpha_i = \frac{(2i-1)h}{2E} \tag{2-15}$$

$$\cos\alpha_1 = \sqrt{1 - \left(\frac{h}{2E}\right)^2} \tag{2-16}$$

$$\cos\alpha_i = \sqrt{1 - \left[\frac{(2i-1)h}{2E}\right]^2} \tag{2-17}$$

Expanding the right-hand side of Eq. (2-13), we can show that

$$Y_1 = \frac{4h}{\pi}\sum_{i=1}^{n}\cos\alpha_i \tag{2-18}$$

Substituting Eq. (2-17) into Eq. (2-18), we have

$$Y_1 = \frac{4h}{\pi}\sum_{i=1}^{n}\left\{1 - \left[\frac{(2i-1)h}{2E}\right]^2\right\}^{1/2} \tag{2-19}$$

The describing function of the quantizer is written as

$$N(E/h) = \frac{Y_1}{E} = \frac{4h}{\pi E}\sum_{i=1}^{n}\left\{1 - \left[\frac{(2i-1)h}{2E}\right]^2\right\}^{1/2} \tag{2-20}$$

Figure 2-4 shows the plot of N(E/h) as a function of E/h. We shall show in the following that

$$\lim_{\frac{E}{h}\to\infty} N(E/h) = 1 \tag{2-21}$$

Letting $\chi = E/h$, Eq. (2-20) is written

$$N(\chi) = \frac{4}{\pi\chi} \sum_{i=1}^{n} \left\{1 - \left[\frac{2i - 1}{2\chi}\right]^2\right\}^{1/2} \tag{2-22}$$

Expanding the quantity inside the summation sign in the last equation, we have

$$N(\chi) = \frac{4}{\pi\chi} \sum_{i=1}^{n} \left\{1 - \frac{1}{2}\left[\frac{i}{\chi} - \frac{1}{2\chi}\right]^2 - \frac{1}{8}\left[\frac{i}{\chi} - \frac{1}{2\chi}\right]^4 - \frac{3}{48}\left[\frac{i}{\chi} - \frac{1}{2\chi}\right]^6 - \frac{15}{384}\left[\frac{i}{\chi} - \frac{1}{2\chi}\right]^8 - \cdots\right\} \tag{2-23}$$

Or

$$N(\chi) = \frac{4}{\pi\chi} \sum_{i=1}^{n} \left\{1 - \frac{1}{2\chi^2}\left[i - \frac{1}{2}\right]^2 - \frac{1}{8\chi^4}\left[i - \frac{1}{2}\right]^4 - \frac{3}{48\chi^6}\left[i - \frac{1}{2}\right]^6 - \frac{15}{384\chi^8}\left[i - \frac{1}{2}\right]^8 - \cdots\right\} \tag{2-24}$$

Taking limit as χ approaches infinity and n approaches infinity, in the last equation, we get

$$\lim_{\substack{X\to\infty \\ n\to\infty}} N(X) = \lim_{\substack{X\to\infty \\ n\to\infty}} \frac{4}{\pi X} \sum_{i=1}^{n} \left(1 - \frac{i^2}{2X^2} - \frac{i^4}{8X^4} - \frac{3i^6}{48X^6} - \frac{15i^8}{384X^8} - \cdots\right)$$

$$= \lim_{\substack{X\to\infty \\ n\to\infty}} \frac{4}{\pi X} \left(n - \frac{1}{2X^2}\frac{n^3}{3} - \frac{1}{8X^4}\frac{n^5}{5} - \frac{3}{48X^6}\frac{n^7}{7} - \frac{15}{384X^8}\frac{n^9}{9} - \cdots\right)$$

$$= \frac{4}{\pi}\left(1 - \frac{1}{2}\cdot\frac{1}{3} - \frac{1}{8}\cdot\frac{1}{5} - \frac{3}{48}\cdot\frac{1}{7} - \frac{15}{384}\cdot\frac{1}{9} - \cdots\right)$$

$$= \frac{4}{\pi}\int_0^1 \sqrt{1 - X^2}\, dX$$

$$= \frac{4}{\pi}\left(X\sqrt{1 - X^2} + \frac{1}{2}\sin^{-1}X\right)_0^1$$

$$= 1 \qquad (2\text{-}25)$$

Since the describing function of the quantizer nonlinearity is always a real number, the function -1/N(E/h) in the magnitude (db) versus phase coordinates will lie on the -180-degree axis for all values of E/h. The plot in Fig. 2-4 shows that the magnitude of -1/N(E/h) is infinite for $0 \leq E/h < 0.5$. For $0.5 \leq E/h \leq 0.707$, the plot of -1/N(E/h) extends from infinity to -2.09 db along the -180-degree axis. Over the range of $0.707 \leq E/h \leq 1.5$, -1/N(E/h) extends from -2.09 db to 1.9 db along the -180-degree axis, etc. As E/h approaches infinity, the plot of -1/N(E/h) is reduced to the zero-db point. Figure 2-5 shows the plot of N(E/h) in magnitude versus E/h and shows the multivalued property of the function.

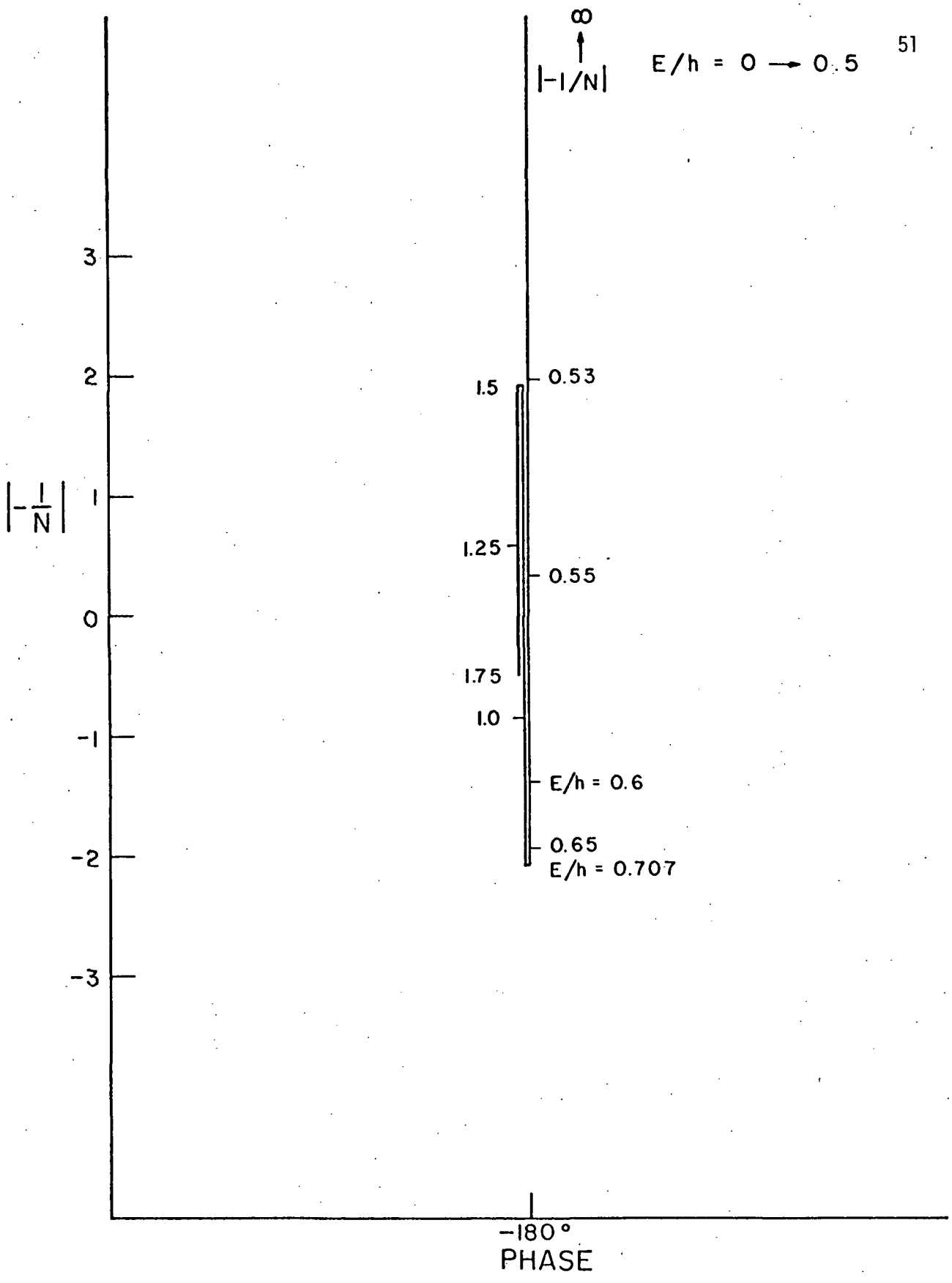

Figure 2-4. Analog describing function for the quantizer nonlinearity.

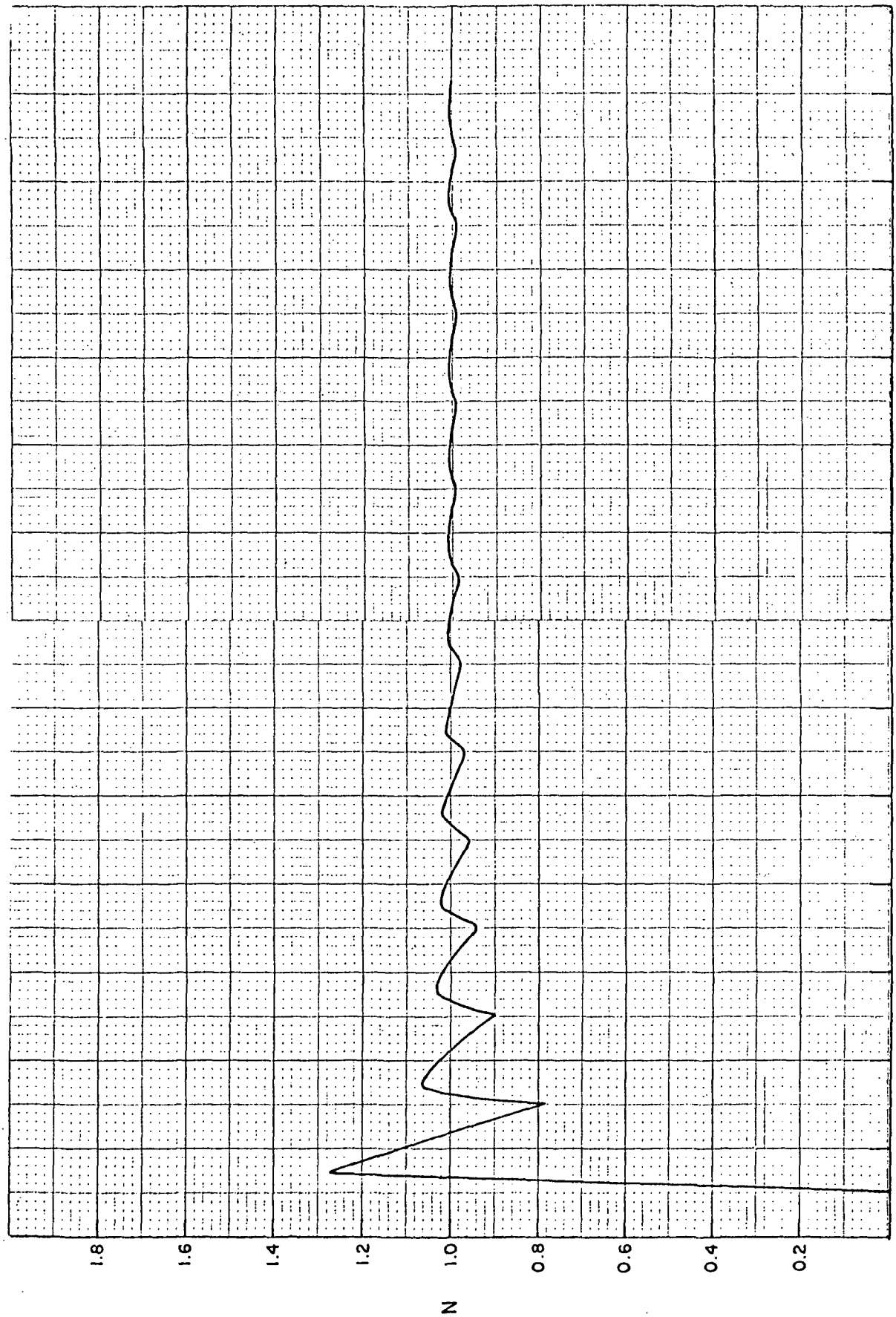

Figure 2-5. Describing function plot for the quantizer nonlinearity.

2-3. Self-Sustained Oscillations of the Analog LST System with Quantization

The transfer functions of the three quantizers, Q_D, Q_T, and Q_R, given by Eqs. (2-5), (2-6), and (2-7), are plotted in Fig. 2-6, together with the -1/N(E/h) trajectory. The following system parameters are used:

$K_p = 1.65 \times 10^6$ $\qquad$ $K_R = 3.71 \times 10^5$

$K_I = 7.33 \times 10^5$ $\qquad$ $J_v = 41822$

Figure 2-6 shows that since the plot of $G_D(s)$ does not intersect the -1/N(E/h) trajectory in the finite domain, the quantizer Q_D will not cause any self-sustained oscillations in the LST system.

Both the curves for $G_T(s)$ and $G_R(s)$ intersect the -180-degree axis and the -1/N(E/h) trajectory at 25 db.

Thus,

$$20 \log_{10}|1/N(E/h)| = 25 \text{ db} \tag{2-26}$$

which gives

$$N(E/h) = 0.05012 \tag{2-27}$$

Figure 2-4 shows that for this value of N(E/h),

$$\frac{E}{h} \cong 0.5 \tag{2-28}$$

or

$$E \cong 0.5\ h \tag{2-29}$$

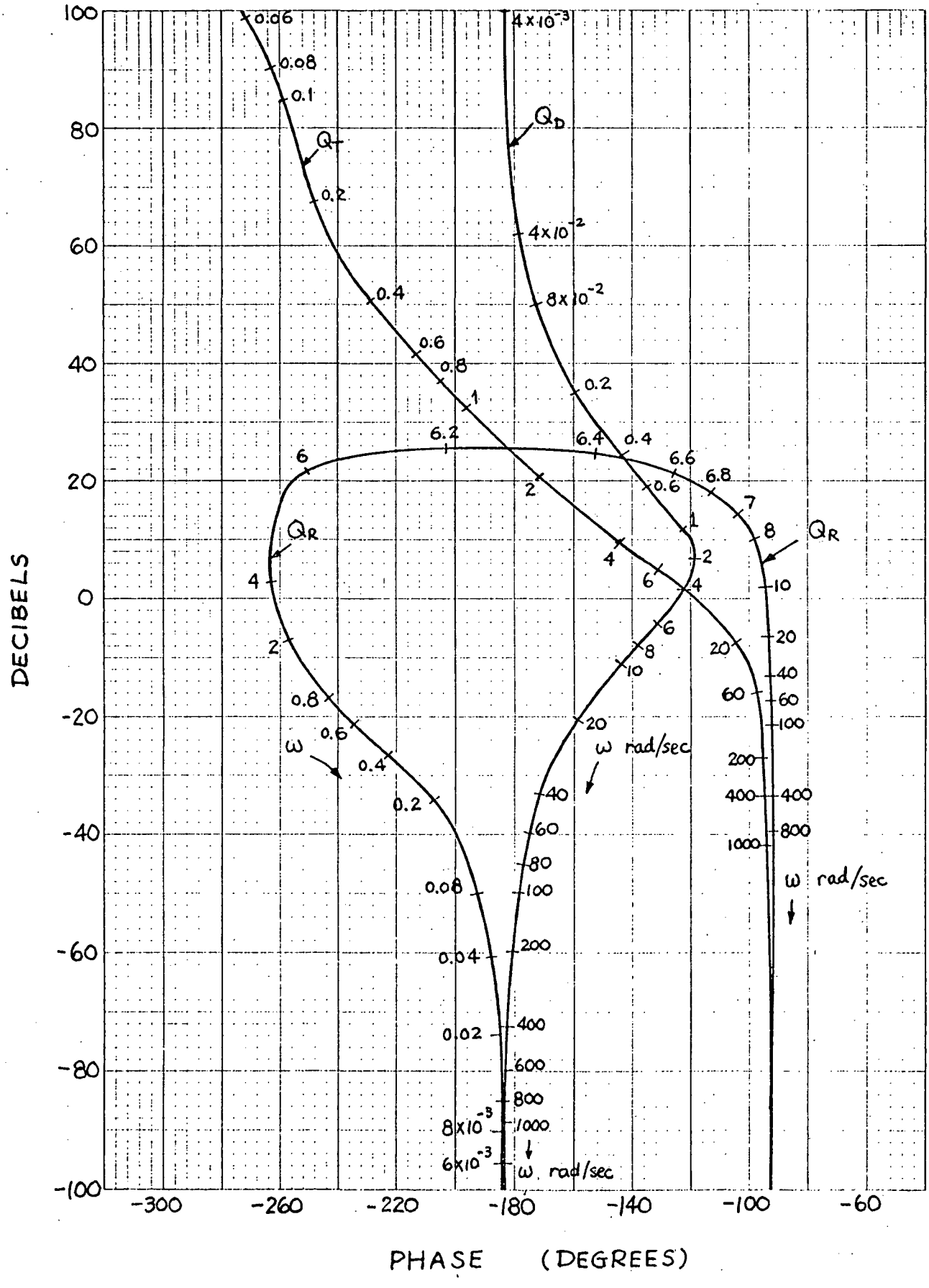

Figure 2-6. G(s) plots for the analog low-cost LST system with various quantizers.

This means that the quantizers Q_T and Q_R each independently may cause self-sustained oscillations to occur in the LST system. Furthermore, the self-sustained oscillations will have an amplitude equal to one-half the level of quantization h. Another point of interest is that the intersect between $G_T(s)$, $G_R(s)$, and $-1/N(E/h)$ corresponds to $n = 1$, so that the quantizers Q_T and Q_R are essentially acting as a simple relay with dead zone.

Figure 2-6 shows that the frequency of the oscillations caused by Q_T is 1.5 rad/sec, and that caused by Q_R is 6.3 rad/sec.

It is interesting to point out that the analysis in Chapter 1 shows that the displacement quantizer Q_D produces far greater quantization error than the torque and rate quantizers. However, the describing function analysis shows that Q_D does not cause self-sustained oscillations, whereas Q_T and Q_R may excite oscillations with amplitudes equal to one-half the level of quantization, h/2. All these factors must be taken into consideration when selecting the quantization level.

3. Stability of the Analog Low-Cost Large Space Telescope with Reaction Wheel Friction Nonlinearity

3-1. Introduction

The objective of this chapter is to conduct an investigation on the pointing stability of the analog model of the low-cost Large Space Telescope (LST) System with the reaction wheel frictional nonlinearity.

Although the LST system is digital, the stability study on the analog model will establish a limiting case when the sampling period becomes very small, thus providing a check on the results of the digital system.

The block diagram of the digital low-cost LST system, including the reaction wheel dynamics, is shown in Fig. 1-1. It has been shown in Section 1-1 that the dynamics of the LST system can be simplified. Figure 3-1 shows the block diagram of the simplified low-cost LST system with the reaction wheel nonlinearity.

The Δ of the system shown in Fig. 3-1 is

$$\Delta = 1 + K_R G_4 + G_1 G_4 G_5 + N G_6 G_7 \tag{3-1}$$

where N denotes the continuous-data describing function of the reaction wheel frictional nonlinearity.

Substitution of the expressions of G_1, G_4, G_5, G_6, and G_7 into Eq. (3-1), we have

$$\Delta = 1 + \frac{K_R}{J_v s} + \left(K_p + \frac{K_I}{s}\right)\frac{1}{J_v s^2} + N\,\frac{1}{J_{RW} s^2} \tag{3-2}$$

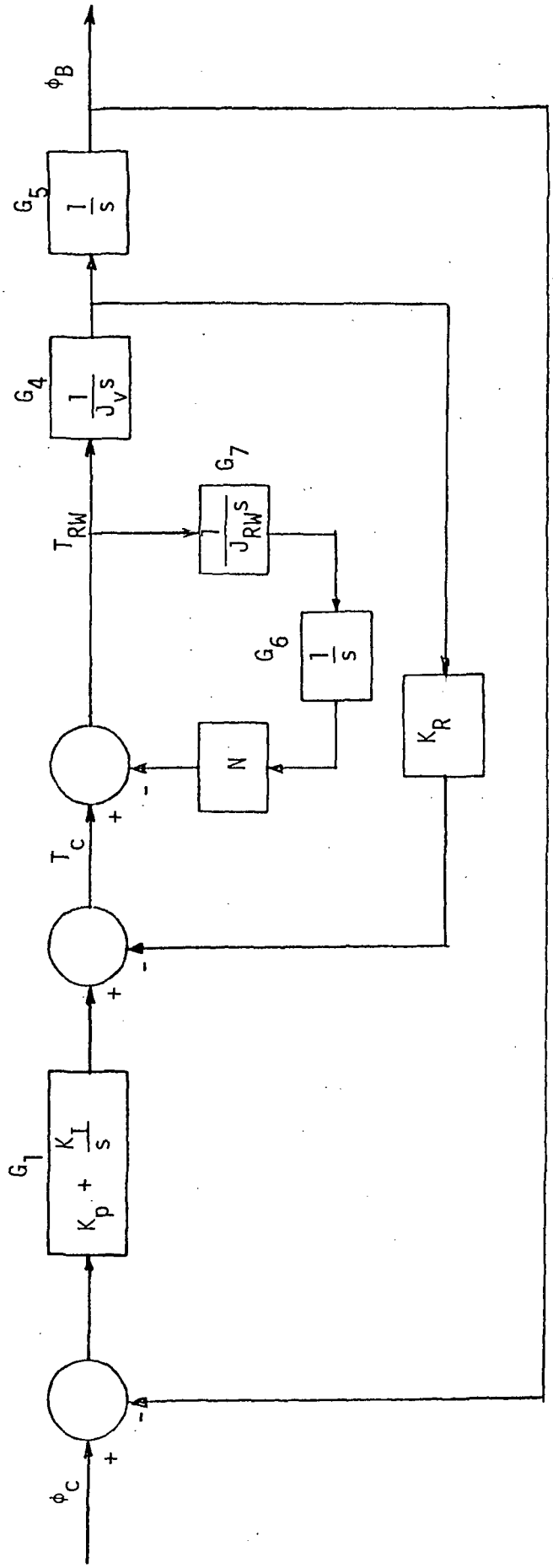

Figure 3-1. Simplified low-cost LST system with reaction wheel nonlinearity.

Setting Δ to zero, and rearranging Eq. (3-2), we get

$$J_v J_{RW} s^3 + J_{RW} K_R s^2 + J_{RW}(K_p s + K_I) + N J_v s = 0 \qquad (3\text{-}3)$$

which is the "characteristic equation" of the system.

3-2. Condition of Self-Sustained Oscillations in the Analog LST System with Reaction Wheel

It has been shown [1] that the nonlinear frictional characteristics of a reaction wheel can be described by the Dahl model. Therefore, the analog describing function of the CMG frictional nonlinearity derived in [5] can be directly utilized.

The equivalent transfer function that N sees is determined from Eq. (3-3) by dividing both sides of the equation by the terms that do not contain N. We have

$$1 + \frac{NJ_v s}{J_{RW}(J_v s^3 + K_R s^2 + K_p s + K_I)} = 0 \tag{3-4}$$

Thus,

$$G_{eq}(s) = \frac{J_v s}{J_{RW}(J_v s^3 + K_R s^2 + K_p s + K_I)} \tag{3-5}$$

The condition of self-sustained oscillation is investigated by plotting $G_{eq}(j\omega)$ and $-1/N$ in the magnitude (db) versus phase coordinates. Figure 3-2 shows the plot of $G_{eq}(j\omega)$ of the LST system with

$K_R = 3.71 \times 10^5$

$K_p = 1.65 \times 10^6$

$K_I = 7.33 \times 10^5$

$J_v = 41822$

$J_{RW} = 0.2$

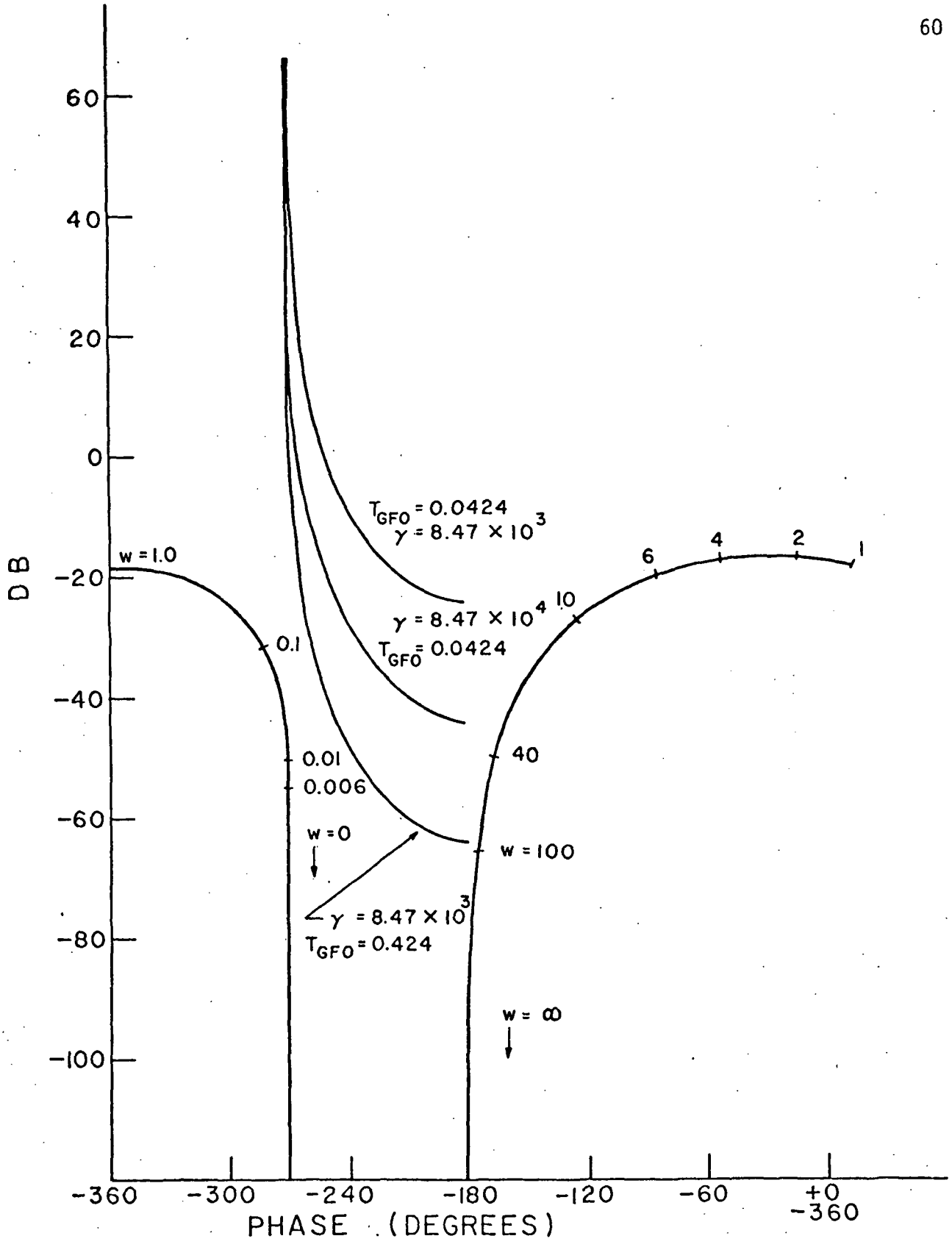

Figure 3-2. $G_{eq}(j\omega)$ and -1/N plots of analog LST with reaction wheel and frictional nonlinearity.

and the plots of -1/N with

(i) $\gamma = 8470$ $T_{GFO} = 0.0424$

(ii) $\gamma = 84700$ $T_{GFO} = 0.0424$

(iii) $\gamma = 8470$ $T_{GFO} = 0.424$

Since the $G_{eq}(j\omega)$ plot never enters the region bounded by -180° and -270° in which the plot of -1/N lies, the analog LST system will not have self-sustained oscillations, due to the reaction wheel frictional nonlinearity.

4. Stability of the Digital Low-Cost Large Space Telescope With Reaction Wheel Friction Nonlinearity

4-1. Introduction

In this chapter we shall investigate the condition of self-sustained oscillations of the digital low-cost LST system with reaction wheel friction nonlinearity.

The block diagram of the simplified LST system is shown in Fig. 4-1. The equations written for the outputs of the samplers are:

$$\Phi_e(z) = -G_A(z)\Phi_e(z) + N(z)G_B(z)\Theta_{RW}(z) \tag{4-1}$$

$$\Theta_{RW}(z) = G_c(z)\Phi_e(z) - N(z)G_D(z)\Theta_{RW}(z) \tag{4-2}$$

where N(z) denotes the discrete describing function of the reaction wheel friction nonlinearity. Since the friction nonlinearity of the reaction wheel can be represented by the Dahl model, N(z) is identical to the discrete describing function of the CMG nonlinearity [5].

The transfer functions in Eqs. (4-1) and (4-2) are

$$G_A(z) = \mathcal{Z}\left[\frac{G_{ho}G_1G_2G_3}{1 + K_RG_2}\right] \tag{4-3}$$

$$G_B(z) = \mathcal{Z}\left[\frac{G_{ho}G_2G_3}{1 + K_RG_2}\right] \tag{4-4}$$

$$G_c(z) = \mathcal{Z}\left[\frac{G_{ho}G_1G_4G_5}{1 + K_RG_2}\right] \tag{4-5}$$

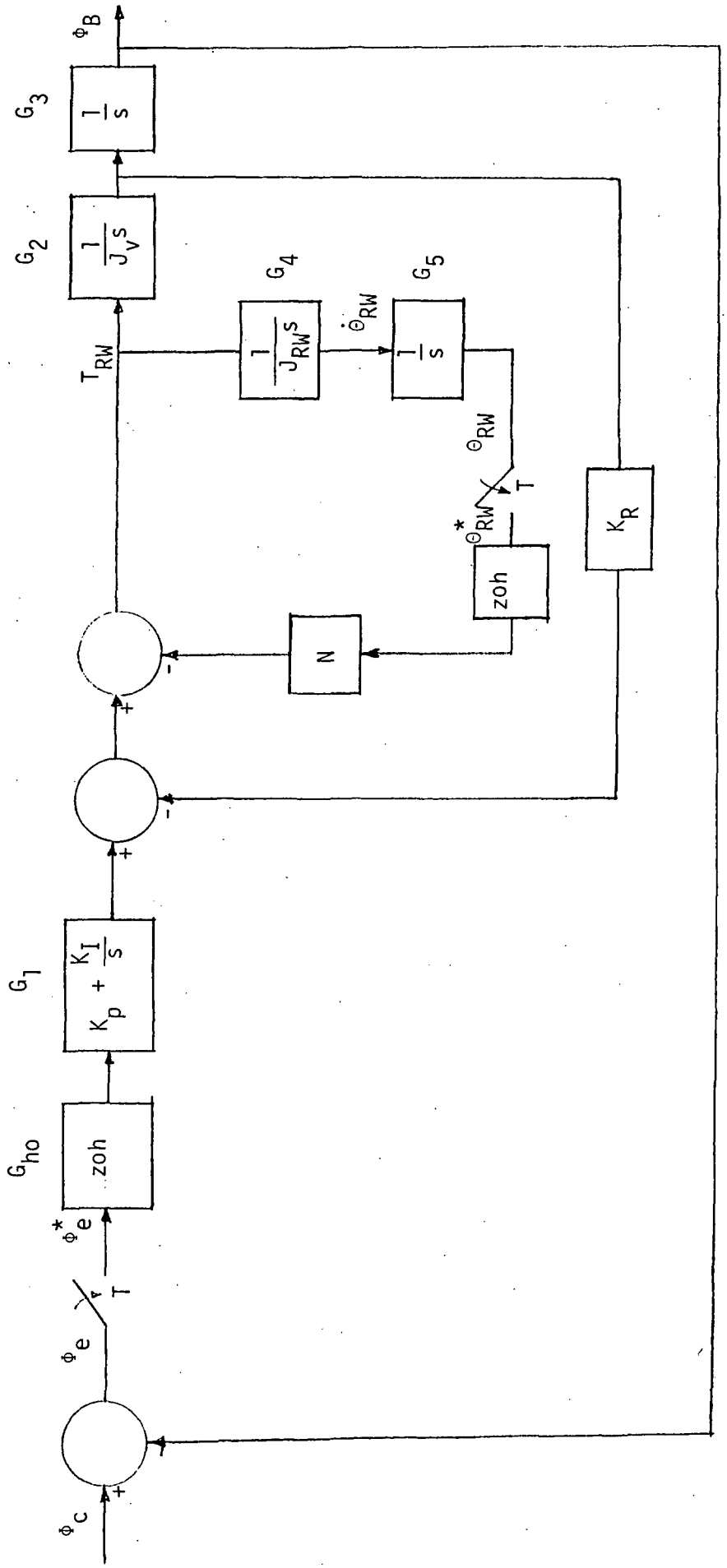

Figure 4-1. Block diagram of digital low-cost LST system with reaction wheel nonlinearity.

$$G_D(z) = \mathcal{Z}\left[\frac{G_{ho}G_4G_5}{1 + K_RG_2}\right] \tag{4-6}$$

The signal flow graph representing Eqs. (4-1) and (4-2) is shown in Fig. 4-2. The Δ of the system is obtained from Fig. 4-2,

$$\Delta = 1 + G_A(z) + N(z)[G_A(z)G_D(z) - G_B(z)\,G_c(z) + G_D(z)] \tag{4-7}$$

Setting Δ to zero, the last equation can be written in the form of

$$1 + N(z)G_{eq}(z) = 0 \tag{4-8}$$

where

$$G_{eq}(z) = \frac{G_A(z)G_D(z) - G_B(z)G_c(z) + G_D(z)}{1 + G_A(z)} \tag{4-9}$$

The individual transfer functions are evaluated as follows:

$$G_A(z) = (1 - z^{-1})\,\frac{1}{J_v}\,\mathcal{Z}\left[\frac{K_p}{s^2(s + a)} + \frac{K_I}{s^3(s + a)}\right]$$

$$= K_pG_B(z) + \frac{K_I}{J_v}\left[\frac{T^2(z + 1)}{2a(z - 1)^2} - \frac{T}{a^2(z - 1)} + \frac{1}{a^3} - \frac{z - 1}{a^3(z - e^{-aT})}\right] \tag{4-10}$$

$$a = K_R/J_v$$

$$G_B(z) = \frac{1}{K_R}\left[\frac{T}{z - 1} - \frac{1 - e^{-aT}}{a(z - e^{-aT})}\right] \tag{4-11}$$

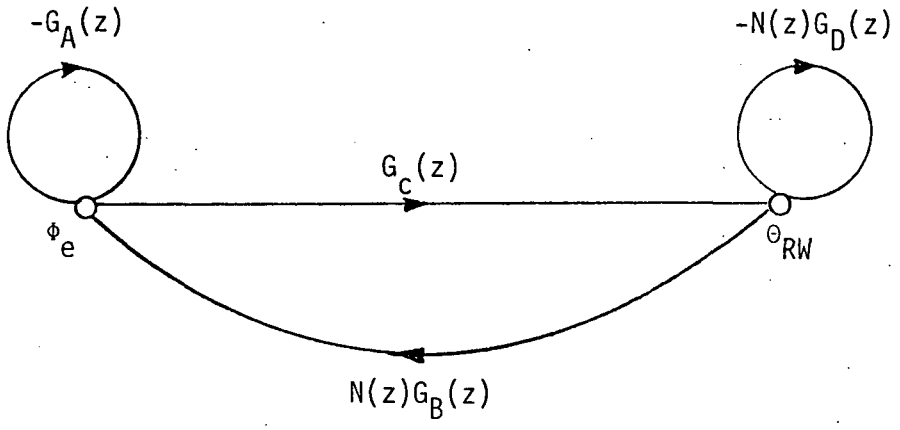

Figure 4-2. Signal flow graph.

(4-12)

$$G_c(z) = \frac{J_v}{J_{RW}} G_A(z)$$

(4-13)

$$G_D(z) = \frac{J_v}{J_{RW}} G_B(z)$$

4-2. Self-Sustained Oscillations in the Digital LST System With Reaction Wheel Nonlinearity

Figure 4-3 shows the plots of $G_{eq}(z)$ in Eq. (4-9) for various values of n with T as a parameter. The integer n and sampling period T are related to the frequency of oscillation by the following equation:

$$\omega_c = \frac{2\pi}{nT} \tag{4-14}$$

The following system parameters are used:

$K_p = 1.65 \times 10^6$ $\quad$ $K_R = 3.71 \times 10^5$

$K_I = 7.33 \times 10^5$ $\quad$ $J_v = 41822$

$J_{RW} = 0.2$

In Fig. 4-3 the curve for n = 2 extends up to approximately 30 db at T = 0.7 sec. Also, as n is increased the curves for $G_{eq}(z)$ approach the curve for $G_{eq}(s)$ presented in Fig. 3-2. The plots of $G_{eq}(z)$ together with the plots of $-1/N(z)$ allow the study of self-sustained oscillations in the digital LST system.

Figures 4-4 through 4-6 show the plots for $-1/N(z)$ for various n. In these plots $\gamma = 84700$ and $T_{GFO} = 0.424$. In all cases, the magnitude of the lowest point of the $-1/N(z)$ curve as E approaches 0 is given by

$$\lim_{E \to 0} \frac{1}{|N(z)|} = \frac{1}{\gamma T_{GFO}^2} \tag{4-15}$$

With the given parameters this point is at -83.66 db. The curves for n = 2 are shown in Fig. 4-4 and consist of two straight lines at

$-180°$ (for $0 \leq \phi < \pi/2$) and $-360°$ (for $\pi/2 < \phi \leq \pi$). The plots for $n = 3$ and $n = 4$ are shown in Figs. 4-5 and 4-6, respectively. Several values of ϕ are plotted in each case to illustrate the effect of the phase of the input signal. It should be noted that for odd n the curves repeat every 180/n degrees starting from $\phi = 0$, and for even n the curves repeat every 360/n degrees starting from $\phi = 0$. As the input amplitude E goes to infinity, the curves also go to infinity and span a region 180/n degrees or 360/n degrees wide for odd or even n, respectively. This region is centered about the $-270°$ line. Thus, as n goes to infinity these curves approach the $-1/N$ curve of the continuous system shown in Fig. 3-2.

For stability analysis it is sufficient to consider only the bounds of the $-1/N(z)$ plot for a fixed n. Self-sustained oscillations can occur if the $G(z)$ curve corresponding to the same n intersects with the $F(z)$ plot. Figures 4-3 through 4-6 show that self-sustained oscillations can readily occur in this system with the choice of T determining the possible n values which can exist. As the critical regions for higher values than $n = 4$ can be easily visualized, it is apparent that this system will have self-sustained oscillations for integral values beyond $n = 4$. However, as n increases, the amplitude of oscillation decreases and the oscillation will eventually cease as T gets smaller and smaller and n gets larger and larger.

If γ and T_{GRO} are increased then the curves of $-1/N(z)$ move up with the end point shifting according to Eq. (4-15). Figures 4-7 through 4-9 show the plots of $-1/N(z)$ for $n = 2$, 3 and 4, respectively, with $\gamma = 8470$ and $T_{GFO} = 0.0424$. In this case the lowest point is at -23.66 db and

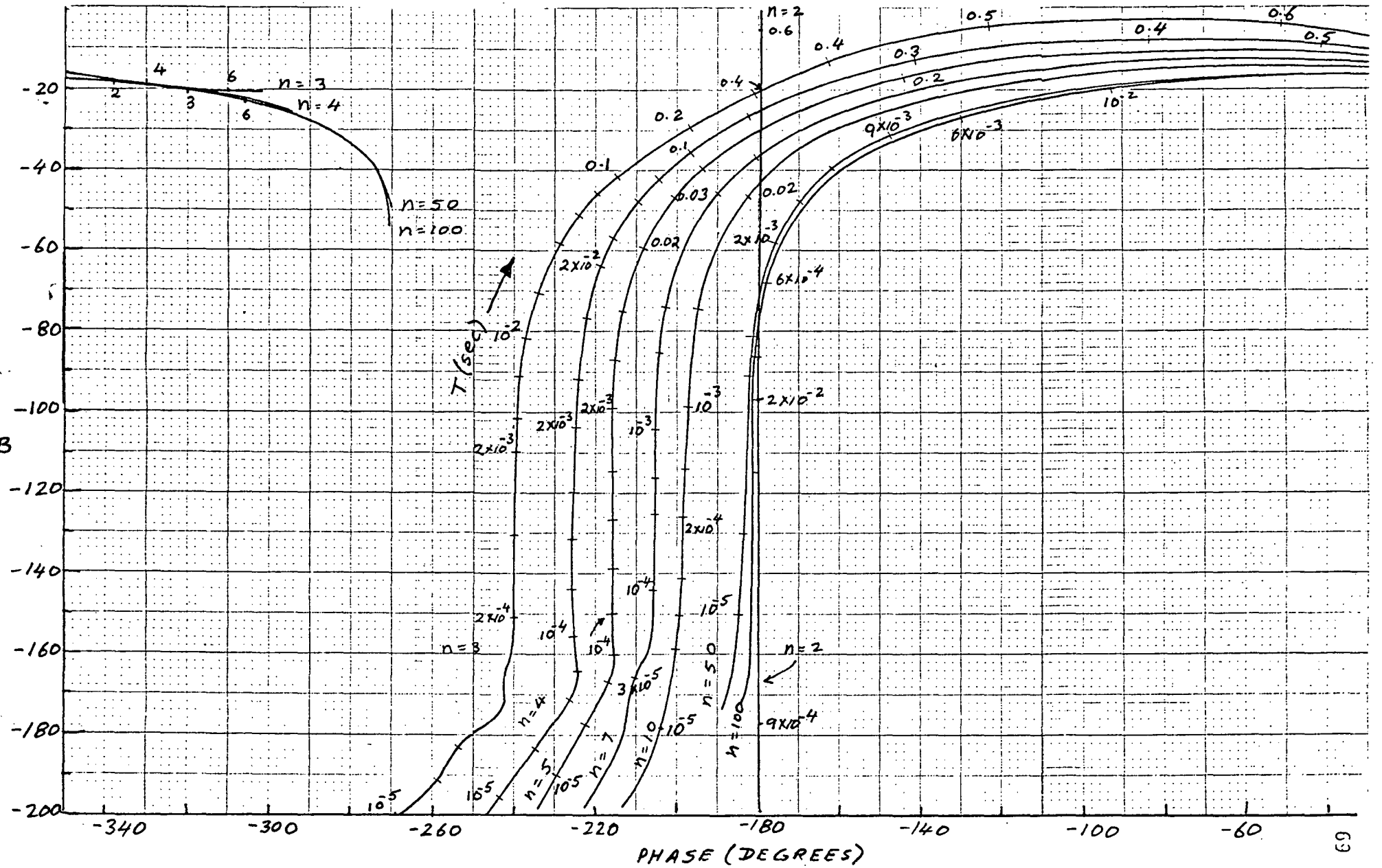

Figure 4-3. G(z) curves of the low-cost LST with frictional nonlinearity.

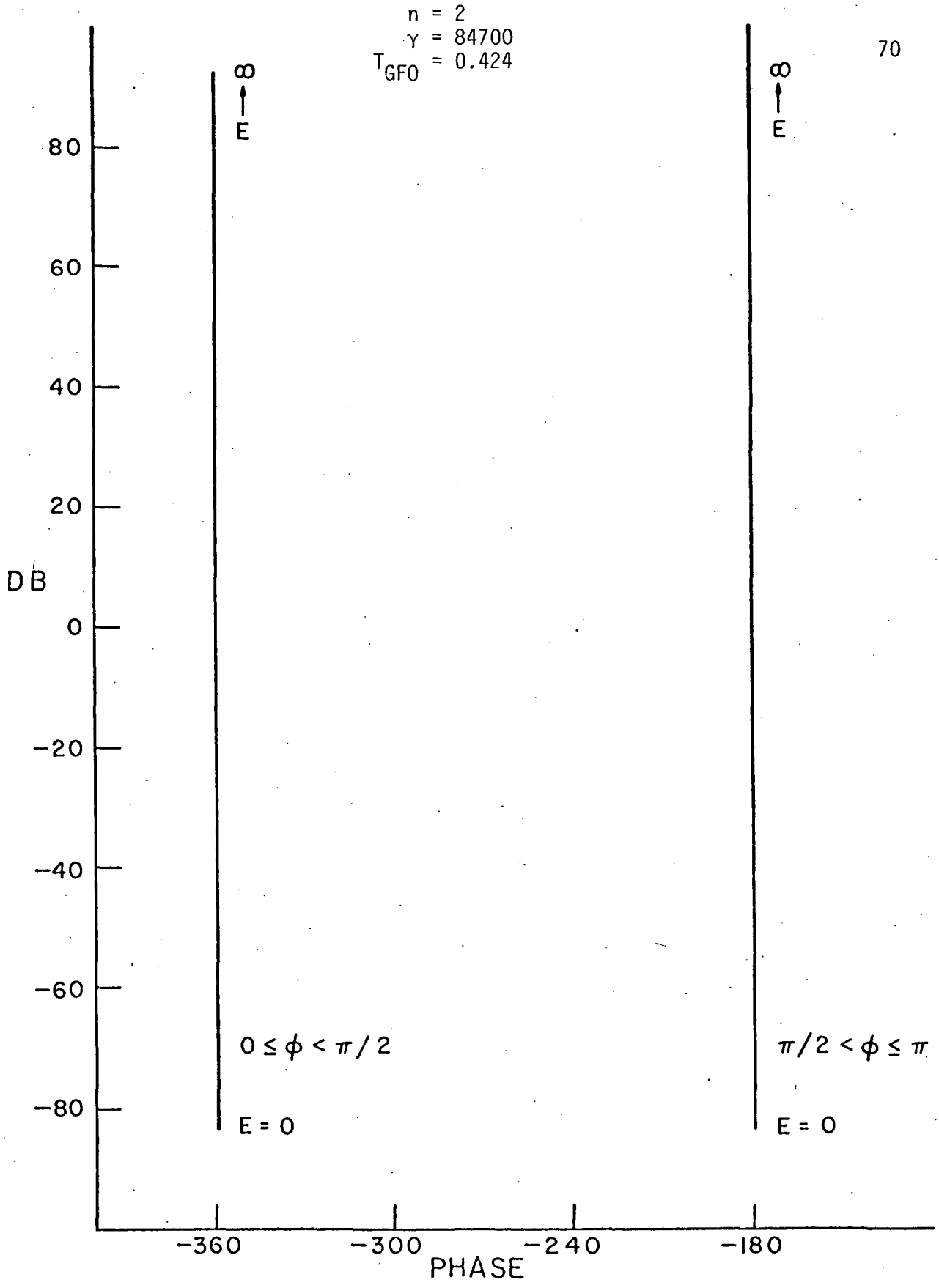

Figure 4-4. Discrete describing function for the frictional nonlinearity, n = 2.

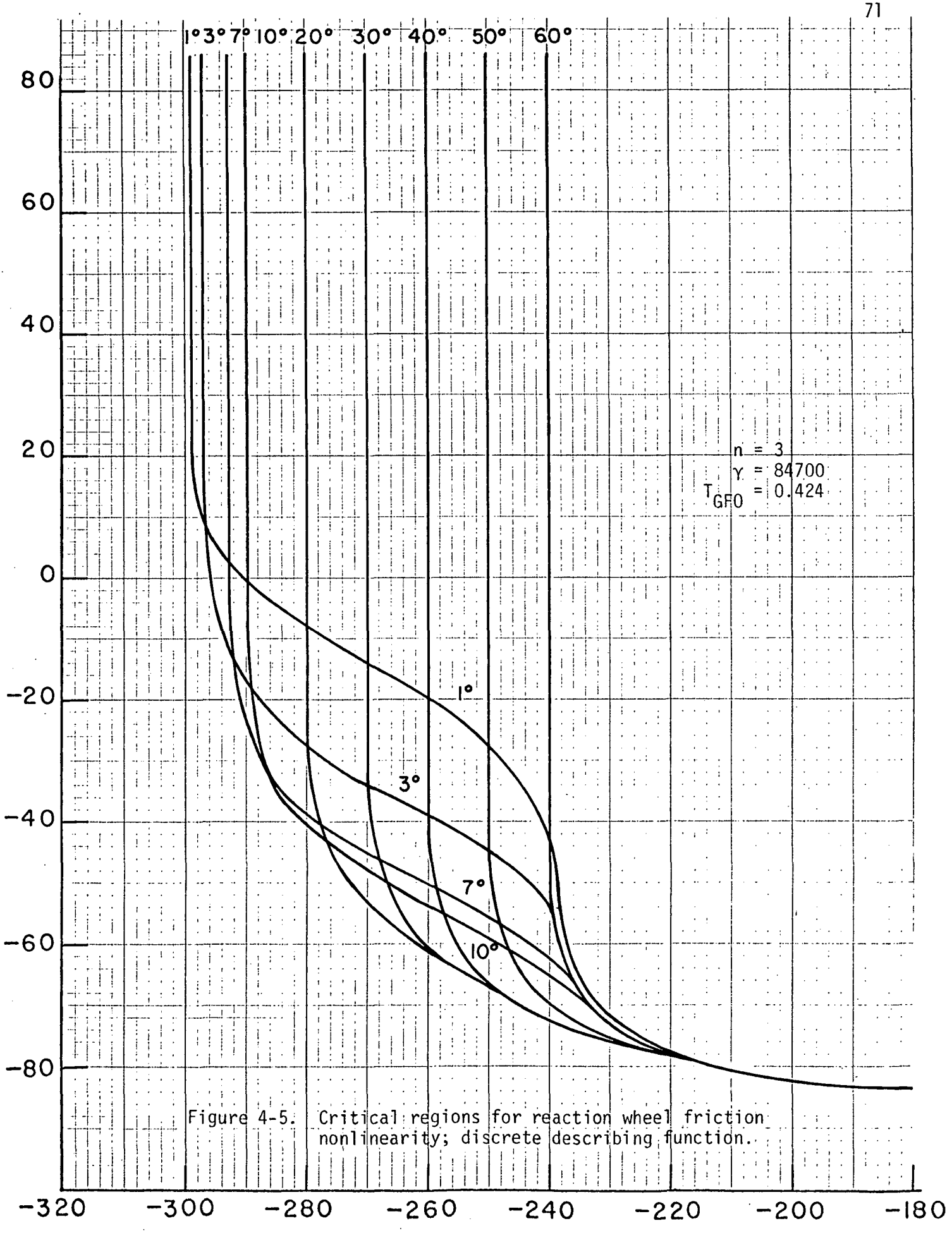

Figure 4-5. Critical regions for reaction wheel friction nonlinearity; discrete describing function.

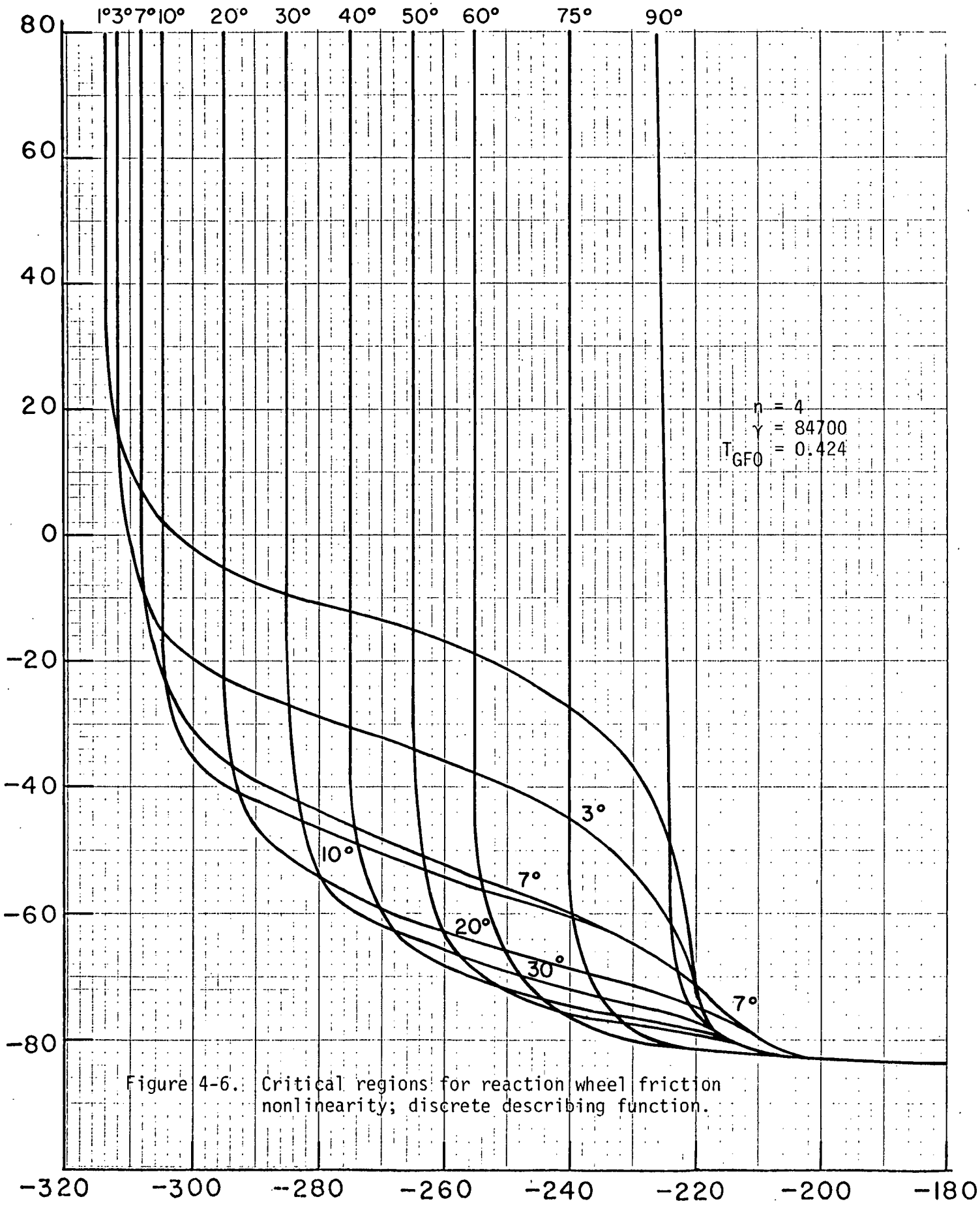

Figure 4-6. Critical regions for reaction wheel friction nonlinearity; discrete describing function.

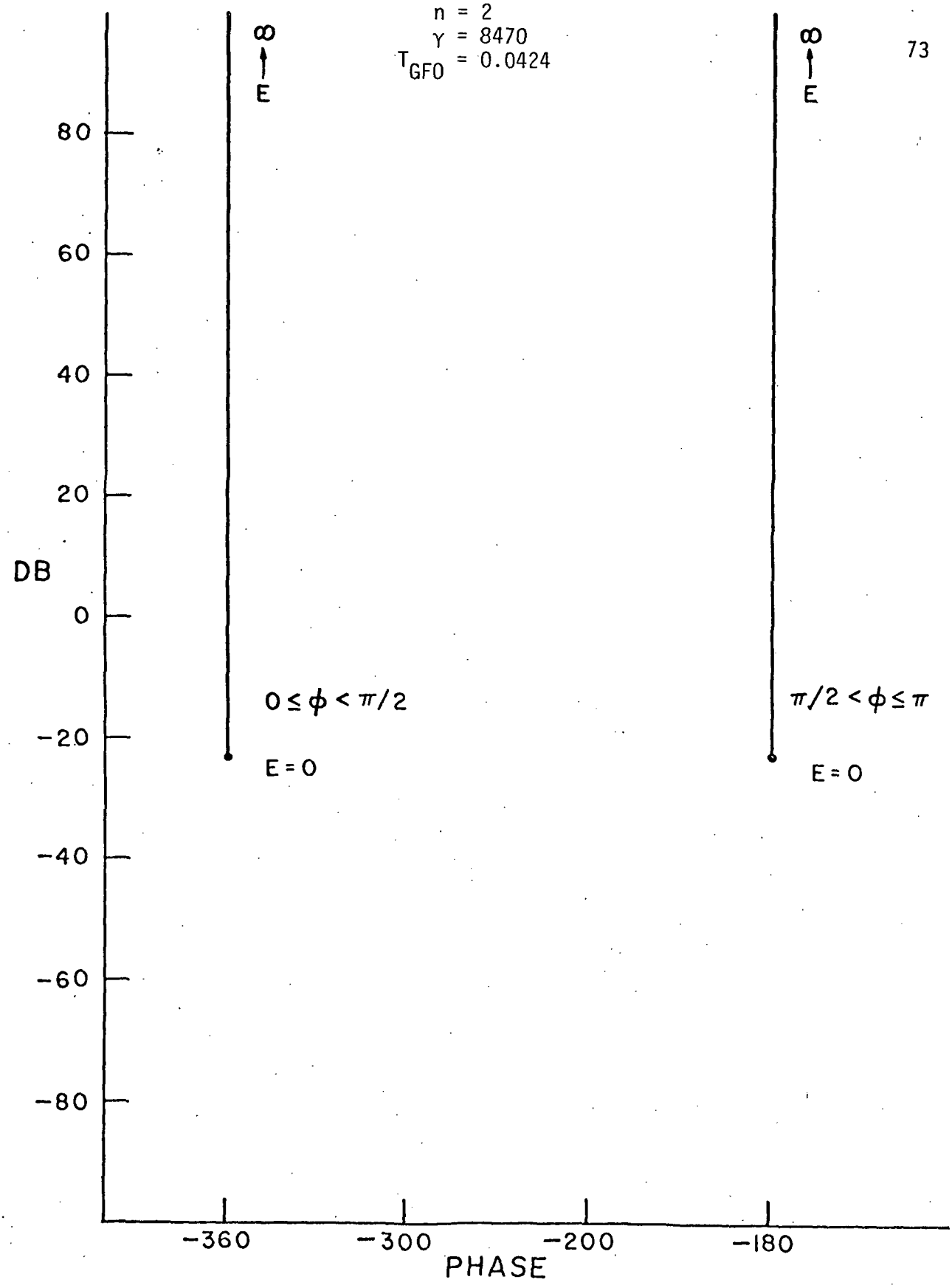

Figure 4-7. Discrete describing function for the frictional nonlinearity, n = 2.

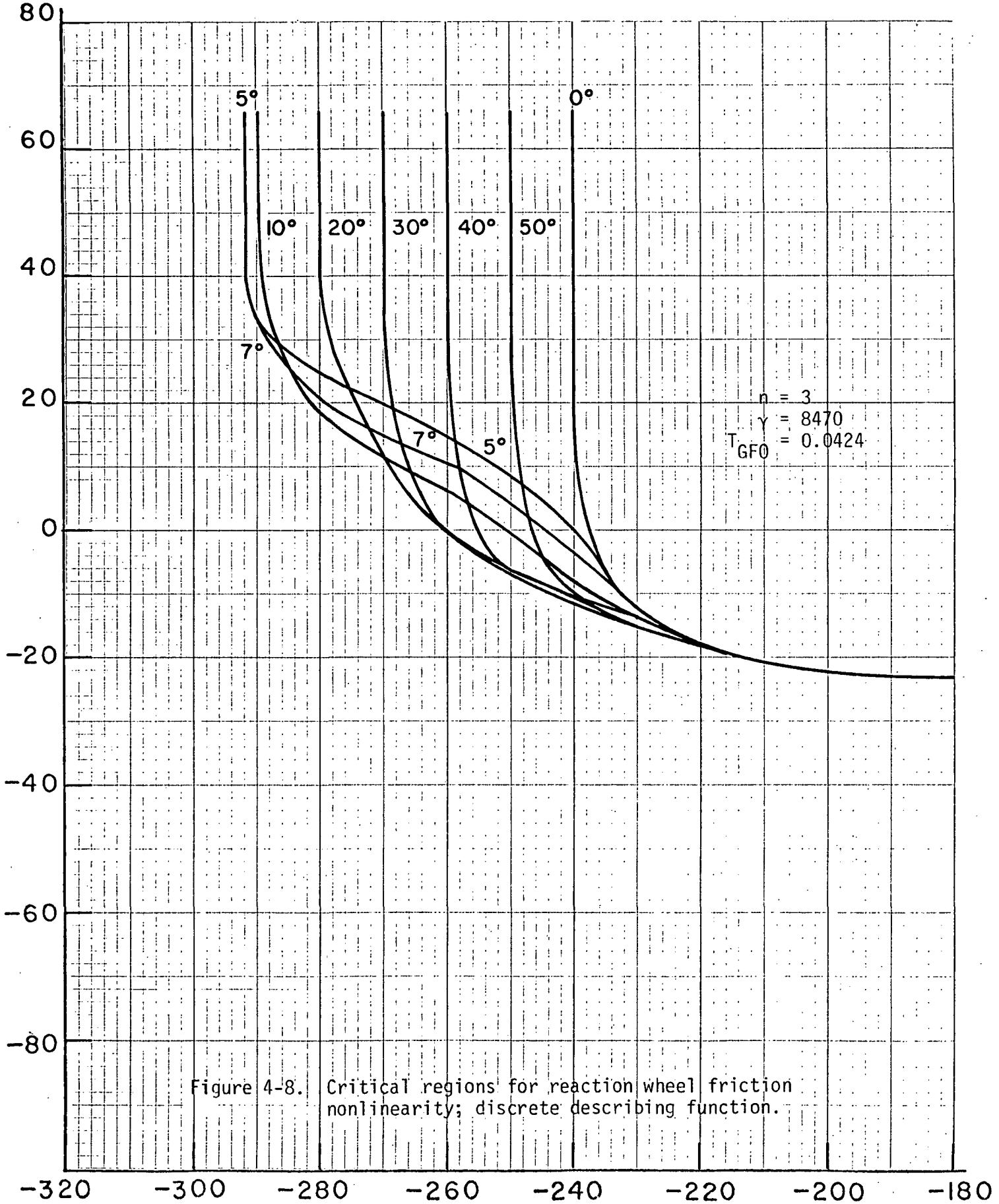

Figure 4-8. Critical regions for reaction wheel friction nonlinearity; discrete describing function.

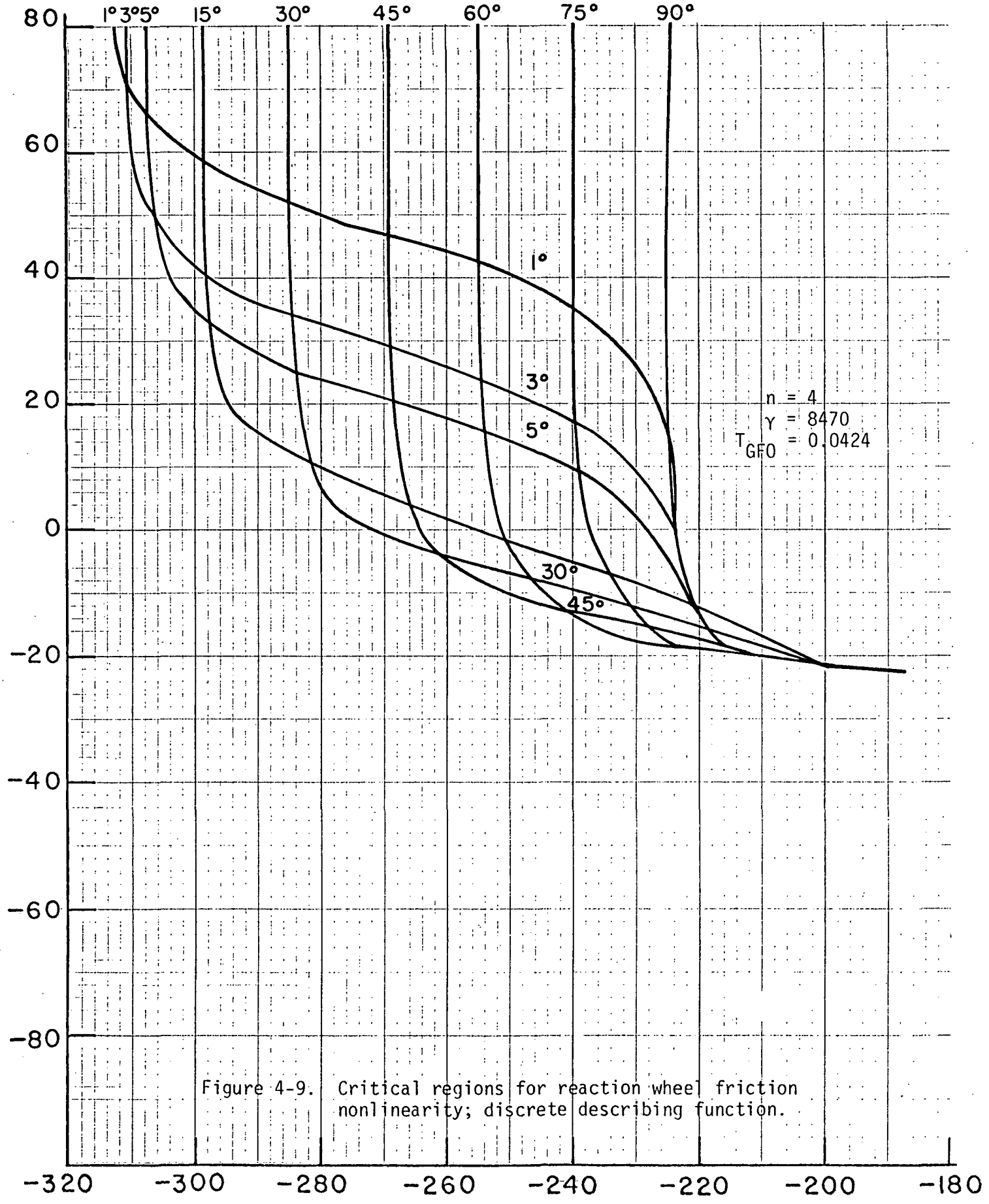

Figure 4-9. Critical regions for reaction wheel friction nonlinearity; discrete describing function.

self-sustained oscillations are possible only for n = 2 over a fixed small range of sampling periods. If T is chosen to exclude the critical region, self-sustained oscillations can be avoided.

5. Discrete Describing Function of A Quantizer

5-1. Introduction

The effects of quantization and the study of quantization error conducted in Chapter 1 are all based on the assumption that the digital system with quantization is stable and free from sustained oscillations. Since a quantizer is a nonlinear element, it can cause self-sustained oscillations. In Chapter 2 the condition of self-sustained oscillations in the analog low-cost LST system with quantizer is studied by use of the continuous-data describing function. However, in reality, the low-cost LST system is a digital system. The interaction between the sampling operation and the quantizer will bring about phenomena which can be grossly different from that in an analog system. Therefore, it is essential that the discrete describing function (DDF) of a quantizer be derived. To the authors' knowledge the DDF of a quantizer has not been derived in the past.

Figure 5-1 shows the input-output characteristics of a quantizer. The input of the quantizer is denoted by $e^*(t)$, and the output by $y^*(t)$. It is assumed that the input of the quantizer is the output of an ideal sampler. Therefore, $e^*(t)$ and $y^*(t)$ are trains of impulses. Furthermore, it is assumed that the input to the sampler, $e(t)$, is a cosine wave, and thus the amplitude of $e^*(t)$ is modulated by a cosine wave; that is,

$$e(t) = E \cos (\omega t + \phi) \tag{5-1}$$

$$e^*(t) = E \sum_{k=0}^{\infty} \cos (k\omega T + \phi)\delta(t - kT) \tag{5-2}$$

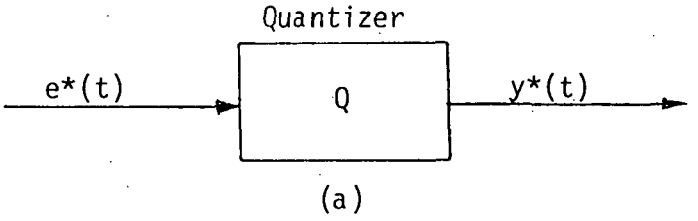

(a)

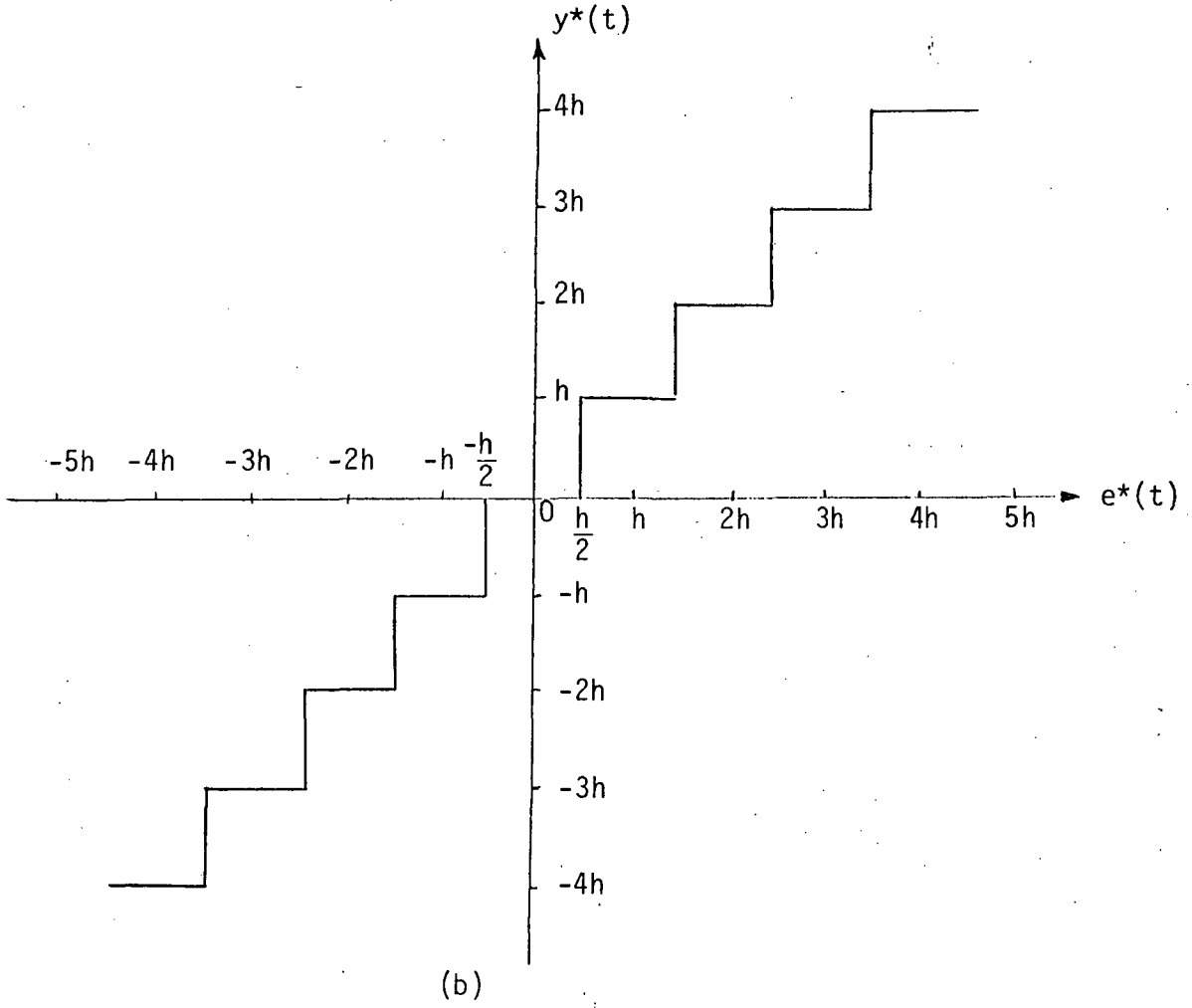

(b)

Figure 5-1. (a) Quantizer nonlinearity.

(b) Input-output relation of quantizer.

where E is a constant, ω is the frequency in radians per second, T is the sampling period in seconds, and $\delta(t)$ denotes the unit impulse function. The z-transform of $e^*(t)$ is

$$E(z) = \frac{Ez}{z^2 - 2z\cos\omega T + 1}\left[(z - \cos\omega T)\cos\phi - \sin\omega T \sin\phi\right] \tag{5-3}$$

The z-transform of $y^*(t)$ is denoted by $Y(z)$.

The discrete describing function of the quantizer nonlinearity is defined as

$$N(z) = \frac{Y(z)}{E(z)} \tag{5-4}$$

As in the case of the relay-type nonlinearity, we assume that because of the periodic nature of the sampler, $e^*(t)$ and $y^*(t)$ are all periodic functions of period nT, where n is a positive integer greater than or equal to two. Thus,

$$\omega = \frac{2\pi}{nT} \tag{5-5}$$

or

$$\omega T = \frac{2\pi}{n} \tag{5-6}$$

$n = 2, 3, 4, \ldots$.

The DDF N(z) is incorporated in the "characteristic equation" of the system,

$$1 + N(z)G_{eq}(z) = 0 \tag{5-7}$$

for the determination of the condition of self-sustained oscillations, where $G_{eq}(z)$ denotes the linear transfer function which the quantizer nonlinearity sees. Graphically, the condition of self-sustained oscillation characterized by the period nT is determined by the intersections of the $G_{eq}(z)$ trajectories with the critical regions of $-1/N(z)$, all for the same n. Therefore, the DDF problem involves the determination of the critical regions of $-1/N(z)$ for the quantizer for $n = 2, 3, \ldots$.

5-2. The DDF of A Quantizer for n = 2

In order to illustrate the derivation of the DDF of the quantizer nonlinearity, we shall first consider the case of n = 2; that is, the self-sustained oscillation is characterized by the period which is equal to twice the sampling period.

For this mode of oscillation, the waveforms of e(t), e*(t), and y*(t) are shown in Fig. 5-2.

For n = 2, Eq. (5-6) gives $\omega T = \pi$; Eq. (5-3) becomes

$$E(z) = \frac{Ez \cos \phi}{z + 1} \tag{5-8}$$

The z-transform of y*(t) is written

$$Y(z) = \frac{khz}{z + 1} \tag{5-9}$$

where k is a positive integer. In this case it is assumed that the value of E is constrained by the following equation:

$$\frac{(2k - 1)h}{2} < E \cos \phi < \frac{(2k + 1)h}{2} \tag{5-10}$$

Using Eqs. (5-8) and (5-9), we have

$$-\frac{1}{N(z)} = -\frac{E \cos \phi}{kh} \tag{5-11}$$

For a given set of values of k, h, and ϕ, the constraints on the values of E for n = 2 are

$$E_{max} = \frac{(2k + 1)h}{2 \cos \phi} \tag{5-12}$$

$$E_{min} = \frac{(2k - 1)h}{2 \cos \phi} \tag{5-13}$$

Substituting E_{max} and E_{min} into Eq. (5-11), we have

$$- \frac{1}{N(z)}\bigg|_{max}(k) = - \frac{(2k + 1)}{2k} \tag{5-14}$$

$$- \frac{1}{N(z)}\bigg|_{min}(k) = - \frac{(2k - 1)}{2k} \tag{5-15}$$

The last two equations indicate that the critical region for $-1/N(z)$ for $n = 2$ is the line which extends from $-(2k - 1)/2k$ to $-(2k + 1)/2k$ on the negative real axis in the polar coordinates.

It can be shown that

$$\frac{1}{N(z)}\bigg|_{max}(k+1) < \frac{1}{N(z)}\bigg|_{max}(k) \tag{5-16}$$

Since

$$\frac{1}{N(z)}\bigg|_{max}(k+1) = \frac{2(k + 1) + 1}{2(k + 1)} = 1 + \frac{1}{2(k + 1)} \tag{5-17}$$

and

$$\frac{1}{N(z)}\bigg|_{max}(k) = \frac{2k + 1}{2k} = 1 + \frac{1}{2k} \tag{5-18}$$

thus, Eq. (5-16) is verified.

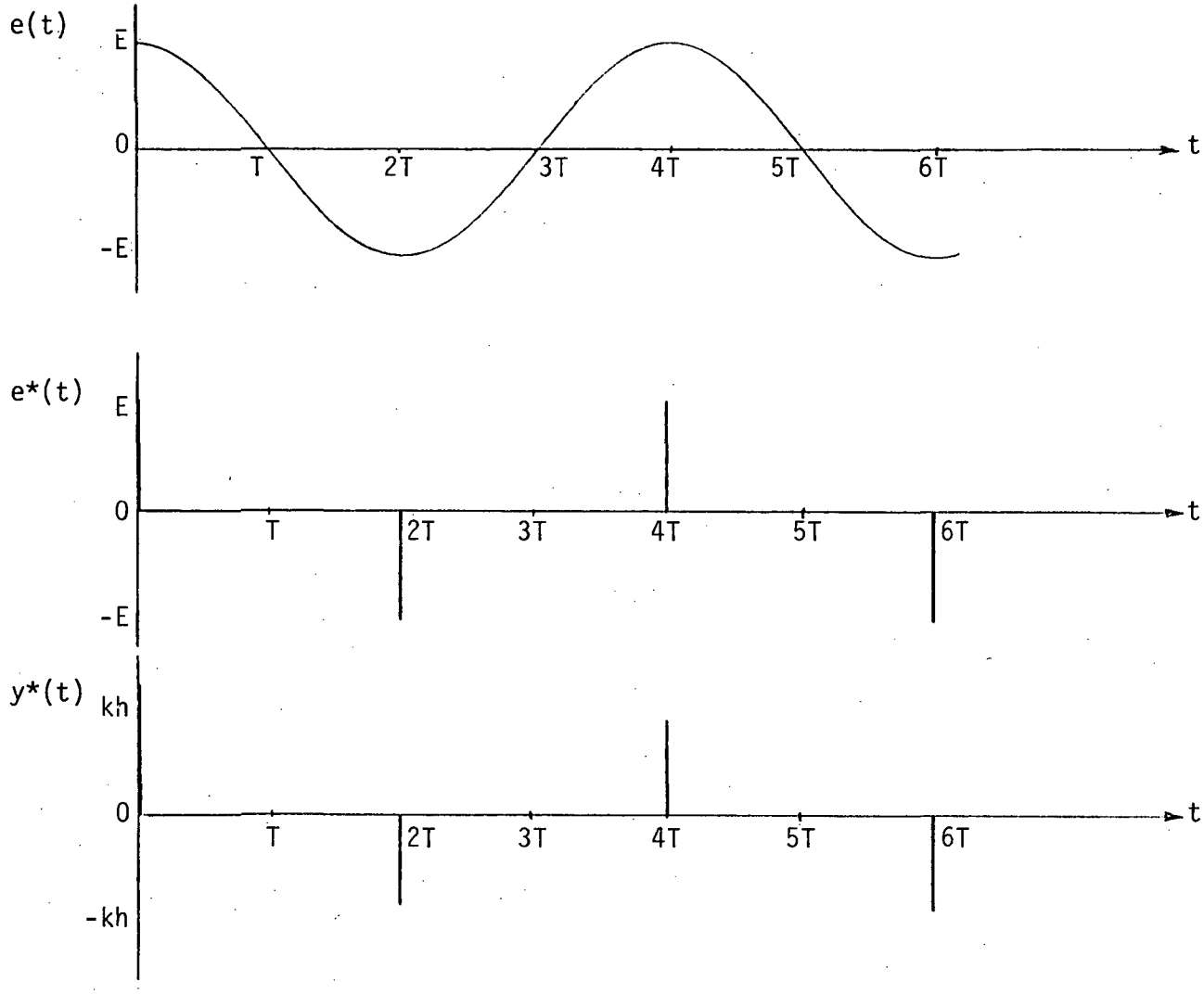

Figure 5-2. Waveforms for n = 2.

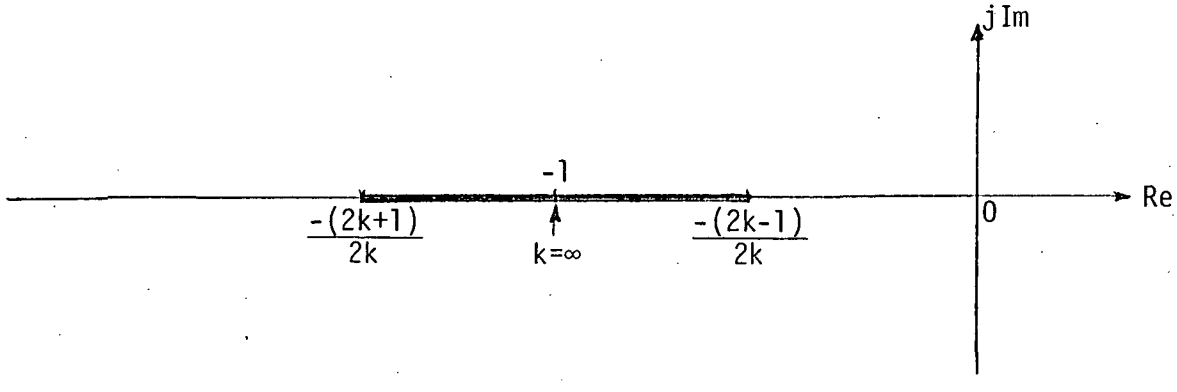

Figure 5-3. Critical region of -1/N(z) for quantizer for n = 2.

Similarly, using Eq. (5-15) we can show that, in general,

$$\left.\frac{1}{N(z)}\right|_{min}(k+1) > \left.\frac{1}{N(z)}\right|_{min}(k) \tag{5-19}$$

Thus, let S(k) be the set which is bounded by

$$-\left.\frac{1}{N(z)}\right|_{max}(k) \quad \text{and} \quad -\left.\frac{1}{N(z)}\right|_{min}(k) \quad ,$$

and S(k+1) be the set which is bounded by

$$-\left.\frac{1}{N(z)}\right|_{max}(k+1) \quad \text{and} \quad -\left.\frac{1}{N(z)}\right|_{min}(k+1) \quad ,$$

then

$$S(k+1) \subset S(k) \tag{5-20}$$

for k = 1, 2, 3, ...

Equations (5-14) and (5-15) also show that

$$\lim_{k\to o}\left[-\left.\frac{1}{N(z)}\right|_{max}(k)\right] = \lim_{k\to o}\left[-\left.\frac{1}{N(z)}\right|_{min}(k)\right] = -1 \tag{5-21}$$

This result implies that as the number of quantization levels increases, the quantizer characteristics approach a linear gain, and the critical region reduces to the (-1, j0) point in the complex plane.

The critical region for n = 2 is shown in Fig. 5-3.

5-3. The DDF of A Quantizer for n = 4

Before embarking on the derivations of general expressions of $-1/N(z)$ for all $n > 2$, the case for $n = 4$ will be considered as an illustrative example.

For $n = 4$, the input pulse train of the quantizer can assume a maximum of two different pulse amplitudes, k_0 and k_1. The mode of oscillation is thus characterized by $\Delta = (k_0, k_1)$, where k_0 and k_1 are positive integers. Figure 5-4 illustrates the input and the output of the sampler when the former is shifted through 360 degrees. It is observed from these waveforms, as well as will be verified later by equations, that the critical region for $n = 4$ repeats every 90 degrees for ϕ, so that only the range for $-45° \leq \phi \leq 45°$ needs be considered.

For $n = 4$, $\cos \omega T = \cos 90° = 0$, $z = j$. Thus, Eq. (5-3) becomes

$$E(z) = \frac{Ez}{z^2 + 1} (z \cos \phi - \sin \phi) \tag{5-22}$$

With reference to Fig. 5-4, the expressions of the input to the quantizer for the various ranges of ϕ are written as follows:

$$-90° \leq \phi \leq 0° \qquad Y(z) = \frac{h(k_0 z + k_1)z}{z^2 + 1} \tag{5-23}$$

$$-180° \leq \phi \leq -90° \qquad Y(z) = \frac{h(-k_0 z + k_1)z}{z^2 + 1} \tag{5-24}$$

$$0° \leq \phi \leq 90° \qquad Y(z) = \frac{h(k_0 z - k_1)z}{z^2 + 1} \tag{5-25}$$

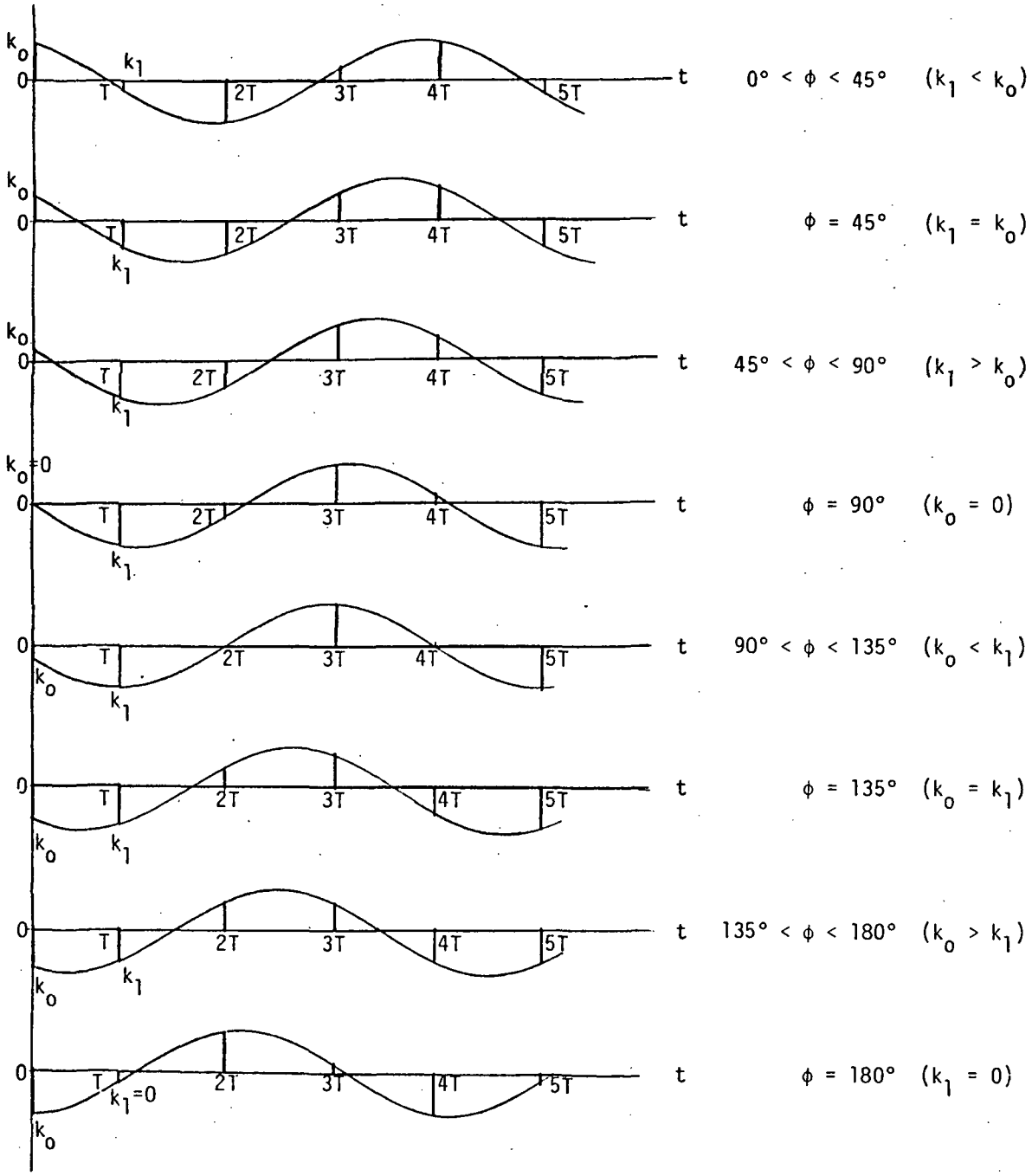

Figure 5-4. Input and output signal waveforms of sampler preceding the quantizer as ϕ varies through 360°.

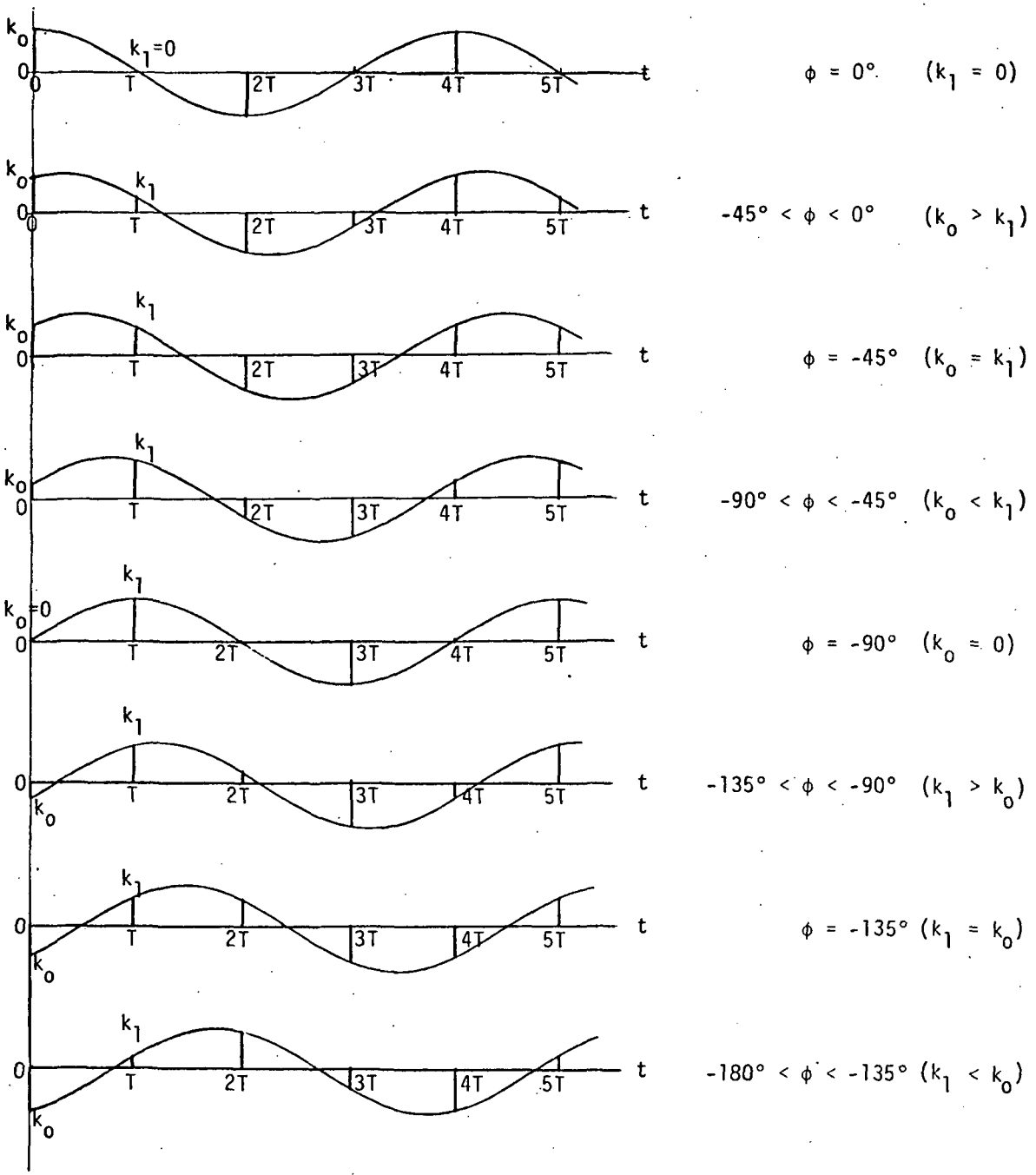

Figure 5-4. Input and output signal waveforms of sampler preceding the quantizer as ϕ varies through 360°.

$$90° \leq \phi \leq 180° \qquad Y(z) = \frac{h(-k_o z - k_1)z}{z^2 + 1} \tag{5-26}$$

The constraints on the magnitude of E over these ranges of ϕ are tabulated as follows:

$$\frac{(2k_o - 1)h}{2} \leq |E \cos \phi| \leq \frac{(2k_o + 1)h}{2} \tag{5-27}$$

and

$$\frac{(2k_1 - 1)h}{2} \leq |E \sin \phi| \leq \frac{(2k_1 + 1)h}{2} \tag{5-28}$$

These inequality conditions lead to maximum and minimum bounds on E. When these E_{max} and E_{min} are substituted into

$$-\frac{1}{N(z)} = -\frac{E(z)}{Y(z)} \tag{5-29}$$

and along with Eqs. (5-23) through (5-26), the equations that define the boundaries of the critical regions are obtained as

$$-\frac{1}{N(z)}\bigg|_{max} \qquad \text{and} \qquad -\frac{1}{N(z)}\bigg|_{min}$$

For instance, for $-90° \leq \phi \leq 0°$, from Eq. (5-27),

$$E_{min\,1} = \frac{(2k_o - 1)h}{2 \cos \phi} \tag{5-30}$$

Using Eqs. (5-22), (5-23), and (5-29), we have

$$-\left.\frac{1}{N(z)}\right|_{\min 1} = \frac{2k_o - 1}{2(k_o j + k_1)}(\tan\phi - j) \tag{5-31}$$

Rationalizing the last equation, we have

$$-\left.\frac{1}{N(z)}\right|_{\min 1} = \frac{2k_o - 1}{2(k_o^2 + k_1^2)}[(k_1 \tan\phi - k_o) + j(-k_o \tan\phi - k_1)] \tag{5-32}$$

Let

$$-\left.\frac{1}{N(z)}\right|_{\min 1} = R + jI \tag{5-33}$$

where

$$R = \frac{2k_o - 1}{2(k_o^2 + k_1^2)}(k_1 \tan\phi - k_o) \tag{5-34}$$

$$I = \frac{2k_o - 1}{2(k_o^2 + k_1^2)}(-k_o \tan\phi - k_1) \tag{5-35}$$

Then, solving for $\tan\phi$ from Eq. (5-34) gives

$$\tan\phi = \frac{R + k_o C}{k_1 C} \tag{5-36}$$

where

$$C = \frac{2k_o - 1}{2(k_o^2 + k_1^2)} \tag{5-37}$$

Substitution of Eq. (5-36) into Eq. (5-35) yields after simplification,

$$I = -\frac{k_o}{k_1} R - \frac{2k_o - 1}{2k_1} \tag{5-38}$$

which is the equation of a straight line in the complex $-1/N(z)$ domain.

Similarly, from Eq. (5-27),

$$E_{max\,1} = \frac{(2k_o + 1)h}{2\cos\phi} \qquad -90° \leq \phi \leq 0° \tag{5-39}$$

Following through the same procedure as described above, we have

$$-\frac{1}{N(z)}\bigg|_{max\,1} = \frac{2k_o + 1}{2(k_o j + k_1)}(\tan\phi - j) \tag{5-40}$$

which is represented by a straight line with the equation

$$I = -\frac{k_o}{k_1} R - \frac{2k_o + 1}{2k_1} \tag{5-41}$$

The boundaries for $-1/N(z)$ when the constraint equation of Eq. (5-28) is used are denoted as

$$-\frac{1}{N(z)}\bigg|_{max\,2} \qquad \text{and} \qquad -\frac{1}{N(z)}\bigg|_{min\,2}$$

The equations which define the boundaries of $-1/N(z)$ for the entire range of ϕ are tabulated below:

$-90° \leq \phi \leq 0°$	$I = -\frac{k_o}{k_1} R - \frac{2k_o - 1}{2k_1}$	(min 1)
$90° \leq \phi \leq 180°$		

$$I = -\frac{k_o}{k_1} R - \frac{2k_o + 1}{2k_1} \qquad \text{(max 1)}$$

$$I = \frac{k_1}{k_o} R + \frac{2k_1 - 1}{2k_o} \qquad \text{(min 2)}$$

$$I = \frac{k_1}{k_o} R + \frac{2k_1 + 1}{2k_o} \qquad \text{(max 2)} \qquad (5\text{-}42)$$

$-180° \leq \phi \leq -90°$

$0° \leq \phi \leq 90°$

$$I = \frac{k_o}{k_1} R + \frac{2k_o - 1}{2k_1} \qquad \text{(min 1)}$$

$$I = \frac{k_o}{k_1} R + \frac{2k_o + 1}{2k_1} \qquad \text{(max 1)}$$

$$I = -\frac{k_1}{k_o} R - \frac{2k_1 - 1}{2k_o} \qquad \text{(min 2)}$$

$$I = -\frac{k_1}{k_o} R - \frac{2k_1 + 1}{2k_o} \qquad \text{(max 2)} \qquad (5\text{-}43)$$

These equations show that for the oscillatory mode of n = 4 and $\Delta \approx (k_o, k_1)$, the critical regions are bounded by straight lines, and that it is sufficient to consider the range of $-90° \leq \phi \leq 90°$. However, Fig. 5-4 shows that $k_o \geq k_1$ for $-45° \leq \phi \leq 45°$ and $k_o \leq k_1$ for $45° \leq |\phi| \leq 90°$, thus, the critical regions for modes $\Delta = (k_o, k_1)$ and $\Delta = (k_1, k_o)$ are identical. It is necessary only to consider the range of ϕ from -45° to +45°. In general, one does not have to use the constraints on ϕ, as the intersects of the eight equations in Eqs. (5-42) and (5-43) will naturally define the critical region.

Modes $\Delta = (k_o, 0)$ and $\Delta = (0, k_1)$

Figure 5-4 shows that when $\phi = 0°$ or $180°$, $k_1 = 0$, and the mode is described as $\Delta = (k_o, 0)$. Similarly, when $\phi = \pm 90°$, the mode is $\Delta = (0, k_1)$.

For the mode $\Delta = (k_o, 0)$, Eqs. (5-42) and (5-43) are reduced to

$$R = -\frac{2k_o - 1}{2k_o} \qquad \text{(min 1)}$$

$$R = -\frac{2k_o + 1}{2k_o} \qquad \text{(max 1)}$$

$$I = -\frac{1}{2k_o} \qquad \text{(min 2)}$$

$$I = \frac{1}{2k_o} \qquad \text{(max 2)} \qquad (5\text{-}44)$$

These four lines define a square as shown in Fig. 5-5.

For the mode $\Delta = (0, k_1)$, it is simple to show that the critical region is described by equations of the same form of Eq. (5-44) with k_o replaced by k_1. Therefore, the square region shown in Fig. 5-5 is also for the mode $\Delta = (0, k_1)$ with k_o replaced by k_1.

Mode $\Delta = (k_o, k_1)$, $k_o = k_1$

When $\phi = \pm 45°, \pm 135°$, $k_o = k_1$, as shown in Fig. 5-4. The critical region is now described by the following four equations:

$$I = -R - \frac{2k_o - 1}{2k_o}$$

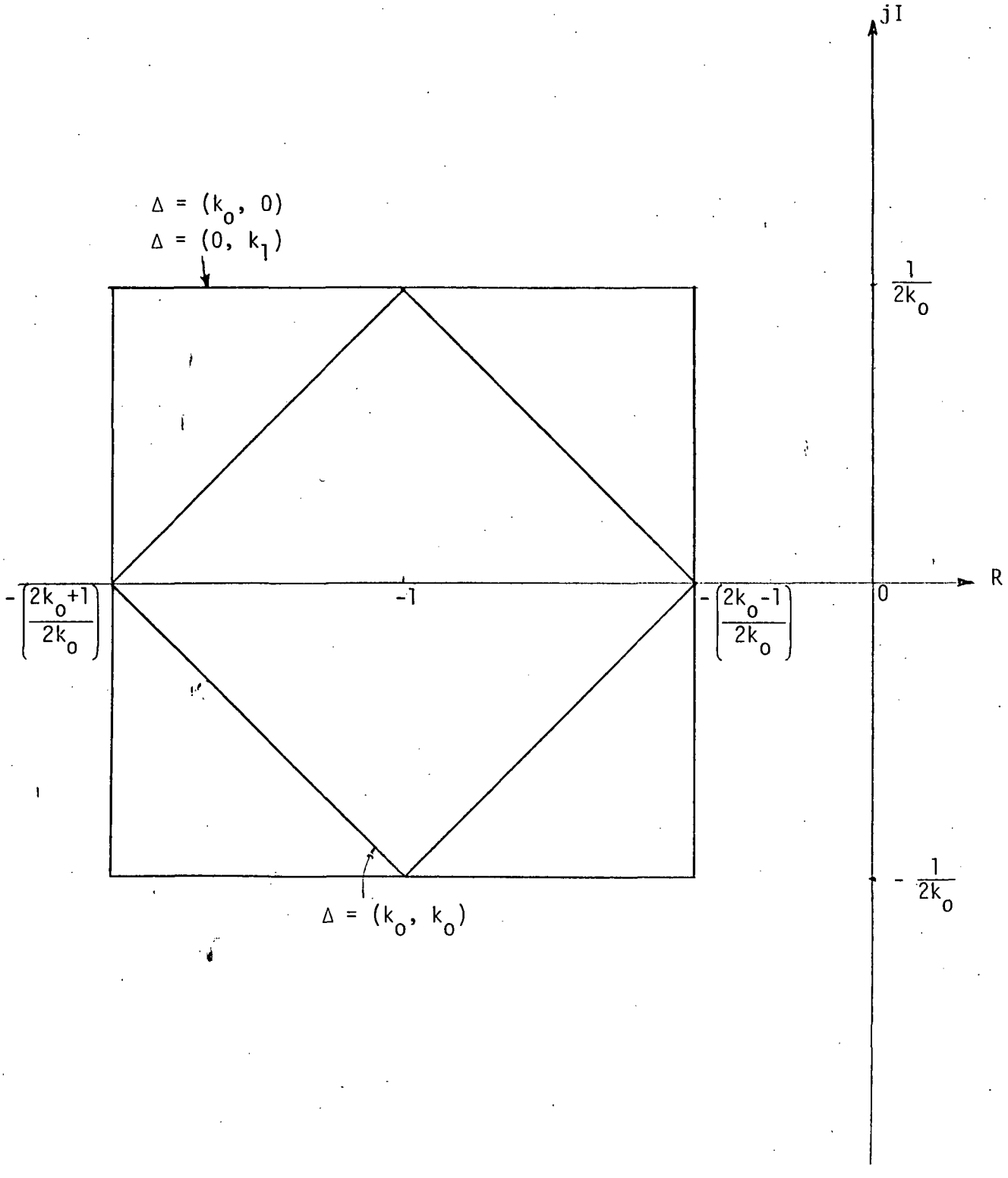

Figure 5-5. Critical regions of $\Delta = (k_o, 0)$, $(0, k_1)$, and (k_o, k_o).

$$I = -R - \frac{2k_o + 1}{2k_o}$$

$$I = R + \frac{2k_o - 1}{2k_o}$$

$$I = R + \frac{2k_o + 1}{2k_o} \qquad (5\text{-}45)$$

The critical region is again a square, as shown in Fig. 5-5.

In general, the critical region for the mode $\Delta = (k_o, k_1)$ is defined by the intersects of the eight equations in Eqs. (5-42) and (5-43). As an illustration, Fig. 5-6 shows the critical region for $\Delta = (2, 1)$ which is also for $\Delta = (1, 2)$. Notice that this critical region is bounded by that of $\Delta = (2, 0)$ or $\Delta = (0, 2)$.

(1) I = -2R - 3/2
(2) I = -2R - 5/2
(3) I = 2R + 3/2
(4) I = 2R + 5/2
(5) I = R/2 + 1/4
(6) I = R/2 + 3/4
(7) I = -R/2 - 1/4
(8) I = -R/2 - 3/4

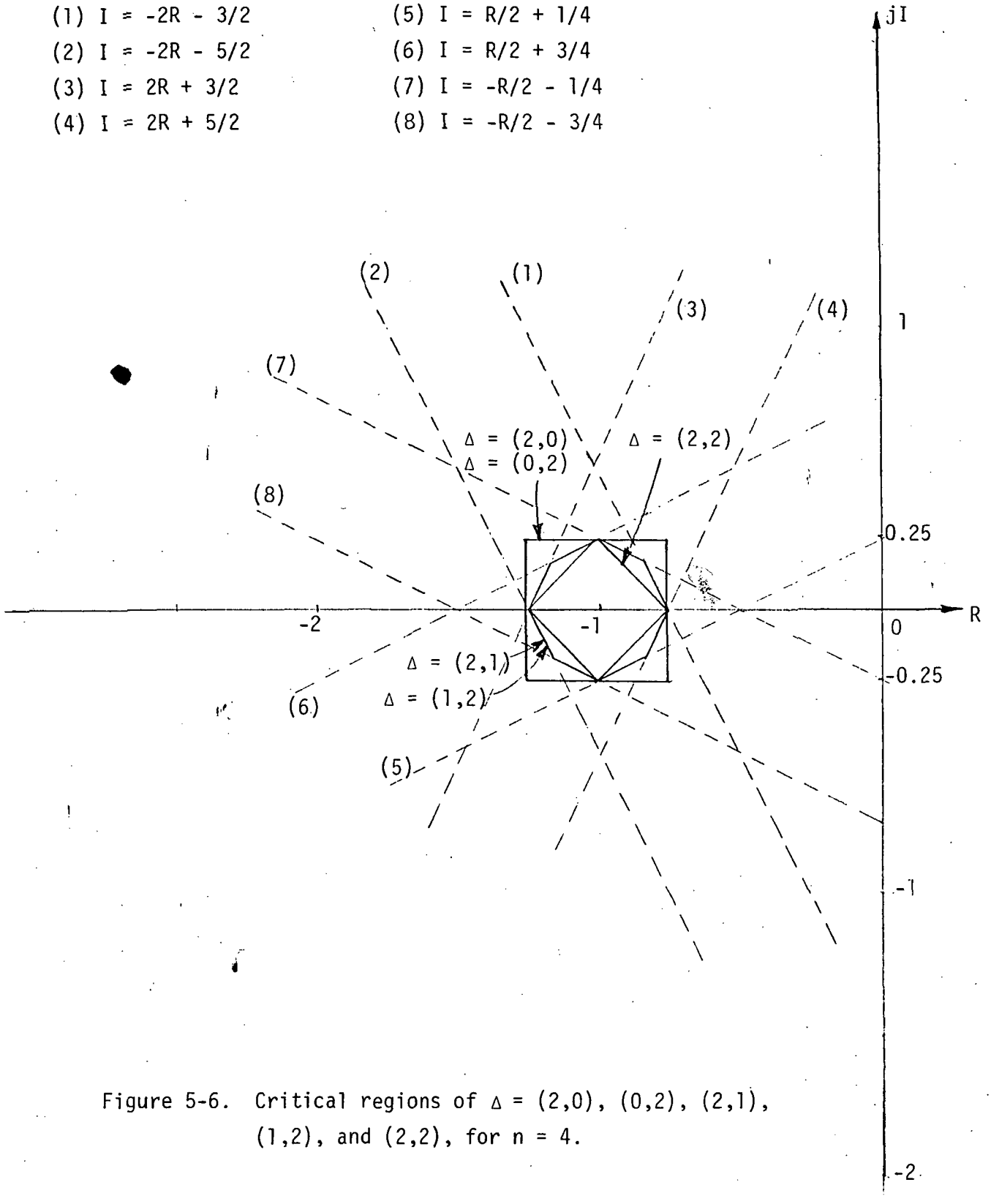

Figure 5-6. Critical regions of $\Delta = (2,0)$, $(0,2)$, $(2,1)$, $(1,2)$, and $(2,2)$, for $n = 4$.

5-4. A General DDF of a Quantizer for n > 2

In this chapter we will generalize the results of the previous sections and derive a DDF of a quantizer which is valid for all n > 2. Thus, for an oscillation of any order, n, we seek expressions which will define the critical regions of $-1/N(z)$ for all possible modes that can exist.

The derivations for the case of odd n and for the case of even n differ substantially and are therefore considered separately.

A. Even n

When n is even, the input pulse train to the quantizer can assume a maximum of n/2 different amplitudes. The mode of oscillation is thus characterized by

$$\Delta = (k_0, k_1, k_2, \ldots, k_{n_1-1}) \tag{5-46}$$

where

$$n_1 = n/2 \tag{5-47}$$

and

k_i = a positive integer, $i = 0, 1, 2, \ldots, n_1-1$.

The corresponding expression for the output of the quantizer can be written as

$$Y(z) = h(k_0b_0 + k_1b_1z^{-1} + k_2b_2z^{-2} + \ldots + k_{n_1-1}b_{n_1-1}z^{-(n_1-1)}$$

$$- k_0 b_0 z^{-n_1} - k_1 b_1 z^{-n_1-1} - \ldots - k_{n_1-1} b_{n_1-1} z^{-(2n_1-1)} + \ldots)$$

$$= h(1 - z^{-n_1} + z^{-2n_1} - \ldots)(k_0 b_0 + k_1 b_1 z^{-1} + \ldots + k_{n_1-1} b_{n_1-1} z^{-(n_1-1)})$$

$$= h(1 + z^{-n_1})^{-1} \left(\sum_{i=0}^{n_1-1} k_i b_i z^{-i} \right)$$

$$= \frac{hz^{n_1} \left(\sum_{i=0}^{n_1-1} k_i b_i z^{-i} \right)}{z^{n_1} + 1}$$

$$= \frac{h \sum_{i=0}^{n_1-1} k_i b_i z^{n_1-i}}{z^{n_1} + 1} \qquad (5\text{-}48)$$

where

h = level of quantization

b_i = +1 or -1, depending on the phase of the input; $i = 0, 1, \ldots, n_1-1$.

The variables b_i, $i = 0, 1, 2, \ldots, n_1-1$, determine the sign of the corresponding input and output pulses of the quantizer. The value of b_i is determined by the variable i and the phase shift ϕ associated with the input cosine signal.

The input to the sampler is written as

$$e(t) = E \cos(\omega t + \phi) \qquad (5\text{-}49)$$

and the input to the quantizer is

$$e^*(t) = E \sum_{k=0}^{\infty} \cos(k\omega T + \phi)\delta(t - kT) \tag{5-50}$$

For an oscillation of order n, we have

$$\omega T = \frac{2\pi}{n} \tag{5-51}$$

or

$$\omega T = \frac{\pi}{n_1} \qquad \text{when n is even} \tag{5-52}$$

Thus, Eq. (5-50) becomes

$$e^*(t) = E \sum_{k=0}^{\infty} \cos\left(\frac{k\pi}{n_1} + \phi\right)\delta(t - kT) \tag{5-53}$$

Let

$$\alpha_i = \frac{i\pi}{n_1} \qquad i = 0, 1, 2, \ldots, n_1 - 1 \tag{5-54}$$

Then the variable b_i is given by

$$b_i = \text{SIGN}[\cos(\alpha_i + \phi)] \tag{5-55}$$

With a given input amplitude E, an output of $k_i h$ at time α_i requires the following relation to exist:

$$\frac{(2k_i - 1)h}{2} < |E\cos(\alpha_i + \phi)| < \frac{(2k_i + 1)h}{2} \tag{5-56}$$

Equation (5-56) implies that for a given even n, all combinations of k_i's in the mode expression in Eq. (5-46) may not exist. Further, the range of ϕ over which a particular mode exists will vary from mode to mode. These facts provide useful insight into the operation of a quantizer and play an important role in the implementation of any scheme which is used to calculate the critical regions.

In general, the range of ϕ which must be considered in describing function derivations is 2π radians, but due to symmetry the required variation of ϕ can be reduced substantially. In the case of a quantizer and with n being even, the output waveform repeats after every $2\pi/n$ radians change in ϕ. This fact was illustrated for n = 4 by the waveforms of Fig. 5-4. Thus, it is sufficient to consider the range $-\pi/n \leq \phi \leq \pi/n$.

The expression for the output of the quantizer, Eq. (5-48), is valid over that range of ϕ where the k_i's and b_i's do not change from their selected values. The expression in Eq. (5-56) provides the restriction on ϕ because of possible variation in k_i. To determine the influence of ϕ on b_i, it is necessary to determine minimum domains of constant b_i's when ϕ is varied. With reference to Fig. 5-7, the time of pulse occurrence of the quantizer input/output is according to the sequence

$$0, \frac{2\pi}{n}, \frac{4\pi}{n}, \ldots, \frac{i2\pi}{n}, \ldots, \frac{(n-1)2\pi}{n}$$

or

$$\frac{i2\pi}{n}, \qquad i = 0, 1, 2, \ldots, n-1$$

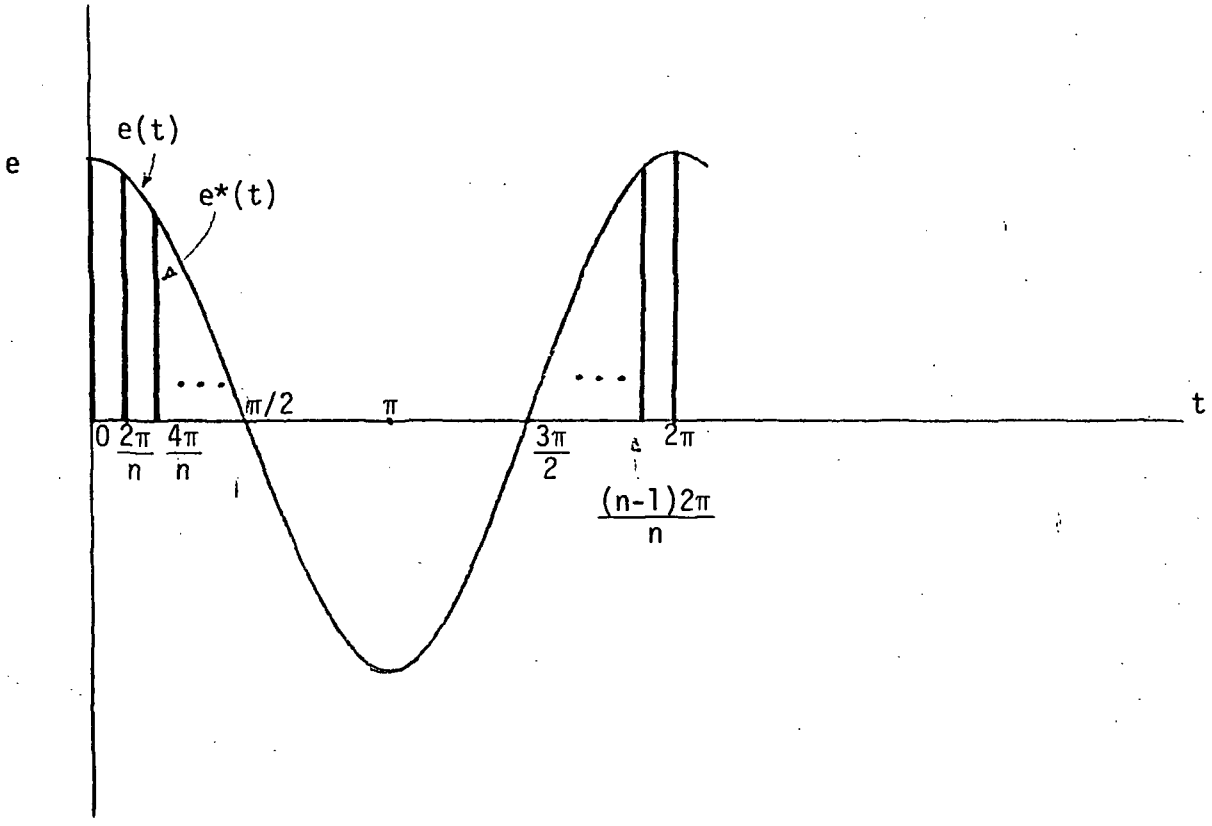

Figure 5-7.

With $\phi = 0$ as reference, the range of ϕ for constant b_i is defined by the angle when any of the b_i's first change sign. Thus, the pulses located nearest to the $\pi/2$ and $3\pi/2$ points must be considered; i.e., we need to determine those values of i for which $|\pi/2 - 2\pi i/n|$ and $|3\pi/2 - 2\pi i/n|$ achieve a minimum.

First, note that

$$\min_i \left|\frac{3\pi}{2} - \frac{2\pi i}{n}\right| = \min_i \left|\frac{\pi}{2} + \pi - \frac{2\pi i}{n} - 2\pi + \frac{2\pi n}{n}\right|$$

$$= \min_i \left|-\frac{\pi}{2} + \frac{2\pi}{n}(n - i)\right|$$

$$= \min_j \left|\frac{\pi}{2} - \frac{2\pi j}{n}\right| \qquad (5\text{-}57)$$

$j = n - i, \quad i = 0, 1, 2, \ldots, n, \quad j = 0, 1, 2, \ldots, n.$

Thus, it is sufficient to consider the minimum of $|\pi/2 - 2\pi i/n|$ only. Two separate cases have to be considered:

Case a: n_1 is even

When n_1 is even, let

$$n_1 = 2n_r \qquad (5\text{-}58)$$

then

$$n = 4n_r \qquad (5\text{-}59)$$

If we choose $i = n_r = n/4$, then

$$\left|\frac{\pi}{2} - \frac{2\pi i}{n}\right| = \left|\frac{\pi}{2} - \frac{\pi}{2}\right| = 0$$

which is then the desired minimum. In this case, there is a pulse at $\alpha_i = \pi/2$ and also at $\alpha_i = 3\pi/2$. The pulses nearest to these lie $2\pi/n$ radians on either side; thus, the b_i's will remain constant for the ranges $0 \leq \phi \leq 2\pi/n$ and $-2\pi/n \leq \phi \leq 0$. Since the range of ϕ variation is $-\pi/n \leq \phi \leq \pi/n$, two ranges of ϕ have to be considered

$$\begin{aligned} &\text{Range 1:} \quad 0 \leq \phi \leq \pi/n \\ &\text{Range 2:} \quad -\pi/n \leq \phi \leq 0 \end{aligned} \tag{5-60}$$

Case b: n_1 is odd

In this case the pulse nearest to $\pi/2$ is given by $i = (n_1/2 \pm 1/2)$, thus

$$\begin{aligned} \min_i \left|\frac{\pi}{2} - \frac{2\pi i}{n}\right| &= \left|\frac{\pi}{2} - \frac{2\pi}{n}\left(\frac{n_1}{2} \pm \frac{1}{2}\right)\right| \\ &= \left|\frac{\pi}{2} - \frac{2\pi}{n}\left(\frac{n}{4} \pm \frac{1}{2}\right)\right| \\ &= \left|\pm \frac{\pi}{n}\right| \\ &= \frac{\pi}{n} \end{aligned} \tag{5-61}$$

Since the b_i's will remain unchanged for $0 \leq \phi \leq \pi/n$ and $-\pi/n \leq \phi \leq 0$, the two ranges of ϕ are the same as in case a, Eq. (5-60).

The ranges of ϕ defined by Eq. (5-60) must therefore be considered separately when the expression for the quantizer output in Eq. (5-48) is

utilized. Although, the choice of the k_i's further restricts the range of ϕ, this restriction will not be considered in advance, and will appear naturally when the critical regions are calculated. In fact, for some combination of the k_i's the range of ϕ will be nonexistent.

In order to derive a general expression for $-1/N(z)$ when n is even, we write the expression for the input from Eq. (5-3) and the expression for the output from Eq. (5-48):

$$E(z) = \frac{Ez[(z - \cos\omega T)\cos\phi - \sin\omega T \sin\phi]}{z^2 - 2z\cos\omega T + 1} \tag{5-62}$$

$$Y(z) = \frac{h \sum_{i=0}^{n_1-1} k_i b_i z^{n_1-i}}{z^{n_1} + 1} \tag{5-63}$$

The negative inverse of the describing function is given by

$$-\frac{1}{N(z)} = -\frac{E(z)}{Y(z)}$$

$$= -\frac{Ez[(z - \cos\omega T)\cos\phi - \sin\omega T \sin\phi][z^{n_1} + 1]}{(z^2 - 2z\cos\omega T + 1)h \sum_{i=0}^{n_1-1} k_i b_i z^{n_1-i}} \tag{5-64}$$

Since z is given by

$$z = e^{j\omega T} = \cos\omega T + j\sin\omega T \tag{5-65}$$

Eq. (5-64) becomes

$$-\frac{1}{N(z)} = -\frac{Ezj \sin \omega T(\cos \phi + j \sin \phi)(z^{n_1} + 1)}{(z^2 - 2z \cos \omega T + 1)h \sum_{i=0}^{n_1-1} k_i b_i z^{n_1-i}} \tag{5-66}$$

Define

$$C_n = \frac{-zj \sin \omega T(z^{n_1} + 1)}{(z^2 - 2z \cos \omega T + 1) \sum_{i=0}^{n_1-1} k_i b_i z^{n_1-i}} \tag{5-67}$$

The term $(z^{n_1} + 1)$ can be expanded as

$$z^{n_1} + 1 = \prod_{k=0}^{n_1-1} (z - e^{j(2k+1)\pi/n_1})$$

$$= (z - e^{j\pi/n_1})(z - e^{-j\pi/n_1}) \prod_{k=1}^{n_1-2} (z - e^{j(2k+1)\pi/n_1})$$

$$= (z^2 - 2z \cos \omega T + 1) \prod_{k=1}^{n_1-2} (z - e^{j(2k+1)\pi/n_1}) \tag{5-68}$$

Substituting Eq. (5-68) into Eq. (5-67) yields

$$C_n = -\frac{zj \sin \omega T \prod_{k=1}^{n_1-2} (z - e^{j(2k+1)\pi/n_1})}{\sum_{i=0}^{n_1-1} k_i b_i z^{n_1-i}} \tag{5-69}$$

or

$$C_n = - \frac{j \sin \omega T \prod_{k=1}^{n_1-2} (z - e^{j(2k+1)\pi/n_1})}{\sum_{i=1}^{n_1} k_{i-1} b_{i-1} z^{n_1-i}} \tag{5-70}$$

let

$$C_n = C_{nR} + jC_{nI} \tag{5-71}$$

where C_{nR} and C_{nI} are the real and imaginary parts of the constant C_n.

The expression in Eq. (5-66) can now be written as

$$- \frac{1}{N(z)} = \frac{E}{h} (C_{nR} + jC_{nI})(\cos \phi + j \sin \phi) \tag{5-72}$$

The constraints on the magnitude of E are

$$\frac{(2k_i - 1)h}{2} \leq |E \cos (\phi + \alpha_i)| \leq \frac{(2k_i + 1)h}{2} \tag{5-73}$$

$i = 0, 1, 2, \ldots, n_1-1$; $k_i \neq 0$.

Since E is a positive quantity, the expression in Eq. (5-73) can be written as

$$\frac{(2k_i - 1)h}{2} \leq E|\cos (\phi + \alpha_i)| \leq \frac{(2k_i + 1)h}{2} \tag{5-74}$$

Let the range of ϕ be defined as

$$\phi_1 \leq \phi \leq \phi_2 \tag{5-75}$$

where ϕ_1 and ϕ_2 can take the values as specified in Eq. (5-60).

Define ϕ_N as

$$\phi_N = \frac{\phi_1 + \phi_2}{2} \tag{5-76}$$

The absolute value sign in Eq. (5-74) can be removed by use of a new variable α_i' as

$$\alpha_i' = \alpha_i \quad \text{if} \quad \frac{3\pi}{2} < (\phi_N + \alpha_i) < 2\pi \quad \text{or} \quad 0 < (\phi_N + \alpha_i) < \frac{\pi}{2}$$

and

$$\alpha_i' = \alpha_i - \pi \quad \text{if} \quad \frac{\pi}{2} < (\alpha_i + \phi_N) < \frac{3\pi}{2} \tag{5-77}$$

Equation (5-74) now becomes

$$\frac{(2k_i - 1)h}{2} \leq E \cos(\phi + \alpha_i') \leq \frac{(2k_i + 1)h}{2} \tag{5-78}$$

Thus, the maximum and minimum values of E can be written as

$$E_{\max i} = \frac{(2k_i + 1)h}{2 \cos(\phi + \alpha_i')} \tag{5-79}$$

$$E_{\min i} = \frac{(2k_i - 1)h}{2 \cos(\phi + \alpha_i')} \tag{5-80}$$

$i = 0, 1, 2, \ldots, n_1 - 1.$

The corresponding maximum and minimum values of $-1/N(z)$ are

$$-\frac{1}{N}\bigg|_{\max i} = \frac{(2k_i + 1)(C_{nR} + jC_{nI})(\cos\phi + j\sin\phi)}{2\cos(\phi + \alpha_i')} \tag{5-81}$$

$$-\frac{1}{N}\bigg|_{\min i} = \frac{(2k_i - 1)(C_{nR} + jC_{nI})(\cos\phi + j\sin\phi)}{2\cos(\phi + \alpha_i')} \tag{5-82}$$

In order to eliminate ϕ from Eqs. (5-81) and (5-82) consider Eq. (5-81) first; expanding the denominator and numerator yields

$$-\frac{1}{N}\bigg|_{\max i} = \frac{(2k_i + 1)[(C_{nR}\cos\phi - C_{nI}\sin\phi) + j(C_{nR}\sin\phi + C_{nI}\cos\phi)}{2(\cos\phi\cos\alpha_i' - \sin\phi\sin\alpha_i')} \tag{5-83}$$

Let

$$-\frac{1}{N}_{\max i} = x + jy \tag{5-84}$$

By comparing Eqs. (5-83) and (5-84), we have

$$x = \frac{(2k_i + 1)}{2}\frac{C_{nR}\cos\phi - C_{nI}\sin\phi}{\cos\phi\cos\alpha_i' - \sin\phi\sin\alpha_i'}$$

$$= K_i^+ \frac{C_{nR} - C_{nI}\tan\phi}{\cos\alpha_i' - \sin\alpha_i'\tan\phi} \tag{5-85}$$

where

$$K_i^+ = (2k_i + 1)/2 \tag{5-86}$$

and

$$y = K_i^+ \frac{C_{nR}\sin\phi + C_{nI}\cos\phi}{\cos\phi\cos\alpha_i' - \sin\phi\sin\alpha_i'}$$

$$= K_i^+ \frac{C_{nR}\tan\phi + C_{nI}}{\cos\alpha_i' - \sin\alpha_i'\tan\phi} \tag{5-87}$$

Equation (5-85) is solved for $\tan\phi$ to yield

$$\tan\phi = \frac{K_i^+ C_{nR} - x\cos\alpha_i'}{K_i^+ C_{nI} - x\sin\alpha_i'} \tag{5-88}$$

If Eq. (5-88) is substituted into Eq. (5-87), we have

$$y = K_i^+ \frac{C_{nR}\left(\dfrac{K_i^+ C_{nR} - x\cos\alpha_i'}{K_i^+ C_{nI} - x\sin\alpha_i'}\right) + C_{nI}}{\cos\alpha_i' - \sin\alpha_i'\left(\dfrac{K_i^+ C_{nR} - x\cos\alpha_i'}{K_i^+ C_{nI} - x\sin\alpha_i'}\right)} \tag{5-89}$$

After some algebraic manipulation, Eq. (5-89) yields

$$y = K_i^+ \frac{C_{nR}^2 + C_{nI}^2}{C_{nI}\cos\alpha_i' - C_{nR}\sin\alpha_i'} - \frac{C_{nR}\cos\alpha_i' + C_{nI}\sin\alpha_i'}{C_{nI}\cos\alpha_i' - C_{nR}\sin\alpha_i'}\, x \tag{5-90}$$

Equation (5-90) which is obtained from Eq. (5-81) by eliminating ϕ shows that the $-1/N|\max i$ locus in the complex plane is a straight line. Similarly, when ϕ is eliminated from the $-1/N|\min i$ expression, Eq. (5-82), we have

$$y = K_i^- \frac{C_{nR}^2 + C_{nI}^2}{C_{nI}\cos\alpha_i' - C_{nR}\sin\alpha_i'} - \frac{C_{nR}\cos\alpha_i' + C_{nI}\sin\alpha_i'}{C_{nI}\cos\alpha_i' - C_{nR}\sin\alpha_i'}\, x \tag{5-91}$$

which is also a straight line in the complex plane, and

$$K_i^- = \frac{(2k_i - 1)}{2} \tag{5-92}$$

Note that the lines defined by Eqs. (5-90) and (5-91) are parallel but have different intercepts on the imaginary axis. Thus, each magnitude constraint of Eqs. (5-79) and (5-80) on the input expression of

Eq. (5-62) generates two parallel lines which represent the maximum and minimum values of $-1/N(z)$, respectively.

Since there are n_1 magnitude constraints, Eq. (5-73), each output expression generates $2n_1$ lines, where n_1 lines are the maximum values of $-1/N(z)$, and n_1 lines are the minimum values of $-1/N(z)$.

When n is even, the number of ϕ ranges to be considered is two, as in Eq. (5-60), then Eq. (5-63) gives two output expressions which have to be considered. The difference between these two output expressions would be that some of the b_i's are different due to the different ϕ range. Therefore, each mode as defined by Eq. (5-46) yields the following number of lines:

$$n_L = 4n_1 \tag{5-93}$$

where n_L represents the number of lines generated in the complex plane.

Among the lines in Eq. (5-93), $2n_1$ represent maximum conditions for $-1/N(z)$, and $2n_1$ represent minimum conditions. Also, each maximum line is parallel to the corresponding minimum line.

The critical region for $-1/N(z)$ is thus the region enclosed by the n_L lines and satisfying the maximum and minimum requirements associated with each line. In some cases if the choice of the k_i's in Eq. (5-46) is such that there may be no region enclosed, then that particular mode will not exist.

The procedure for determining the critical region for the quantizer describing function when n is even, can be summarized as follows:

1. Select an even integral n.

2. Select a mode by choosing the k_i's in Eq. (5-46).
3. There are two ranges of ϕ, $0 \leq \phi \leq \pi/n$ and $-\pi/n \leq \phi \leq 0$. For each range of ϕ determine the b_i's and thus the output, Eq. (5-63).
4. Calculate the coefficient C_n as in Eq. (5-70) for each range of ϕ.
5. Determine the α_i's, Eq. (5-54), and α_i''s, Eq. (5-77), for the chosen n.
6. For each α_i' and each range of ϕ, calculate the slope and intercepts of the n_L lines, Eqs. (5-90) and (5-91) which define the maximum and minimum values of $-1/N(z)$.
7. Determine the region enclosed by these lines. This is the critical region.

As n is increased, the number of equations defined by Eq. (5-93) quickly rises and it is useful to consider utilizing a digital computer for determining the critical regions. The following table illustrates the number of lines associated with various even values of $n \geq 4$.

n	ranges of ϕ (degrees)	no. of lines per ϕ range ($2n_1$)	total number of lines ($4n_1$)
4	$0 \leq \phi \leq 45$ $-45 \leq \phi \leq 0$	8	16
6	$0 \leq \phi \leq 30$ $-30 \leq \phi \leq 0$	12	24
8	$0 \leq \phi \leq 22.5$ $-22.5 \leq \phi \leq 0$	16	32
10	$0 \leq \phi \leq 18$ $-18 \leq \phi \leq 0$	20	40
20	$0 \leq \phi \leq 9$ $-9 \leq \phi \leq 0$	40	80

B. Odd n

When n is odd, the input pulse train to the quantizer can assume a maximum of n different values. The mode of oscillation is thus characterized by

$$\Delta = (k_0, k_1, k_2, \ldots, k_{n-1}) \tag{5-94}$$

The output of the quantizer is written as

$$\begin{aligned} Y(z) &= h(k_0 b_0 + k_1 b_1 z^{-1} + k_2 b_2 z^{-2} + \ldots + k_{n-1} b_{n-1} z^{-(n-1)} \\ &\quad + k_0 b_0 z^{-n} + k_1 b_1 z^{-(n+1)} + \ldots) \\ &= h(1 + z^{-n} + z^{-2n} + \ldots)(k_0 b_0 + k_1 b_1 z^{-1} + \ldots + k_{n-1} b_{n-1} z^{-(n-1)}) \\ &= h(1 - z^{-n})\left(\sum_{i=0}^{n-1} k_i b_i z^{-i}\right) \\ &= \frac{h z^n \left(\sum_{i=0}^{n-1} k_i b_i z^{-i}\right)}{z^n - 1} \\ &= \frac{h \sum_{i=0}^{n-1} k_i b_i z^{n-i}}{z^n - 1} \end{aligned} \tag{5-95}$$

where h and b_i have the same meaning as in the even n case.

The input to the sampler is again written as

$$e(t) = E \cos(\omega t + \phi) \tag{5-96}$$

and the input to the quantizer is

$$e^*(t) = E \sum_{k=0}^{\infty} \cos(k\omega T + \phi)\delta(t - kT)$$

$$= E \sum_{k=0}^{\infty} \cos\left(\frac{2k\pi}{n} + \phi\right)\delta(t - kT) \qquad (5\text{-}97)$$

Let

$$\alpha_i = \frac{2\pi i}{n} \qquad i = 0, 1, 2, \ldots, n-1 \qquad (5\text{-}98)$$

then, b_i is given by

$$b_i = \text{SIGN}[\cos(\alpha_i + \phi)] \qquad (5\text{-}99)$$

The input and output of the quantizer are constrained by the following relation:

$$\frac{(2k_i - 1)h}{2} < |E\cos(\alpha_i + \phi)| < \frac{(2k_i + 1)h}{2} \qquad (5\text{-}100)$$

As in the case of even n, Eq. (5-100) restricts the possible combinations of k_i's in the mode expression of Eq. (5-94).

In order to determine the range of ϕ, consider the waveforms in Fig. 5-8. In this figure n = 3 and the waveforms repeat every 120 degrees. In general, for odd n, the output waveform will repeat when ϕ is changed by $2\pi/n$ radians. Thus, the range of ϕ is chosen as $-\pi/n \leq \phi \leq \pi/n$.

It is now necessary to divide the chosen range of ϕ into smaller ranges depending on the variation of b_i's in the chosen full range.

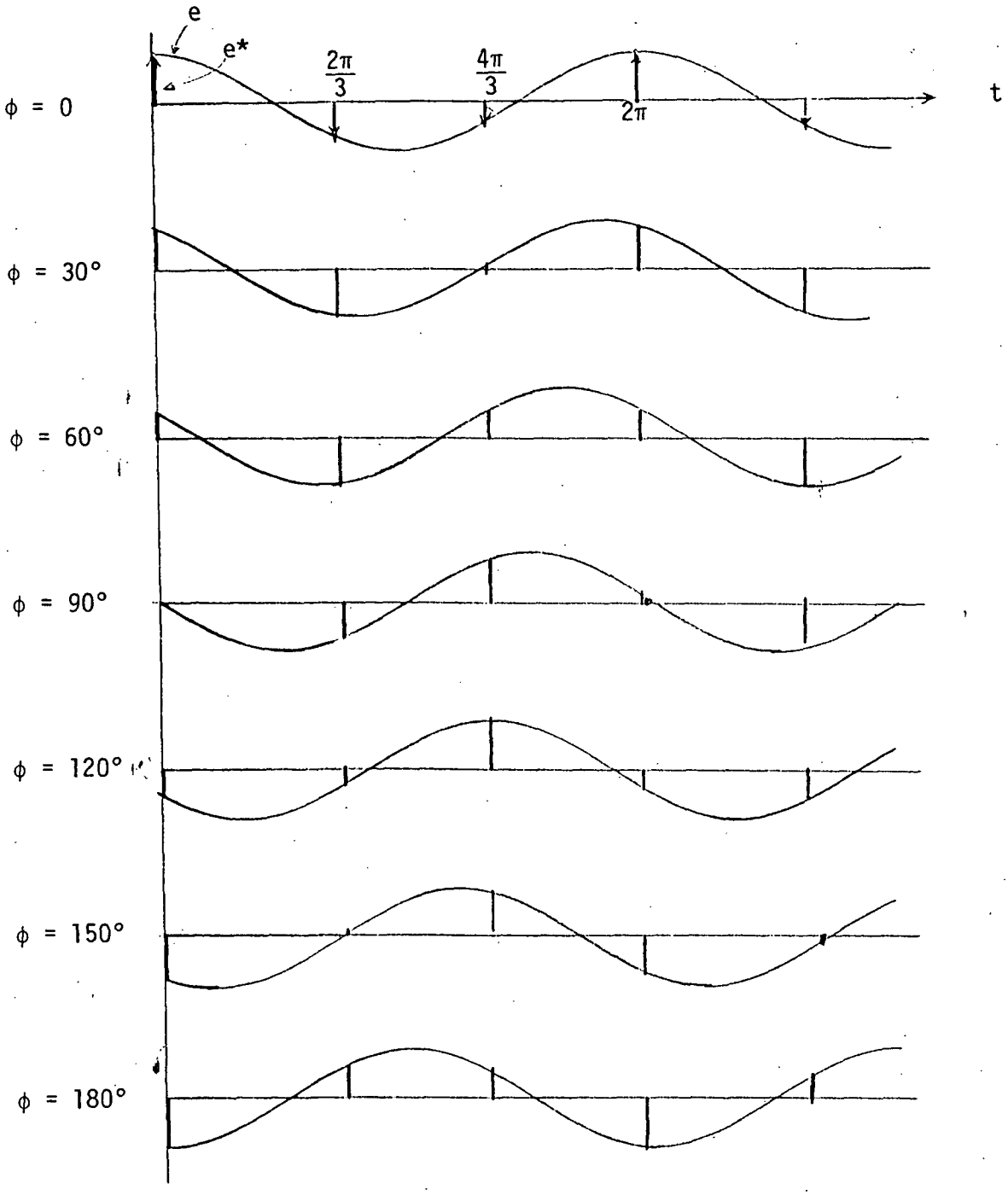

Figure 5-8.

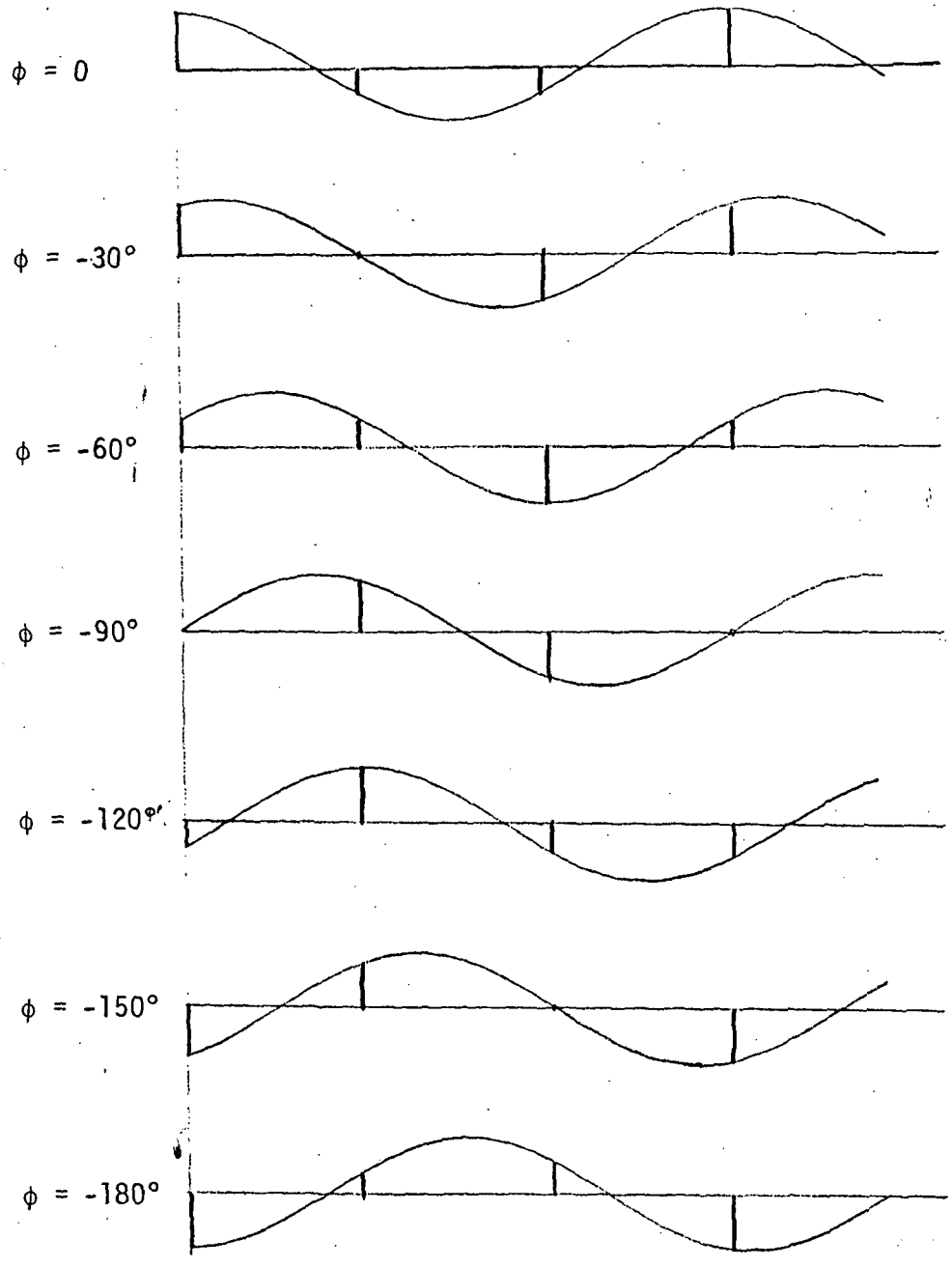

Figure 5-8.

The effect of k_i's on restricting the range of ϕ will be accounted for when the limits on the input magnitude as described by Eq. (5-100) are considered. To determine the influence of b_i's on ϕ, we again calculate the domains of constant b_i when ϕ is varied in the chosen range. The pulse occurrence timing is written as

$$0, \frac{2\pi}{n}, \ldots, \frac{(n-1)2\pi}{n}$$

or

$$\frac{2\pi i}{n}, \qquad i = 0, 1, 2, \ldots, n-1.$$

Taking $\phi = 0$ as reference, it is necessary to determine the values of i for which $|\pi/2 - 2\pi i/n|$ becomes a minimum. The result of Eq. (5-57) is still valid and allows us to ignore the $3\pi/2$ point while considering the $\pi/2$ point only.

The minimum of $|\pi/2 - 2\pi i/n|$ will be achieved by one of the two pulse occurrences on either side of the $\pi/2$ points (when n is odd, no pulse occurs at $\pi/2$ exactly). Thus, the minimum will be given by

$$i = \frac{n}{4} \pm \frac{1}{4} \quad ,$$

which ever sign makes i an integer. Thus, when n = 3, the + sign is used and when n = 5 the - sign is used, i = 1 in each case. Thus,

$$\min_i \left|\frac{\pi}{2} - \frac{2\pi i}{n}\right| = \left|\frac{\pi}{2} - \frac{2\pi}{n}\left(\frac{n}{4} \pm \frac{1}{4}\right)\right|$$

$$= \left|\pm \frac{\pi}{2n}\right|$$

$$= \frac{\pi}{2n} \qquad (5\text{-}101)$$

The chosen range of ϕ, $-\pi/n \leq \phi \leq \pi/n$ has to be subdivided into sections given by Eq. (5-101), over which the b_i's are constant. Four ranges of ϕ must therefore be considered.

$$\begin{aligned} &\text{Range 1:} \quad \pi/2n \leq \phi \leq \pi/n \\ &\text{Range 2:} \quad 0 \leq \phi \leq \pi/2n \\ &\text{Range 3:} \quad -\pi/2n \leq \phi \leq 0 \\ &\text{Range 4:} \quad -\pi/n \leq \phi \leq -\pi/2n \end{aligned} \tag{5-102}$$

A general expression for $-1/N(z)$ with odd n is now derived. The input signal will change when ϕ is varied beyond its range as defined by Eq. (5-102). Accordingly, each range in Eq. (5-102) will have to be calculated separately.

The input and the output of the quantizer are written as

$$E(z) = -\frac{Ezj \sin \omega T(\cos \phi + j \sin \phi)}{z^2 - 2z \cos \omega T + 1} \tag{5-103}$$

$$Y(z) = \frac{h \sum_{i=0}^{n-1} k_i b_i z^{n-i}}{z^n + 1} \tag{5-104}$$

respectively.

The negative inverse of the describing function is

$$\begin{aligned} -\frac{1}{N(z)} &= -\frac{E(z)}{Y(z)} \\ &= -\frac{Ezj \sin \omega T(\cos \phi + j \sin \phi)(z^n + 1)}{(z^2 - 2z \cos \omega T + 1)h \sum_{i=0}^{n-1} k_i b_i z^{n-i}} \end{aligned} \tag{5-105}$$

Define

$$C_n = - \frac{zj \sin \omega T(z^n + 1)}{(z^2 - 2z \cos \omega T + 1)(\sum_{i=0}^{n-1} k_i b_i z^{n-i})} \tag{5-106}$$

In Eq. (5-106), the term $(z^n - 1)$ is written as

$$(z^n - 1) = \prod_{i=0}^{n-1} (z - e^{j2\pi i/n})$$

$$= (z - 1)(z^2 - 2z \cos \omega T + 1) \prod_{i=2}^{n-2} (z - e^{j2\pi i/n}) \tag{5-107}$$

Substituting Eq. (5-107) into Eq. (5-106) yields

$$C_n = - \frac{zj \sin \omega T(z - 1) \prod_{i=2}^{n-2} (z - e^{j2\pi i/n})}{\sum_{i=0}^{n-1} k_i z^{n-i}}$$

$$= - \frac{j \sin \omega T(z - 1) \prod_{i=2}^{n-2} (z - e^{j2\pi i/n})}{\sum_{i=1}^{n} k_{i-1} b_{i-1} z^{n-i}} \tag{5-108}$$

Dividing Eq. (5-108) into real and imaginary components, we write

$$C_n = C_{nR} + jC_{nI} \tag{5-109}$$

The expression in Eq. (5-105) then becomes

$$- \frac{1}{N(z)} = \frac{E}{h} (C_{nR} + jC_{nI})(\cos \phi + j \sin \phi) \tag{5-110}$$

The magnitude of E is constrained by

$$\frac{(2k_i - 1)h}{2} \leq |E \cos(\phi + \alpha_i)| \leq \frac{(2k_i + 1)h}{2} \tag{5-111}$$

$i = 0, 1, 2, \ldots, n-1$, $k_i \neq 0$.

Let the range of ϕ under consideration be

$$\phi_1 \leq \phi \leq \phi_2 \tag{5-112}$$

where ϕ_1 and ϕ_2 can take on values as specified in Eq. (5-102), we define

$$\phi_N = \frac{\phi_1 + \phi_2}{2} \tag{5-113}$$

Select α_i' such that

$$\alpha_i' = \alpha_i \quad \text{if} \quad \frac{3\pi}{2} < (\phi_N + \alpha_i) < 2\pi$$

$$\text{or} \quad 0 < (\phi_N + \alpha_i) < \pi/2$$

$$\alpha_i' = \alpha_i - \pi \quad \text{if} \quad \frac{\pi}{2} < (\phi_N + \alpha_i) < 3\pi/2 \tag{5-114}$$

Then, Eq. (5-111) can be written as

$$\frac{(2k_i - 1)h}{2} \leq E \cos(\phi + \alpha_i') \leq \frac{(2k_i + 1)h}{2} \tag{5-115}$$

The maximum and minimum values of E from Eq. (5-115) become

$$E_{\max i} = \frac{(2k_i + 1)h}{2\cos(\phi + \alpha_i')} \tag{5-116}$$

$$E_{\min i} = \frac{(2k_i - 1)h}{2\cos(\phi + \alpha_i')} \tag{5-117}$$

The corresponding maximum and minimum values of $-1/N(z)$ are

$$-\frac{1}{N}\bigg|_{\max i} = \frac{(2k_i + 1)(C_{nR} + jC_{nI})(\cos\phi + j\sin\phi)}{2\cos(\phi + \alpha_i')} \tag{5-118}$$

$$-\frac{1}{N}\bigg|_{\min i} = \frac{(2k_i - 1)(C_{nR} + jC_{nI})(\cos\phi + j\sin\phi)}{2\cos(\phi + \alpha_i')} \tag{5-119}$$

Equations (5-118) and (5-119) are similar to Eqs. (5-81) and (5-82), respectively, obtained earlier for even n. Thus, as in that case, it is possible to eliminate ϕ and determine the straight lines defined by the locus of each expression which ϕ is varied. The result is identical to Eqs. (5-90) through (5-92).

Each magnitude constraint in Eq. (5-115) again generates two parallel straight lines, one representing the maximum value of $-1/N(z)$ and the other representing the minimum value of $-1/N(z)$.

With n magnitude constraints and four ranges of ϕ, the total number of straight lines in the complex plane is

$$n_L = 8n \tag{5-120}$$

As before, the critical region for $-1/N(z)$ is the region enclosed by the n_L lines and simultaneously satisfying the maximum and minimum requirements associated with each line. Also, if the choice of k_i's is such that no region may be enclosed, that particular mode will not exist.

The procedure for determining the critical region for the quantizer describing function when n is odd is summarized below:

1. Select an odd integral n.
2. Select a mode by choosing the k_i's in Eq. (5-94).
3. Four ranges of ϕ can exist, as defined by Eq. (5-102). Determine the b_i's for each range.
4. Calculate coefficients C_n as given by Eq. (5-108) for each range of ϕ.
5. Determine the α_i''s, Eq. (5-114).
6. For each α_i' and each range of ϕ calculate the two lines of Eqs. (5-118) and (5-119) which define the maximum and minimum values of $-1/N(z)$.
7. Determine the critical region by finding the region enclosed by all the lines.

The following table indicates the number of lines associated with several values of odd n:

n	Ranges of ϕ (degrees)	no. of lines per ϕ range (2n)	total number of lines (8n)
3	$0 \leq \phi \leq 30$, $30 \leq \phi \leq 60$ $-60 \leq \phi \leq -30$, $-30 \leq \phi \leq 0$	6	48
5	$0 \leq \phi \leq 18$, $18 \leq \phi \leq 36$ $-36 \leq \phi \leq -18$, $-18 \leq \phi \leq 0$	10	80
7	$0 \leq \phi \leq 12.9$, $12.9 \leq \phi \leq 25.8$ $-25.8 \leq \phi \leq -12.9$, $-12.9 \leq \phi \leq 0$	14	112

5-5. Computer Implementation and Results with the General Quantizer Describing Function

The DDF derived in the previous sections has been programmed on a digital computer. Input data consists of the order of oscillation n and the modes which are to be investigated. The program calculates the ϕ ranges, the α_i''s, the b_i's and generates all the possible lines for the given mode. These lines are then plotted by hand and the critical region determined.

As examples of the utility of the program, two values of n, n = 4 (even case) and n = 3 (odd case) are selected.

A. Results for n = 4

Figure 5-9 shows a typical printed output from the program for one mode, Δ = (1, 2). In Fig. 5-9 the following information is provided:

1. N = the order of oscillation n
   N1 = n/2 for even n and N1 = n for odd n
   NPR = no. of ϕ ranges
   NLS = NPR × N1
   NL = no. of lines n_L
   N1NT = no. of intersections of the lines, $\frac{n_i(n_L - 2)}{2}$
2. The ϕ range is printed next as PHI RANGE
3. The α_i''s are written as ALPHA VALUES
4. Sequence of b_0k_0, b_1k_1, b_2k_2, ... is written as SEQUENCE OF KO, K1, etc.
5. C_{nR} and C_{nI} are printed next

```
DISCRETE DESCRIBING FUNCTION FOR A QUANTIZER NONLINEARITY
N= 4    N1= 2    NPR= 2    NLS=  4    NL=  8    NINT=  24
PHI RANGE IS-45.00 TO   0.00
ALPHA VALUES ARE     0.000E-01    9.000E+01
SEQUENCE OF K0,K1,...ETC IS  1.  2.
CN-REAL=-2.00000E-01  CN-IMAG=-4.00000E-01
THE LINES ARE GIVEN BY Y=X*SLOPE+CROSS
       SLOPE           CROSS1           CROSS2
  -5.00000E-01    -7.49999E-01    -2.50000E-01
   2.00001E+00     2.50001E+00     1.50000E+00
PHI RANGE IS  0.00 TO  45.00
ALPHA VALUES ARE     0.000E-01   -9.000E+01
SEQUENCE OF K0,K1,...ETC IS  1. -2.
CN-REAL=-2.00000E-01  CN-IMAG= 4.00000E-01
THE LINES ARE GIVEN BY Y=X*SLOPE+CROSS
       SLOPE           CROSS1           CROSS2
   5.00000E-01     7.50001E-01     2.50000E-01
  -2.00001E+00    -2.50001E+00    -1.50000E+00
```

Figure 5-9.

6. The lines for this ϕ range are then written, where SLOPE refers to the slope of the maximum and minimum lines. CROSS1 is the intercept of the maximum line and CROSS2 is the same for the minimum line. The lines are written in the same order as the α_i''s, or the occurrence of the pulses.
7. All information is repeated for the other ϕ range.

The lines are plotted and the critical region is determined. Figure 5-10 shows the plots for several different modes with n = 4. In this case the critical regions are symmetrically located around the (-1, 0) point in the complex plane. Also, as k_0, k_1 increase the critical region tends to shrink towards the (-1, 0) point.

B. Results for n = 3

With n = 3 the mode of oscillation is defined by three different variables, k_0, k_1 and k_2. Also, in this case, many of the combinations of k_i's cannot exist. Figure 5-11 shows the critical regions obtained with the computer program for Δ = (1, 0, 0) and Δ = (1, 1, 1). The critical region was found not to exist for the modes Δ = (2, 0, 0), Δ = (1, 2, 2), Δ = (1, 2, 3).

Results for other modes and other values of n can be obtained similarly. However, as n gets larger, the number of lines increases substantially and the procedure for determining the critical region gets more involved. It would be desirable if the computer program were able to calculate these regions itself from the straight lines. In order to expand the scope of the program to include this calculation, several special cases, which can occur have to be resolved first:

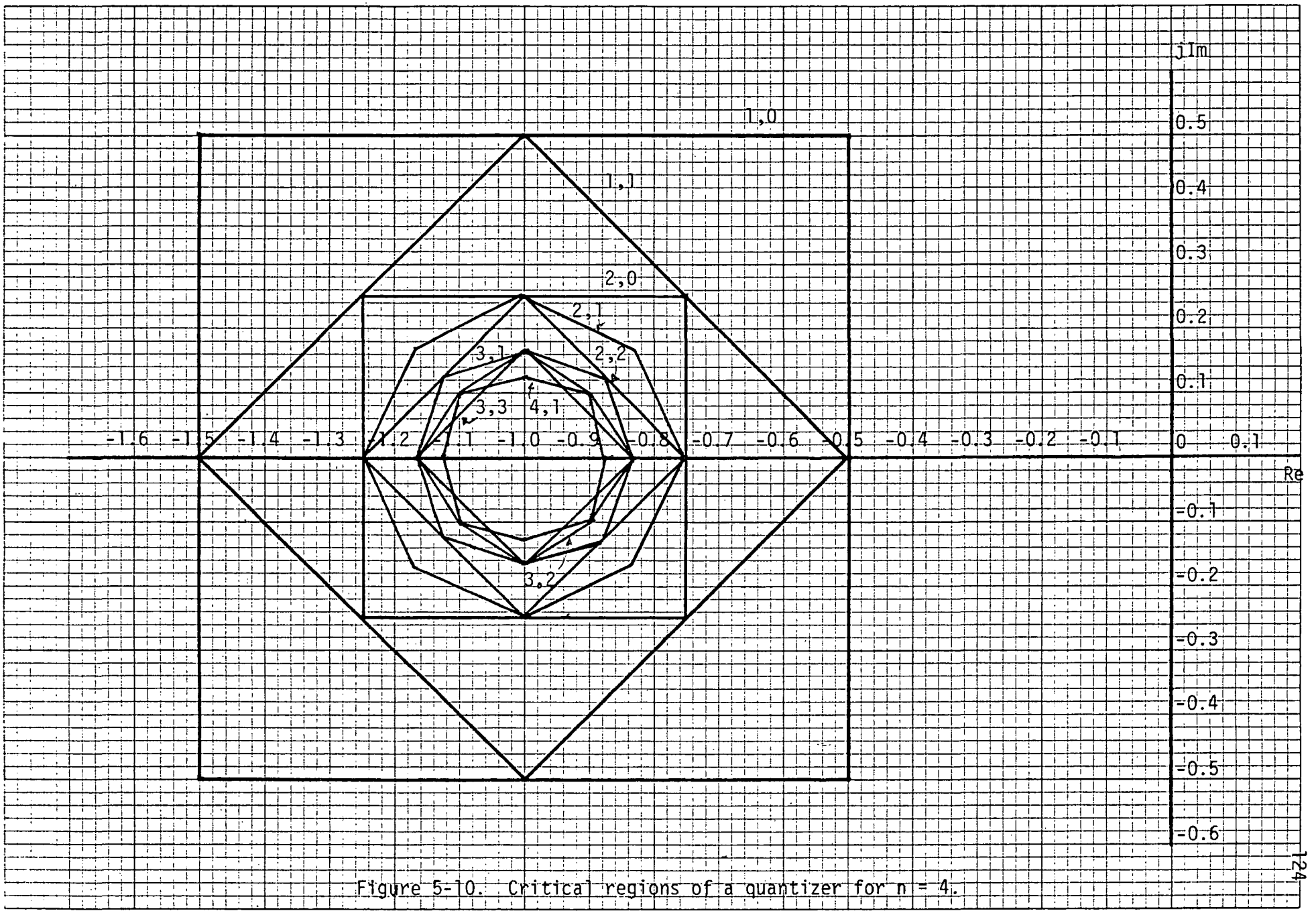

Figure 5-10. Critical regions of a quantizer for n = 4.

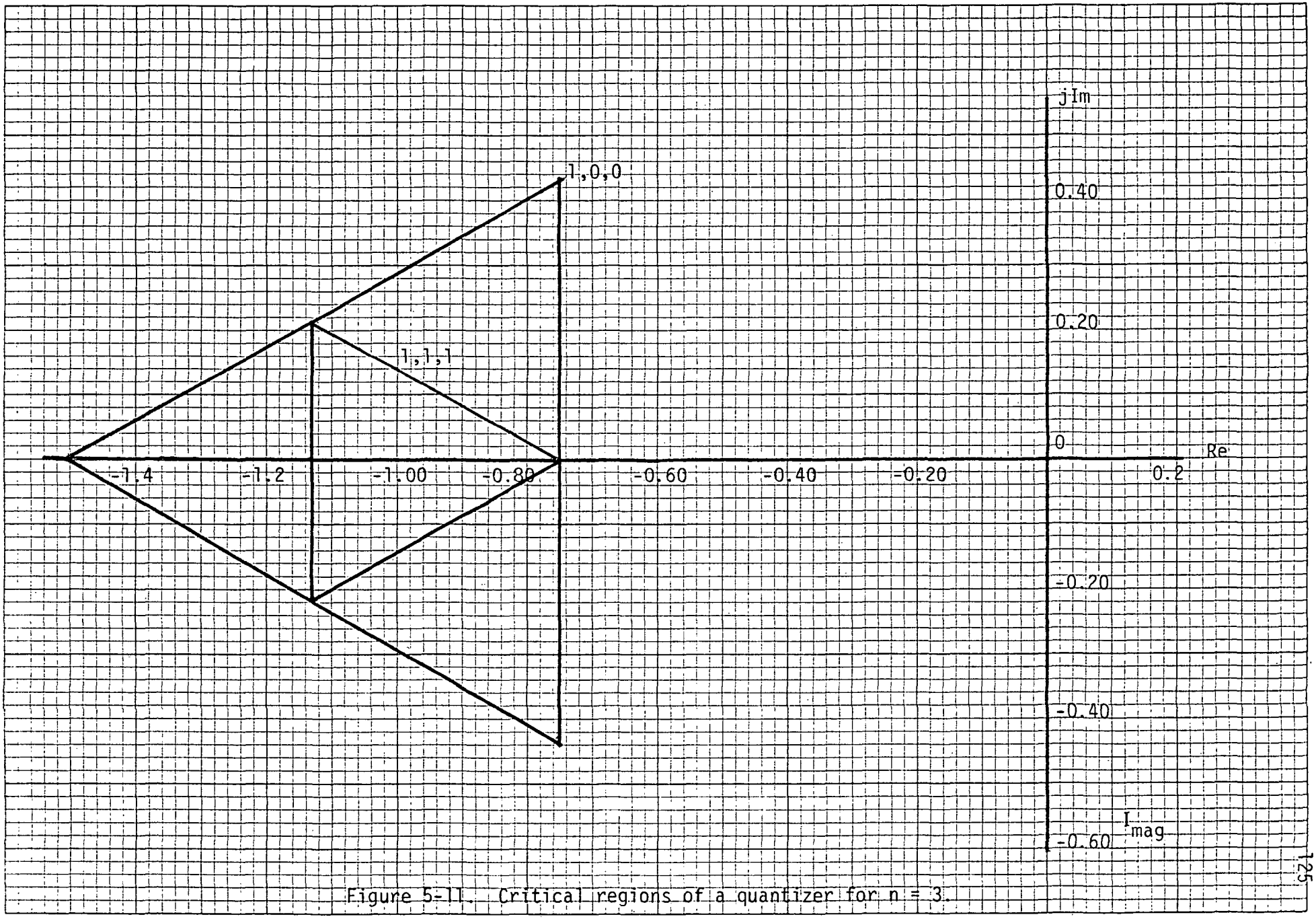

Figure 5-11. Critical regions of a quantizer for n = 3.

1. In certain modes, the duplication of the lines results in many parallel lines, and their intersection calculations can cause singularities. Such duplicate lines and repetitions should be recognized and eliminated, thus removing any singularities as well as reducing the computation.
2. In certain modes, the straight line can be a line with infinite slope. This happens when certain combinations of C_{nR}, C_{nI} and α_i's yield zero denominator in the slope expression, Eq. (5-90). This condition should be recognized and the line should be redefined as $x = f(c, \alpha)$, with no occurrence of y in the line equation.
3. Sometimes the straight line has zero slope and this must also be recognized and eliminated. The line must be redefined using y only.

These comments can provide a basis for extending the results presented here and using them in a more general situation.

REFERENCES

1. K. Frevert and R. Joyce, "Pointing Stability of A Fine Pointing Control System For A Low-Cost LST With A Reaction Wheel Model And Dahl Nonlinearity," Northrop Services, Inc., Memorandom No. 9250C-74-51, December 20, 1974.

2. K. Frevert and R. Joyce, "Effects of Dahl Nonlinear Friction Model On Pointing Stability," Northrop Services, Inc., Memorandom No. 9250C-75-10, January 28, 1975.

3. R. W. Troop, "An Equivalent Gain Analysis of Nonlinear Sampled-Data Systems Subjected to Stochastic Inputs," M.S. Thesis, Air University, USAF, Wright-Patterson AFB, Ohio, 1968.

4. R. F. Prueher, "An Equivalent Gain and Stochastic Analysis For Nonlinear Sampled-Data Control Systems," Ph.D Thesis, Department of Electrical Engineering, University of Illinois, Urbana, Illinois, 1966.

5. B. C. Kuo and G. Singh, "Continuous And Discrete Describing Function Analysis of the LST System" Chapter 1, Final Report, IV-73, Systems Reserach Laboratory, January 1, 1974.